Semi-leptonic Decays on the Lattice

Nicholas Mark Hazel

Doctor of Philosophy

The University of Edinburgh

1996

To Mum and Dad.

Abstract

This thesis describes a lattice calculation of the matrix elements of the vector and axial-vector currents which are relevant to the semi-leptonic decays $D \to K$ and $D \to K^*$. The simulation was performed in the quenched approximation to lattice QCD on a $24^3 \times 48$ space-time lattice at $\beta = 6.2$, using an $O(a)$-improved fermionic action. In the limit of zero lepton masses the $D \to K$ and $D \to K^*$ decays are described by four form factors: f_K^+, V_{K^*}, $A_{K^*}^1$ and $A_{K^*}^2$ which are dimensionless functions of q^2, where q^μ is the four-momentum transfer. The main results, for the form factors at $q^2 = 0$, are as follows:

$$
\begin{aligned}
f_K^+(0) &= 0.67 \,{}^{+\,0.05}_{-\,0.03}\,{}^{+\,0.03}_{-\,0.04} \\
V_{K^*}(0) &= 1.01 \,{}^{+\,0.25}_{-\,0.05}\,{}^{+\,0.05}_{-\,0.06} \\
A_{K^*}^1(0) &= 0.69 \,{}^{+\,0.06}_{-\,0.03}\,{}^{+\,0.01}_{-\,0.05} \\
A_{K^*}^2(0) &= 0.63 \,{}^{+\,0.12}_{-\,0.12}\,{}^{+\,0.01}_{-\,0.05}
\end{aligned}
$$

where the first set of errors are statistical and the second are an estimate of the systematic error. These results are in good agreement with experiment. The form factors were determined for different q^2 values; their q^2 dependence is found to be reasonably well described by a simple pole-dominance model. The form factors corresponding to the semi-leptonic decays $D \to \pi$ and $D \to \rho$ were also computed.

Declaration

This thesis has been composed wholly by me and contains my own work carried out as a member of the UKQCD Collaboration. The analysis described in Chapter 3 was performed under the initial guidance of Dave Richards and in the later stages in collaboration with Juan Nieves in preparation for publication. The basic routines for statistical analysis were written in conjunction with Henning Hoeber, David Henty and Hugh Shanahan.

The results in Chapter 2 are compatible with values published in

- C.R. Allton *et. al.* (UKQCD Collaboration), *Phys. Rev.* **D49** (1994) 474.
- R.M. Baxter *et. al.* (UKQCD Collaboration), *Phys. Rev.* **D49** (1994) 1594.

and the results in Chapter 3 are published in

- K.C. Bowler *et. al.* (UKQCD Collaboration), *Phys. Rev.* **D51** (1995) 4905.

Other related publications to which I have contributed include

- N.M. Hazel (UKQCD Collaboration), *Nucl. Phys.* **B (Proc. Suppl.) 34** (1994) 471.
- S.P. Booth *et. al.* (UKQCD Collaboration), *Phys. Rev. Lett.* **72** (1994) 462.
- K.C. Bowler *et. al.* (UKQCD Collaboration), *Phys. Rev. Lett.* **72** (1994) 1398.
- K.C. Bowler *et. al.* (UKQCD Collaboration), *Phys. Rev.* **D51** (1995) 4955.
- K.C. Bowler *et. al.* (UKQCD Collaboration), *Phys. Rev.* **D52** (1995) 5067.
- D.R.Burford *et. al.* (UKQCD Collaboration), *Nucl. Phys.* **B447** (1995) 425.
- J.M. Flynn *et. al.* (UKQCD Collaboration), *Nucl. Phys.* **B461** (1996) 327.

Nicholas Mark Hazel

Acknowledgements

I dedicate this thesis to my family whose support and encouragement have made it possible. I would also like to thank my supervisors Ken Bowler and Brian Pendleton, and Professor Richard Kenway, for their guidance and support, and for providing access to the funds to attend *Lattice* 93. Thanks to Dave Richards and David Henty for useful discussions and suggestions during my research. I also enjoyed collaborating with Juan Nieves from Southampton University in the preparation of a UKQCD publication.

I had the pleasure to work alongside my fellow postgrads Henning Hoeber, Hugh Shanahan, Nick Stanford and John Mehegan. I wish them all the best in their future careers. I have also enjoyed sharing an office, and far too many coffee breaks, with Harry Newton, Orlando Oliveira, Mike Peardon and Sinead Ryan. I am particularly in debt to Harry and Mike for letting me stay at Montague Street during my 'homeless' period.

During my stay in Edinburgh I spent two great years at 5 Roseneath St. with my extended family Dave, James and Mark - the 'boyz from the flat'. These 'guys' provided me with an escape from the social isolation of the physics department and an appallingly bad taste in music. Good luck with your respective careers in Medicine ($\times 2$) and Veterinary Practice. More recently, I have enjoyed sharing a flat with Pete Evans, Chris Jowett and David Parratt.

I have had the good fortune to know Adam Davis, Graham Ford and Charlie Tripp with whom I have shared the more memorable experiences in my life. Thanks for the epic expeditions, wild drinking escapades and disturbing philosophical debates.

Finally I acknowledge the financial support of the Particle Physics and Astronomy Research Council, and my personal sponsors Mr. Access and Mr. Visa.

Henry IV, Part 1

(Close of Act 1, Scene 2)

Prince Henry

I know you all, and will awhile uphold
The unyoked humour of your idleness:
Yet herein will I imitate the sun,
Who doth permit the base contagious clouds
To smother up his beauty from the world,
That, when he please again to be himself,
Begin wanted, he may be more wonder'd at,
By breaking through the fowl and ugly mists
Of vapours that did seem to strangle him.
If all the year were playing holidays,
To sport would be as tedious as to work;
But when they seldom come, they wish'd for come,
And nothing pleaseth but rare accidents.
So, when this loose behavior I throw off
And pay the debt I never promised,
By how much better than my word I am,
By so much shall I falsify men's hopes;
And like bright metal on a sullen ground,
My reformation, glittering o'er my fault,
Shall show more goodly and attract more eyes
Than that which hath no foil to set it off.
I'll so offend, to make offence a skill;
Redeeming time when men think least I will.

[Exit]

William Shakespeare

Contents

Introduction

The Standard Model (SM) of Particle Physics [1, 2, 3] describes the interaction of the elementary particles, the quarks and leptons, in terms of the strong, weak and electromagnetic forces. These forces are mediated by gauge bosons: the gluon, W^+_- and Z, and the photon respectively. This model has been successful in explaining many of the observed experimental phenomena, over a wide range of energies. However, the SM has some unsatisfactory features: the large number of free parameters (> 20) required as input, and no quantum theory of gravity. Tests of the SM have focused on determining these free parameters in a search for new physics.

Many parameters in the weak sector of the SM are under-determined. The Cabibbo-Kobayashi-Maskawa (CKM) matrix elements describe how the quarks participate in the weak interaction. However, only the weak decays of mesons and baryons are observed experimentally; the strong force confines quarks within hadrons. Unfortunately, the relevant weak processes occur at low energies where the quark-gluon coupling is of $O(1)$. Thus, perturbation theory fails and one must rely on non-perturbative approaches, such as quark models and QCD sum rules, in order to extract information on the CKM matrix elements from experimental measurements. On the lattice, the non-perturbative quark-gluon contribution can be computed from first principles.

The semi-leptonic decays of heavy-light mesons provide a window on the CKM matrix elements; the square of the relevant CKM matrix element appears as an overall factor in the decay rate. These decays proceed via the spectator process whereby the heavy quark decays into a 'lighter' quark by emitting a W boson (which decays into a lepton pair); the common light quark plays no part in the interaction. Figure 0.1 shows the Feynman diagram relevant in semi-leptonic $D \to K$, K^* decays. Semi-leptonic decays are particularly simple since there is a single hadron only in the final state. Thus, there are no interference diagrams or final state interactions to take into account, unlike the case of non-leptonic decays.

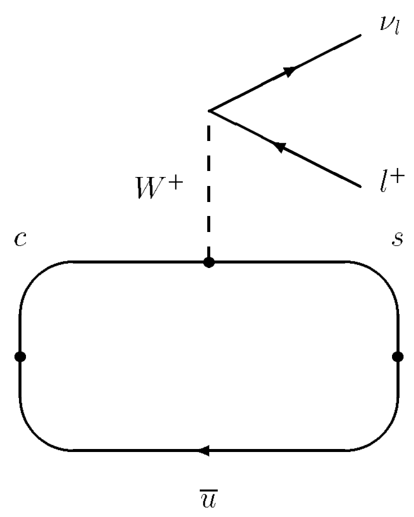

Figure 0.1: Feynman diagram relevant in semi-leptonic $D \to K, K^*$ decays.

Charged Weak Currents

The SM Lagrangian describing the charged-current interaction is given by

$$\mathcal{L}_{CC} = \frac{g}{2\sqrt{2}} \left(J_h^\mu + J_l^\mu\right) W_\mu^+ + \text{h.c.} \tag{0.1}$$

with

$$J_h^\mu = \left(\bar{u},\, \bar{c},\, \bar{t} \right) \gamma^\mu (1 - \gamma^5)\, V_{CKM} \begin{pmatrix} d \\ s \\ b \end{pmatrix} \tag{0.2}$$

and

$$J_l^\mu = \left(\bar{\nu}_e,\, \bar{\nu}_\mu,\, \bar{\nu}_\tau\right) \gamma^\mu (1 - \gamma^5) \begin{pmatrix} e \\ \mu \\ \tau \end{pmatrix} \tag{0.3}$$

where J_h^μ and J_l^μ are the hadronic and leptonic vector-minus-axial-vector (V-A) currents respectively which couple to the massive gauge vector bosons, W_-^+, and g is the $SU(2)$ gauge coupling constant.

The CKM matrix [4, 5] is given by

$$V_{CKM} = \begin{pmatrix} V_{ud} & V_{us} & V_{ub} \\ V_{cd} & V_{cs} & V_{cb} \\ V_{td} & V_{ts} & V_{tb} \end{pmatrix} \tag{0.4}$$

where V_{CKM} is a 3×3 unitary matrix which can be parameterised by three real angles and one complex phase. The CKM matrix arises in the SM through the Higgs mechanism [6] which generates mass terms for both the fermions and the gauge vector bosons, W^+_- and Z, in a renormalisable way.

For momentum transfer much less than the vector gauge boson mass ($m_W \approx 80\ GeV$) an effective Lagrangian can be constructed as follows:

$$\mathcal{L}^{eff}_{CC} = -\frac{G_F}{\sqrt{2}} J^\dagger_\mu J^\mu \tag{0.5}$$

with

$$\frac{G_F}{\sqrt{2}} = \frac{g^2}{8\, m_W^2} \tag{0.6}$$

which corresponds to the low-energy V-A theory [7, 8, 9].

Weak Matrix Elements

Consider the semi-leptonic decay $D \to K\, l^+ \nu$, the transition amplitude is defined as follows:

$$T = \left\langle K\, l^+ \nu \,\middle|\, H_{eff} \,\middle|\, D \right\rangle \tag{0.7}$$

with

$$H_{eff} = \frac{G_F}{\sqrt{2}} J^\dagger_\mu J^\mu \tag{0.8}$$

where H_{eff} is the effective weak Hamiltonian. Factorising the leptonic and hadronic currents in Eqn. (0.7) gives

$$T = \frac{G_F}{\sqrt{2}} |V_{cs}|\, L^\dagger_\mu H^\mu \tag{0.9}$$

with

$$L_\mu = \bar{v}(l^+)\,\gamma_\mu(1-\gamma^5)\,u(\nu) \tag{0.10}$$

$$H^\mu = \left\langle K \,\middle|\, \bar{c}\,\gamma^\mu(1-\gamma^5)\,s \,\middle|\, D \right\rangle \tag{0.11}$$

where v and u are Dirac spinors and H^μ is the weak matrix element required to extract the CKM matrix element $|V_{cs}|$ from the decay rate; the leptonic matrix element L^μ follows from tree-level perturbation theory. Clearly, H^μ includes non-perturbative strong interaction effects. On the lattice this matrix element can be computed from first principles.

In recent years, a machinery has been developed for calculating weak matrix elements on the lattice [10]–[15]. The lattice is the only non-perturbative method for computing strong interaction effects which is systematically improvable. For lattice methods to gain acceptance as a useful phenomenological tool it is essential to show that systematic errors are under control. The study of D decays provides an important test of the lattice method since the relevant CKM matrix elements are well-constrained in the SM by three-generation unitarity. Furthermore, such tests give us confidence in our predictions for B decays [16]–[21] where the relevant CKM matrix elements are under-determined.

Overview

Chapter 1 begins with a brief introduction to Quantum Chromodynamics, the gauge theory which describes the strong interaction. The lattice gauge formulation is then described; this is motivated by a simple geometric interpretation of the gauge principle. Finally, the lattice machinery required to construct weak matrix elements is presented. Chapter 2 presents a lattice calculation of the light-light and heavy-light meson spectrum. These masses and the corresponding two-point amplitudes are required to extract the form factors which describe the semi-leptonic decays. Chapter 3 describes a lattice calculation of the matrix elements of the vector and axial-vector currents which are relevant for the semi-leptonic decays $D \to K$ and $D \to K^*$. The form factors describing these decays are determined and their q^2 dependence investigated, where q^μ is the four-momentum transfer. The decay rates are also computed. Finally, these results are compared with experiment and other theoretical calculations.

Chapter 1

Lattice QCD

This chapter describes the lattice formulation of QCD. At low energies QCD is non-perturbative; it is this non-perturbative nature which is expected to account for the binding of quarks into hadrons. The lattice formulation [22]-[25] provides a systematic first-principles approach to solving QCD.

1.1 QCD

Quantum Chromodynamics (QCD) is the theory of hadronic physics in which quarks interact via the exchange of gluons [26]–[28]. The early quark model (consisting of fractionally charged, spin-half particles) was successful in accounting for many of the observed symmetries in the hadron spectrum. Problems with this model (such as unobserved states) were resolved by postulating that the quarks possess a 'hidden' degree of freedom, called colour.

Each quark flavour is assumed to occur in three colours which form a triplet under a colour $SU(3)$ group. Since colour is a hidden quantity only singlet states are physically observable; and thus quarks cannot be free and must be confined within hadrons. The allowed $q\bar{q}$ and qqq states reproduce the physical spectrum of mesons and baryons respectively.

In deep inelastic scattering experiments, the hadronic constituents (the quarks) behave at short distances as if only weakly bound. Thus phenomenologically, a theory is required which exhibits both asymptotic freedom (the quark coupling decreases at short distance) and quark confinement. The fact that only non-abelian gauge theories are both asymptotically free and renormalisable [29, 30] leads us to QCD.

QCD Derived

QCD can be 'derived' by demanding that the Lagrangian density for a free quark colour triplet ψ (of four-component Dirac spinors)

$$\mathcal{L} = \bar{\psi}(x)\Big(i\gamma^{\mu}\partial_{\mu} - m\Big)\psi(x) \tag{1.1}$$

be invariant under a local $SU(3)$ symmetry transformation in which

$$\psi(x) \;\rightarrow\; \psi^{'}(x) = U(\theta)\,\psi(x) \tag{1.2}$$

$$\bar{\psi}(x) \;\rightarrow\; \bar{\psi}^{'}(x) = \bar{\psi}(x)\,U(\theta)^{-1} \tag{1.3}$$

with

$$U(\theta) = \exp\left(\frac{-i\lambda\cdot\theta(x)}{2}\right) \tag{1.4}$$

where λ^a and $\theta^a(x)$ $(a = 1, 2, \ldots, 8)$ are the generators and group parameters of $SU(3)$ respectively. The λ^as are the Gell-Mann matrices which satisfy the following commutation relation and normalisation condition:

$$\left[\frac{\lambda_a}{2}, \frac{\lambda_b}{2}\right] = i f_{abc}\frac{\lambda^c}{2} \quad , \quad Tr\left(\lambda^a\lambda^b\right) = 2\,\delta^{ab}. \tag{1.5}$$

The derivative term in Eqn. (1.1) spoils gauge invariance. By introducing vector gauge fields $A^a_{\mu}(x)$ (one gauge gluon for each generator) a gauge invariant derivative can be constructed through the minimal coupling as follows:

$$D_{\mu} = \partial_{\mu} - ig\,\frac{\lambda\cdot A_{\mu}}{2} \tag{1.6}$$

where g is the gauge coupling constant. $D_{\mu}\psi(x)$ must transform like $\psi(x)$ which implies the following symmetry transformation:

$$\frac{\lambda\cdot A_{\mu}}{2} \rightarrow \frac{\lambda\cdot A^{'}_{\mu}}{2} = U(\theta)\left(\frac{\lambda\cdot A_{\mu}}{2}\right)U(\theta)^{-1} - \frac{i}{g}\,\partial_{\mu}\Big[U(\theta)\Big]\,U(\theta)^{-1}. \tag{1.7}$$

Finally, a term involving the derivatives of the gauge fields is required to make the gluon a truly dynamical variable. The simplest gauge invariant, renormalisable term (of dimension four or less) is

$$-\frac{1}{4}\,F^a_{\mu\nu}\,F^{a\mu\nu} \tag{1.8}$$

with

$$F^a_{\mu\nu} = \partial_\mu A^a_\nu - \partial_\nu A^a_\mu + g f^{abc} A^b_\mu\, A^c_\nu\,. \tag{1.9}$$

Eqn. (1.8) contains terms which correspond to both trilinear and quadrilinear couplings of the gauge fields, A^a_μ. This self-coupling arises from the non-abelian nature of the theory in which gluons, like quarks, carry colour-charge.

Thus, the QCD Lagrangian can be written as follows:

$$\mathcal{L}_{QCD} = \sum_{k=1}^{n_f} \bar{q}_k\,(i\gamma^\mu D_\mu - m_k)\,q_k - \frac{1}{4}\,F^a_{\mu\nu}\,F^{a\mu\nu} \tag{1.10}$$

where n_f is the number of quark flavours. To satisfy phenomenological requirements, a theory of the strong interaction must exhibit both asymptotic freedom and quark confinement. QCD is asymptotically free 'by design', and it can be shown [25] (in the absence of vacuum polarisation effects) that the inter-quark potential does indeed rise linearly with increasing separation. However, these regimes may be separated by one or more discontinuous phase transitions. Thus, further numerical investigation is required to determine whether QCD allows these two necessary phenomena to coexist in a single phase.

QCD and Geometry

Like all gauge theories, QCD has a deep geometrical foundation. In this section, following Cheng and Li [2], the basic geometrical concepts required to construct a lattice gauge theory are introduced. A more complete description of the gauge principle, using the language of differential geometry, can be found in Ref. [31].

Consider two vectors which are free to move on the circumference of a circle while being held at some fixed angle to their tangent vectors. The relative 'orientation' of these vectors is dependent on their position. In a curved space, a method is required for comparing vectors which is independent of their position; and thus uniquely defined.

In a region of curved space (where the derivative of the metric is non-vanishing), a vector in moving from $x \to x + dx$ will experience a change in 'scale' (due to the change in the measure). The covariant derivative takes this scale transformation into account and is defined as follows:

$$D_\mu \psi(x) = \frac{\psi(x+dx) - [\psi(x) + \delta\psi(x)]}{dx^\mu} \tag{1.11}$$

where $\delta\psi(x)$ is the change in $\psi(x)$ in moving from $x \to x + dx$, in the μ-direction. This change is directly proportional to the vector itself, to the distance travelled, and to a mathematical construction called the 'connection' (a term involving derivatives of the metric).

Comparing Eqn. (1.6) with the general form for a covariant derivative (above) gives the following relation:

$$\delta\psi(x) = ig \left(\frac{\lambda \cdot A_\mu}{2} \right) \psi(x)\, dx^\mu \tag{1.12}$$

where the minimal coupling $ig\,(\lambda \cdot A_\mu)/2$ can be identified as the connection in charge space. Thus, the gauge principle has a geometric description in terms of a curved charge space.

A useful geometric concept is parallel transport: the 'rescaling' of a vector at every point along a path. The infinitesimal parallel transport operator is defined as follows:

$$P(x+dx, x)\, \psi(x) = \psi(x) + \delta\psi(x) \tag{1.13}$$

and using Eqns. (1.12) is given by

$$P(x+dx, x) = \left[I + ig \left(\frac{\lambda \cdot A_\mu(x)}{2} \right) dx^\mu \right] \tag{1.14}$$

where I is the identity operator. The infinitesimal parallel transport operator preserves the 'orientation' of a vector, $\psi(x)$, in moving from $x \to x + dx$.

For parallel transport over a finite interval Eqn. (1.14) is exponentiated to obtain

$$P(x^{'},x) = \exp\left\{ig\int_x^{x^{'}}\left(\frac{\lambda\cdot A_\mu(y)}{2}\right)dy^\mu\right\} \in SU(3) \tag{1.15}$$

where the line integral is ordered along the path joining x and $x^{'}$. Under parallel transport $\psi(x)$ picks up a path-dependent phase factor. Thus, for every path there is a corresponding group element. The quantity $\bar{\psi}(x^{'})\,P(x^{'},x)\,\psi(x)$ is clearly gauge invariant. From Eqns. (1.2) and (1.3) the parallel transport operator must transform as follows:

$$P(x^{'},x) \to P^{'}(x^{'},x) = U(x')\,P(x^{'},x)\,U(x)^{-1} \tag{1.16}$$

which can be shown, using Eqn. (1.14), to be consistent with the original transformation law for the minimal coupling.

Another important geometrical concept is the 'curvature tensor'. A space has non-zero curvature if a vector experiences a change under parallel transport around a closed path. This change is directly proportional to the vector itself, to the area bounded by the path, and to the curvature tensor. By considering parallel transport around an infinitesimal rectangle

$$\begin{aligned} P_\Box &= P(x,y;x,y+dy)\,P(x,y+dy;x+dx,y+dy)\times \\ &\quad P(x+dx,y+dy;x+dx,y)\,P(x+dx,y;x,y) \end{aligned} \tag{1.17}$$

and using the following matrix identity

$$e^{\lambda A}e^{\lambda B} \equiv e^{\lambda(A+B)+\frac{\lambda^2}{2}[A,B]} + O(\lambda^3) \tag{1.18}$$

it can be shown that

$$P_\Box = \exp\left\{ig\left(\frac{\lambda\cdot F_{\mu\nu}}{2}\right)dx\,dy\right\} \tag{1.19}$$

which suggests identifying $\left(\frac{\lambda\cdot F_{\mu\nu}}{2}\right)$ as the curvature tensor in charge space. From Eqn. (1.16) it is clear that parallel transport around any closed path is a gauge invariant operation.

1.2 Lattice QCD

In the Feynman path integral formalism [32] of Quantum Field Theory (QFT), the vacuum expectation value of a time-ordered product of field operators is defined in Minkowski space-time as:

$$\left\langle 0 \left| \hat{T}\left[\hat{\phi}(x_1)\cdots\hat{\phi}(x_N)\right]\right| 0 \right\rangle = \int D[\phi]\,\phi(x_1)\cdots\phi(x_N)\,e^{iS[\phi]} \tag{1.20}$$

with

$$S[\phi] = \int d^4x\,\mathcal{L}(x) \tag{1.21}$$

where the path integral, $D[\phi]$, is over all possible configurations of the field ϕ, weighted by an action, $S[\phi]$, which is expressed in terms of a Lagrangian density $\mathcal{L}(x)$.

For the path integral to be well-defined, in infinite time and volume limits, it is necessary to work in Euclidean space-time. Analytically continuing Eqn. (1.20) to imaginary time gives

$$\left\langle 0 \left| \hat{T}\left[\hat{\phi}(-ix_1^0,\vec{x}_1)\cdots\hat{\phi}(-ix_N^0,\vec{x}_N)\right]\right| 0 \right\rangle = \int D\mu[\phi]\,\phi(x_1)\cdots\phi(x_N) \tag{1.22}$$

with

$$D\mu[\phi] = \frac{D[\phi]\,e^{-S_E[\phi]}}{Z} \tag{1.23}$$

and

$$Z = \int D[\phi]\,e^{-S_E[\phi]} \tag{1.24}$$

where the probability measure, $D\mu[\phi]$, is now well-defined. The Euclidean path integral is equivalent to a statistical mechanics ensemble average with a Boltzmann factor of $\left(\frac{e^{-S_E[\phi]}}{Z}\right)$ where Z is the partition function. This equivalence allows the path integral to be computed using methods borrowed from statistical mechanics.

Lattice Field Theory

To study the long distance properties of QCD (a strong coupling regime), a non-perturbative method of evaluating the path integral is required. The lattice approach is to replace the continuum of space-time by a regular hyper-cubic lattice[1] with lattice spacing a. The integral over space-time is approximated by

$$\int d^4x \to a^4 \sum_{\vec{n}} \tag{1.25}$$

where the sum is over all lattice sites, labelled by a four-vector $\vec{n}$.

The discretisation of space-time introduces a natural cut-off on momenta which are restricted to a domain bounded by π/a; wavelengths less than twice the lattice spacing have no lattice representation. Furthermore, the introduction of periodic boundary conditions quantises the allowed values of momenta:

$$\vec{p} = \frac{2\pi}{L}\,(n_x, n_y, n_z) \tag{1.26}$$

where n_x, n_y and n_z are integers, and L is the spatial extent of the lattice. As with any cut-off prescription, there is considerable freedom in the lattice formulation. This allows the regulation of unwanted lattice artifacts by the addition of non-continuum terms to the lattice action which vanish in the continuum limit.

The physics of any renormalisable field theory should be independent of the cut-off, in this case the lattice spacing. In this regime, the correlation length of the theory should be infinite compared to the lattice spacing. In statistical mechanics, this is achieved by tuning the 'couplings' to criticality so that the correlation length diverges (this corresponds to a second order phase transition). Near criticality, the behaviour of the theory is governed by renormalisation group equations which can be used to remove finite lattice spacing effects.

On a finite lattice, field theory has a finite number of degrees of freedom and is thus amenable to computer simulation. Field configurations are generated with the correct Boltzmann distribution using a Monte Carlo procedure [33]. To recover the continuum field theory, one must establish the limit of the computer simulation as the lattice spacing $a \to 0$ and the number of lattice sites $N \to \infty$.

[1] Alternative discretisation schemes such as random lattices are not considered.

Naive Fermions

The Euclidean action for a four-component Dirac field, $\psi(x)$, is

$$S_E = \int d^4x\, \bar{\psi}(x)\Big(\gamma^\mu \partial_\mu + m\Big)\psi(x) \tag{1.27}$$

where the Euclidean γ matrices satisfy

$$\Big\{\gamma_\mu, \gamma_\nu\Big\} = 2\,\delta_{\mu\nu} \tag{1.28}$$

$$\gamma_\mu^\dagger = \gamma_\mu \tag{1.29}$$

$$\gamma_\mu = g_{\mu\nu}\gamma^\nu \tag{1.30}$$

and $g_{\mu\nu}$ is the Euclidean metric defined as:

$$g_{\mu\nu} = g^{\mu\nu} = \delta^{\mu\nu}. \tag{1.31}$$

On the lattice, the fermion field, $\psi(x)$, is replaced by fermionic variables at the sites of the lattice, $\psi(x) \to \psi_{\vec{n}}$. Replacing the derivative in Eqn. (1.27) with a central difference approximation, and the integral with a sum over lattice sites, one obtains the naive fermion action

$$S_{NF} = \sum_{\vec{n}} \left\{ \frac{a^3}{2} \sum_{\mu=1}^{4} \bar{\psi}_{\vec{n}}\, \gamma_\mu \Big(\psi_{\vec{n}+\hat{\mu}} - \psi_{\vec{n}-\hat{\mu}}\Big) + m a^4 \bar{\psi}_{\vec{n}}\, \psi_{\vec{n}} \right\} \tag{1.32}$$

where $\hat{\mu}$ is a lattice unit vector (length a), pointing in the μ direction.

The continuum limit of Eqn. (1.32) corresponds to a theory with sixteen mass-degenerate, non-interacting fermions. This can be seen by writing the action in the following matrix form:

$$S_{NF} = \bar{\psi}(x)\, M_{NF}(x,y)\, \psi(y) \tag{1.33}$$

with

$$M_{NF}(x,y) = \frac{1}{2}\sum_{\mu=1}^{4} \gamma_\mu \Big\{\delta(x+\hat{\mu},y) - \delta(x-\hat{\mu},y)\Big\} + m\,\delta(x,y) \tag{1.34}$$

where $M_{NF}(x,y)$ is the naive fermion matrix in lattice units ($a = 1$). And by taking the continuum limit of the free fermion propagator

$$M_{NF}^{-1}(x,y) = \int\limits_{BZ} \frac{d^4k}{(2\pi)^4}\, \frac{e^{ik\cdot(x-y)}}{m + i\sum_\mu \gamma_\mu \sin k_\mu} \tag{1.35}$$

where the momentum integral is over a single Brillouin zone ($-\frac{\pi}{2} \leq k_\mu < \frac{3\pi}{2}$). The continuum limit occurs when the correlation length diverges with respect to the lattice spacing. The inverse fermion mass is the only length scale in the theory which implies that the fermion mass $m \to 0$ as the lattice spacing $a \to 0$. In this limit, Eqn. (1.35) has 2^d poles (at $k_\mu = 0$ and $k_\mu = \pi$) each corresponding to an independent continuum fermion. This doubling in the number of fermion species with each dimension, d, is known as the fermion doubling problem.

Wilson Fermions

Recall from Section 1.2, there is a freedom in the lattice formulation which allows terms to be added to the action which vanish in the continuum limit. Wilson [34] suggested modifying Eqn. (1.32) by adding the following non-local term:

$$\Delta\mathcal{L} = -\frac{r}{2a} \sum_{\mu=1}^{4} \bar{\psi}_{\vec{n}} \Big(\psi_{\vec{n}+\hat{\mu}} + \psi_{\vec{n}-\hat{\mu}} - 2\,\psi_{\vec{n}} \Big) \tag{1.36}$$

where r is the dimensionless Wilson parameter. The Wilson fermion action

$$\begin{aligned} S_{WF} \;=\; \sum_{\vec{n}} \frac{a^3}{2} \Bigg\{ -\sum_{\mu=1}^{4} \bar{\psi}_{\vec{n}} \Big[(r-\gamma_\mu)\,\psi_{\vec{n}+\hat{\mu}} \\ + (r+\gamma_\mu)\,\psi_{\vec{n}-\hat{\mu}} \Big] + (2ma + 8r)\,\bar{\psi}_{\vec{n}}\,\psi_{\vec{n}} \Bigg\} \end{aligned} \tag{1.37}$$

corresponds to a free fermion propagator

$$M_{WF}^{-1}(x,y) = \int\limits_{BZ} \frac{d^4k}{(2\pi)^4}\, \frac{e^{ik\cdot(x-y)}}{m + \sum_\mu \{\, i\gamma_\mu \sin(k_\mu) + r\,[\,1 - \cos(k_\mu)\,]\,\}} \tag{1.38}$$

with only a single pole (at $k_\mu = 0$) in the continuum limit. On the lattice, the extra fermion species acquire a mass of $O(r/a)$ and thus decouple from the low energy behaviour of the theory in the continuum.

The Wilson fermion matrix is usually written in the following parameterisation:

$$M_{WF}(x,y) = \frac{1}{2\kappa}\left\{\delta(x,y) - \kappa\, D\!\!\!/(x,y)\right\} \tag{1.39}$$

with

$$D\!\!\!/(x,y) = \sum_{\mu=1}^{4}\left\{(r-\gamma^\mu)\,\delta(x+\vec{\mu},y) + (r+\gamma^\mu)\,\delta(x-\hat{\mu},y)\right\} \tag{1.40}$$

where κ is the hopping parameter. The bare quark mass is given by

$$m = \frac{1}{2}\left(\frac{1}{\kappa} - \frac{1}{\kappa_c}\right) \tag{1.41}$$

where κ_c is the value of the hopping parameter corresponding to zero quark mass; for free Wilson fermions $\kappa_c = 1/8\,r$.

Lattice Gauge Theory

Discretising a gauge theory by replacing the continuum gauge fields, $A^\mu(x)$, by gauge variables at the sites of the lattice, $A^\mu(x) \to A^\mu_{\hat{n}}$, breaks gauge symmetry. This would necessitate establishing its restoration in the continuum limit. Wilson [35] introduced the following formulation in which the gauge fields are represented by elements of the $SU(3)$ gauge group.

Recall from Section 1.1, a field $\psi(x)$ picks up the following path-dependent phase factor under parallel transport from x to x':

$$U(x',x) = \exp\left\{ig\int_x^{x'} A_\mu(y)\,dy^\mu\right\} \tag{1.42}$$

with

$$A_\mu = \frac{\lambda\cdot A_\mu}{2} \tag{1.43}$$

and that every path can be associated with an $SU(3)$ group element. On the lattice, Wilson introduced the *link variable* defined as:

$$U(\vec{n}+\hat{\mu},\vec{n}\,) \equiv U^\dagger(\vec{n},\vec{n}+\hat{\mu}) \in SU(3) \tag{1.44}$$

which represents parallel transport between nearest-neighbour sites, from $\vec{n}$ to

$\vec{n}+\hat{\mu}$. The relation between these link variables and the gauge fields, $A^{\mu}(x)$, is given by

$$U(\vec{n}+\hat{\mu},\vec{n}\,) = 1 + iga\,A_{\mu}\,(\vec{n}+\hat{\mu}/2) + O(a^2) \tag{1.45}$$

where the mid-point rule is used to approximate the line integral in Eqn. (1.42). The phase factor associated with parallel transport across the lattice is the path-ordered product of link variables traversed.

Wilson Quark Action

Consider a local $SU(3)$ symmetry transformation, at the lattice sites, in which

$$\psi_{\vec{n}} \;\rightarrow\; \psi'_{\vec{n}} = \Theta_{\vec{n}}\,\psi_{\vec{n}} \tag{1.46}$$

$$\bar{\psi}_{\vec{n}} \;\rightarrow\; \bar{\psi}'_{\vec{n}} = \bar{\psi}_{\vec{n}}\,\Theta^{\dagger}_{\vec{n}} \tag{1.47}$$

and following Eqn. (1.16)

$$U(\vec{n}+\hat{\mu},\vec{n}\,) \rightarrow U'(\vec{n}+\hat{\mu},\vec{n}\,) = \Theta_{\vec{n}+\hat{\mu}}\,U(\vec{n}+\hat{\mu},\vec{n}\,)\,\Theta^{\dagger}_{\vec{n}} \tag{1.48}$$

where $\Theta_{\vec{n}} \in SU(3)$. Clearly the quantity $\bar{\psi}_{\vec{n}+\mu}\,U(\vec{n}+\hat{\mu},\vec{n}\,)\,\psi_{\vec{n}}$ is gauge invariant as in the continuum. This suggests inserting link variables between non-local terms in Eqn. (1.37) to obtain the Wilson 'quark' action

$$\begin{aligned} S_Q \;=\; \sum_{\vec{n}} \frac{a^3}{2}\Bigg\{ -\sum_{\mu=1}^{4} \bar{\psi}_{\vec{n}}\Big[(r-\gamma_{\mu})\,U(\vec{n},\vec{n}+\hat{\mu})\,\psi_{\vec{n}+\hat{\mu}} & \qquad (1.49) \\ + (r+\gamma_{\mu})\,U(\vec{n},\vec{n}-\hat{\mu})\,\psi_{\vec{n}-\hat{\mu}}\Big] + \frac{1}{\kappa}\,\bar{\psi}_{\vec{n}}\,\psi_{\vec{n}} \Bigg\} & \end{aligned}$$

which is gauge invariant under a local $SU(3)$ symmetry transformation. Substituting Eqn. (1.45) into this action gives

$$S_Q = \int d^4x \left\{ \bar{\psi}(x)\left(\gamma^{\mu}D_{\mu} + m\right)\psi(x) + O(a) \right\} \tag{1.50}$$

which corresponds to the continuum action with a discretisation error of $O(a)$.

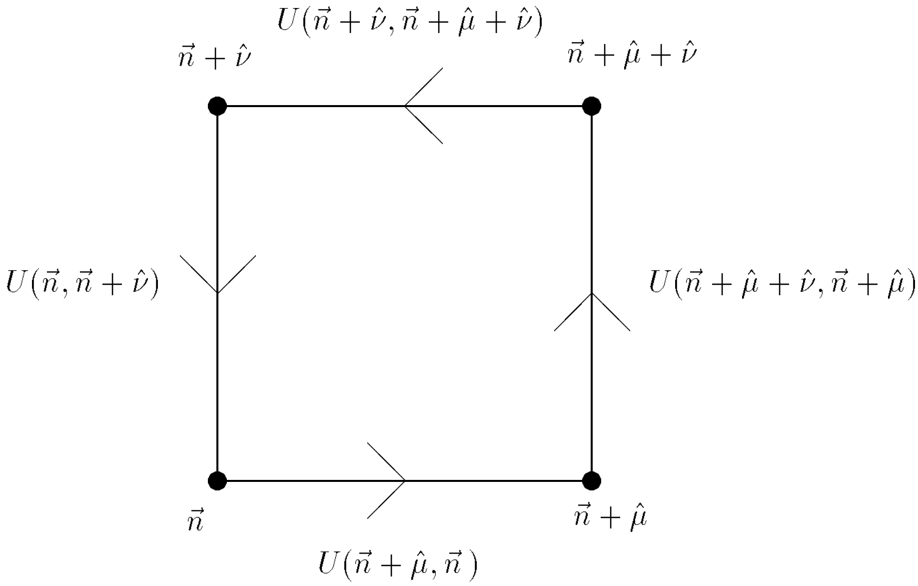

Figure 1.1: The plaquette, $\Box_{\mu\nu}(\vec{n}\,)$, in the μ–ν plane.

Pure Gauge Action

In the lattice QCD action, the dynamical gluon term must be some gauge-invariant combination of link variables. Recall from Section 1.1, parallel transport around an infinitesimal closed path is proportional to the field strength tensor, $F_{\mu\nu}$, and that the trace of this quantity is gauge invariant. This lead Wilson to suggest the following pure gauge action:

$$S_G = -\frac{1}{g^2}\sum_{\vec{n},\,\mu<\nu} Tr\left[\Box_{\mu\nu}(\vec{n}\,) + \Box^{\dagger}_{\mu\nu}(\vec{n}\,)\right] \tag{1.51}$$

with

$$\begin{aligned}\Box_{\mu\nu}(\vec{n}\,) &= U(\vec{n},\vec{n}+\hat{\nu})\,U(\vec{n}+\hat{\nu},\vec{n}+\hat{\mu}+\hat{\nu})\,\times \\ &\quad U(\vec{n}+\hat{\mu}+\hat{\nu},\vec{n}+\hat{\mu})\,U(\vec{n}+\hat{\mu},\vec{n}\,)\end{aligned} \tag{1.52}$$

where $\Box_{\mu\nu}(\vec{n}\,)$ is the product of link variables around an elementary square in the μ–ν plane, called a plaquette. The plaquette is shown in Figure 1.1.

Luscher and Weisz [36] showed that Eqn. (1.51) gives

$$S_G = \int d^4x \left\{ \frac{1}{4} F_{\mu\nu} F^{\mu\nu} + O(a^2) \right\} \tag{1.53}$$

which corresponds to the continuum action with a discretisation error of $O(a^2)$. The Wilson pure gauge action is usually written in the following parameterisation:

$$S_G = \beta \sum_{\vec{n},\, \mu<\nu} \left[1 - \frac{1}{N} Re\, Tr\, \Box_{\mu\nu}(\vec{n}\,) \right] \tag{1.54}$$

with

$$\beta = \frac{2\,N}{g^2} \tag{1.55}$$

where N is the dimension of the $SU(N)$ gauge group.

1.3 Improved Actions

In a lattice calculation there are two sources of systematic error: finite lattice spacing errors ($a > 0$), and finite lattice volume errors ($L < \infty$). The error associated with the lattice spacing can be significantly reduced by removing the lowest-order discretisation terms from the lattice action. The finite volume effects can be minimised by working on a sufficiently large lattice: $L \gg 1/M$ where M is the inverse length scale associated with the problem. This section describes several 'improved' actions.

Wilson Action

The Wilson quark and pure gauge actions, given by Eqns. (1.49) and (1.54), have discretisation errors of $O(a)$ and $O(a^2)$ respectively. The Wilson QCD action is given by

$$S^W_{QCD} = S_Q + S_G \tag{1.56}$$

which differs from the continuum action by a leading discretisation term of $O(a)$.

Recall from Section 1.2, the Wilson fermion action was constructed by adding a term to the naive action to avoid the fermion doubling problem. Further terms can be added (so long as they vanish in the continuum) to try and reduce the discretisation error introduced by the Wilson term.

Two-Link Action

Hamber and Wu [37] suggested adding the following 'two-link' term:

$$\Delta S^{II} = a^4 \sum_{\vec{n},\,\mu} + \frac{r}{8a}\,\bar{\psi}_{\vec{n}} \Big\{ U(\vec{n},\vec{n}+\hat{\mu})\,U(\vec{n}+\hat{\mu},\vec{n}+2\hat{\mu})\,\psi_{\vec{n}+2\hat{\mu}} + U(\vec{n},\vec{n}-\hat{\mu})\,U(\vec{n}-\hat{\mu},\vec{n}-2\hat{\mu})\,\psi_{\vec{n}-2\hat{\mu}} - 2\,\psi_{\vec{n}} \Big\} \tag{1.57}$$

which cancels the $O(a)$ term in the Wilson action. The Two-Link action is

$$S^{II}_{QCD} = S_Q + S_G + \Delta S^{II} \tag{1.58}$$

which differs from the continuum action by terms of $O(a^2)$ at tree level. Heatlie *et al.* have argued [39] that correlation functions computed with the Two-Link action have no discretisation errors of $O(a)$ or $O(\alpha_s^n a \log^n a)$, to all orders in perturbation theory. Unfortunately, the Two-Link term is difficult to implement on a parallel machine because it requires next-to-nearest-neighbour communications.

Sheikholeslami-Wohlert Action

Sheikholeslami and Wohlert [38] proposed the following nearest-neighbour action:

$$S^{SW}_{QCD} = S_Q + S_G + \Delta S^{SW} \tag{1.59}$$

with

$$\Delta S^{SW} = a^4 \sum_{\vec{n},\,\mu,\,\nu} -ig\,\frac{ar}{4}\bar{\psi}_{\vec{n}}\,\sigma_{\mu\nu} P^{\mu\nu}_{\vec{n}}\,\psi_{\vec{n}} \tag{1.60}$$

and

$$\sigma_{\mu\nu} = \frac{1}{2}\Big[\gamma_\mu, \gamma_\nu\Big] \tag{1.61}$$

where $P^{\mu\nu}_{\vec{n}}$ is an appropriate lattice definition of the field strength tensor, $F^{\mu\nu}$. Mandula [40] suggested the following choice of lattice operator:

$$P^{\mu\nu}_{\vec{n}} = \frac{1}{4}\sum_{\square=1}^{4} \frac{1}{2\,iga^2}\Big[\square_{\mu\nu}(\vec{n}\,) - \square^{\dagger}_{\mu\nu}(\vec{n}\,)\Big] \tag{1.62}$$

where the sum is over the four plaquettes, at site $\vec{n}$, lying in the $\mu\!-\!\nu$ plane. The lattice operator $P^{\mu\nu}_{\vec{n}}$ is depicted in Figure 1.2.

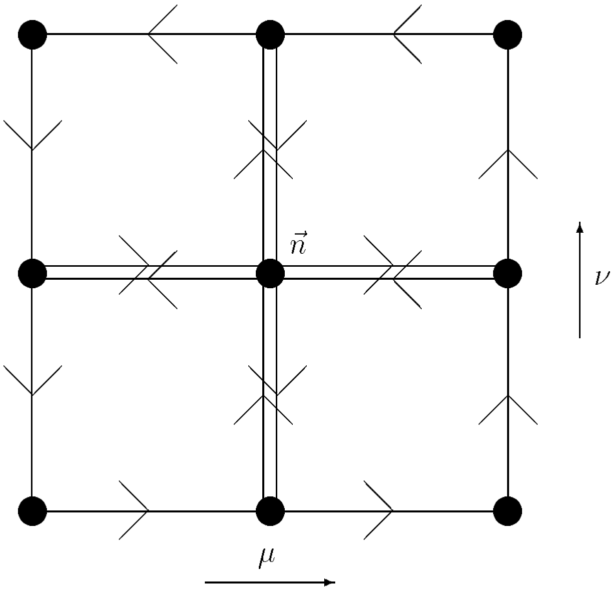

Figure 1.2: The lattice operator $P^{\mu\nu}_{\vec{n}}$.

The Sheikholeslami-Wohlert (SW) action is related to the Two-Link action by the following rotation of the quark fields:

$$\psi_{\vec{n}} \quad \to \quad \psi'_{\vec{n}} = \left[1 - a\frac{r}{4}\left(\overrightarrow{\not{D}} - m\right)\right]\psi_{\vec{n}} + O(a^2) \tag{1.63}$$

$$\bar{\psi}_{\vec{n}} \quad \to \quad \bar{\psi}'_{\vec{n}} = \bar{\psi}_{\vec{n}}\left[1 + a\frac{r}{4}\left(\overleftarrow{\not{D}} + m\right)\right] + O(a^2) \tag{1.64}$$

where the *forward* and *backward* lattice derivatives are given by

$$\overrightarrow{D}_\mu\psi_{\vec{n}} \quad = \quad \frac{1}{2a}\Big[U(\vec{n},\vec{n}+\hat{\mu})\,\psi_{\vec{n}+\hat{\mu}} - U(\vec{n},\vec{n}-\hat{\mu})\,\psi_{\vec{n}-\hat{\mu}}\Big] \tag{1.65}$$

$$\bar{\psi}_{\vec{n}}\overleftarrow{D}_\mu \quad = \quad \frac{1}{2a}\Big[\bar{\psi}_{\vec{n}+\hat{\mu}}\,U(\vec{n}+\hat{\mu},\vec{n}\,) - \bar{\psi}_{\vec{n}-\hat{\mu}}\,U(\vec{n}-\hat{\mu},\vec{n}\,)\Big]. \tag{1.66}$$

These rotations simply constitute a change of variable in the functional integral; and thus results concerning the discretisation errors for the Two-Link action also hold for the SW action. The advantage of using the SW action is that it is nearest-neighbour and can therefore be implemented efficiently on a parallel machine.

Finally, to obtain matrix elements which are $O(a)$-improved, 'improved' operators must be used when computing correlation functions with the SW action. For the following bilinear fermion operators:

$$\hat{O}_\Gamma = \bar{\psi}(x)\,\Gamma\,\psi(x) \tag{1.67}$$

where Γ is any Dirac matrix, the quark fields must be rotated using Eqns. (1.63) and (1.64). For on-shell hadronic matrix elements these rotations simplify to give

$$\psi_{\vec{n}} \quad \rightarrow \quad \psi'_{\vec{n}} = \left(1 - a\frac{r}{2}\overrightarrow{\not{D}}\right)\psi_{\vec{n}} + O(a^2) \tag{1.68}$$

$$\bar{\psi}_{\vec{n}} \quad \rightarrow \quad \bar{\psi}'_{\vec{n}} = \bar{\psi}_{\vec{n}}\left(1 + a\frac{r}{2}\overleftarrow{\not{D}}\right) + O(a^2)\,. \tag{1.69}$$

1.4 Lattice Simulations

On the lattice, particle masses and matrix elements are extracted from correlation functions. These correlators are constructed from quark propagators computed for a fixed number of gauge configurations. The quark propagator is the basic building block in lattice QCD. This section describes how to compute the quark propagator for both local and smeared sources.

Quark Propagator

In QFT the quark propagator is defined as follows:

$$G^{(2)\,ij}_{\alpha\beta}(x,y) \equiv \left\langle\, 0 \left| \psi^i_\alpha(x)\,\bar{\psi}^j_\beta(y) \right| 0 \,\right\rangle = -\left\langle\, 0 \left| \bar{\psi}^j_\beta(y)\,\psi^i_\alpha(x) \right| 0 \,\right\rangle \tag{1.70}$$

where the Greek and Latin indices denote the spin and colour components of the quark fields respectively. In Euclidean space, using the Feynman path integral formalism, Eqn. (1.70) is given by

$$\left\langle\, \psi(x)\,\bar{\psi}(y)\,\right\rangle = \frac{1}{Z}\int D[\mathcal{U}\,]\,D\big[\psi,\bar{\psi}\big]\,\psi(x)\,\bar{\psi}(y)\,e^{-\bar{\psi}\,M_F\,\psi\,-\,S_G} \tag{1.71}$$

where M_F is the fermion matrix, S_G is the pure gauge action and Z is the partition function.

The quark fields in Eqn. (1.71) are Grassmann variables which are difficult to simulate on a computer. Fortunately, the fermionic path integral can be performed analytically to give

$$\left\langle \psi(x)\,\bar{\psi}(y) \right\rangle = \frac{1}{Z} \int D[\,\mathcal{U}\,]\; M_F^{-1}(x,y)\,\det[M_F]\, e^{-\,S_G} \tag{1.72}$$

where $M_F^{-1}(x,y)$ is the inverse of the fermion matrix.

The Monte Carlo estimate of Eqn. (1.72) is given by

$$\left\langle \psi(x)\,\bar{\psi}(y) \right\rangle \simeq \frac{1}{N} \sum_{i=1}^{N} M_F^{-1}(x,y;\mathcal{U}_i\,) \tag{1.73}$$

where $\mathcal{U}_i$ is a statistically independent sample of N gauge configurations generated with the following probability distribution

$$\frac{1}{Z}\, D[\,\mathcal{U}\,]\,\det[M_F]\, e^{-\,S_G}\,. \tag{1.74}$$

Quenched Approximation

The determinant in Eqn. (1.74) connects all lattice sites, and is computed at all stages in the gauge configuration generation algorithm. In the quenched approximation, gauge configurations are computed with $\det[M_F]$ equal to a constant which corresponds to the omission of internal quark loops. Quenched configurations are cheaper to compute, and easier to implement efficiently on a parallel machine. However, there is little physical justification for this procedure which may introduce a significant systematic error.

Fermion Matrix Inversion

The quark propagator is computed using iterative methods [41] to solve linear equations of the form

$$M^{ij}_{\alpha\beta}(x,y;\mathcal{U})\,\psi^j_\beta(y;\mathcal{U}) = \eta^i_\alpha(x) \tag{1.75}$$

with

$$\eta^i_\alpha(x) = \delta_{\alpha\gamma}\,\delta^{ik}\delta(x,0) \tag{1.76}$$

where $\psi^j_\beta(y;\mathcal{U})$ is a fermion vector. In practise, $\psi^j_\beta(y;\mathcal{U})$ is computed for all spin-colour combinations of the point source, $\eta^i_\alpha(x)$. These twelve spin-colour components correspond to the quark propagator, $Q^{jk}_{\beta\gamma}(y,0;\mathcal{U})$, which describes the propagation of a quark from a fixed origin.

Smeared Sources

The Wuppertal group [42] suggested using a source with finite spatial-extent. This 'smeared' source is given by the solution of the three-dimensional Klein-Gordon equation

$$K(\vec{x},\vec{y}\,)\,S(\vec{y},0) = \delta(\vec{x},0) \tag{1.77}$$

with

$$K(\vec{x},\vec{y}\,) = \delta(\vec{x},\vec{y}\,) - \kappa_s\, D^2_s\,(\vec{x},\vec{y}\,) \tag{1.78}$$

and

$$D^2_s\,(\vec{x},\vec{y}\,) = \sum_{\mu=1}^{3}\left\{U(\vec{x},\ \vec{x}+\hat{\mu})\,\delta(\vec{x}+\hat{\mu},\vec{y}) \ +\ U(\vec{x},\ \vec{x}-\hat{\mu})\,\delta(\vec{x}-\hat{\mu},\vec{y})\right\} \tag{1.79}$$

which corresponds to the spatial propagator of a scalar colour particle.

The N^{th} approximation to the solution $S(\vec{x},0)$ is given by

$$S^N(\vec{x},0) = \delta(\vec{x},0) + \kappa_s\, D^2_s\,(\vec{x},\vec{y}\,)\,S^{(N-1)}(\vec{y},0) \tag{1.80}$$

with

$$S^{\,0}(\vec{x},0) = \delta(\vec{x},0) \tag{1.81}$$

which is known as Jacobi Smearing. The Wuppertal smearing function is gauge invariant.

1.5 Two-Point Functions

On the lattice, particle masses are extracted by studying the time-dependence of two-point functions. These correlation functions can be constructed from quark propagators computed for a fixed origin. This section describes how to construct two-point functions corresponding to both pseudoscalar and vector mesons.

Interpolating Operators

In QFT, there is no unique correspondence between particles and fields. Instead, correlation functions are constructed from time-ordered products of field operators, selected to represent the particles. A necessary requirement for such an interpolating operator is

$$\left\langle 0 \middle| \Omega(0) \middle| A, \vec{p} \right\rangle \neq 0 \tag{1.82}$$

where the field operator, Ω, has a non-zero overlap with the single-particle state in question, $A(\vec{p})$. A practical criterion for choosing Ω is that this overlap be maximised[2] while couplings to radial excitations are minimised.

For mesons, this suggests that Ω be a colour singlet with the same spin, parity and valence quark content as the particle of interest. The most general form for a meson interpolating operator is

$$\Omega_M(x) = \int dy\, dz\ \bar{q}_{1\,\alpha}^{\,i}(y)\, \phi^{ij}(x; y, z)\, \Gamma_{\alpha\beta}\, q_{2\,\beta}^{\,j}(z) \tag{1.83}$$

where q_1 and q_2 are different flavour valence quarks with colour indices i and j, and Γ is the Dirac matrix with the correct spin and parity properties. The simplest choice for ϕ is given by

$$\phi^{ij}(x; y, z) = \delta(x, y)\, \delta(x, z)\, \delta^{ij} \tag{1.84}$$

which corresponds to a point meson.

Meson Two-Point Functions

The two-point function describing the propagation of a meson, from a fixed origin with momentum $\vec{p}$, is defined as follows:

$$G_M^{(2)}(t, 0; \vec{p}\,) = \sum_{\vec{x}} e^{i\vec{p}\cdot\vec{x}} \left\langle 0 \middle| \hat{T} \left\{ \Omega_M(x)\, \Omega_M^\dagger(0) \right\} \middle| 0 \right\rangle \tag{1.85}$$

where Ω_M and $\Omega_M^\dagger$ are the meson annihilation and creation operators respectively. Periodic boundary conditions (in the spatial dimensions) quantise the allowed

[2] To extract matrix elements, a good signal-to-noise ratio is required.

values of lattice momenta as follows:

$$\vec{p} = \frac{2\pi}{L}\,(p_1, p_2, p_3) \tag{1.86}$$

where p_1, p_2 and p_3 are integers.

Pseudoscalar Two-Point Functions

Taking $\Gamma = \gamma^5$ in Eqn. (1.83) gives the following pseudoscalar operators:

$$\hat{P}(x) \;=\; \bar{h}(x)\,\gamma^5\,l(x) \tag{1.87}$$

$$\hat{P}^\dagger(x) \;=\; -\bar{l}(x)\,\gamma^5\,h(x) \tag{1.88}$$

where the flavour notation h and l is used to denote a 'heavy' and 'light' quark respectively. Substituting these operators into Eqn. (1.85) one obtains the heavy-light pseudoscalar two-point function

$$G_P^{(2)}(t,0;\vec{p}\,) = -\sum_{\vec{x}} e^{i\frac{2\pi}{L}\vec{p}\cdot\vec{x}} \left\langle 0 \middle| \hat{T}\left\{ \bar{h}^i_\alpha(x)\,\gamma^5_{\alpha\beta}\,l^i_\beta(x)\;\bar{l}^j_\gamma(0)\,\gamma^5_{\gamma\delta}\,h^j_\delta(0)\right\} \middle| 0 \right\rangle . \tag{1.89}$$

The time-ordered product of field operators in Eqn. (1.89) is related by Wick's theorem [43] to the following product of quark propagators

$$\hat{T}\left\{\cdots\right\} \to \left\langle 0 \middle| \bar{h}^i_\alpha(x)\,h^j_\delta(0) \middle| 0 \right\rangle \left\langle 0 \middle| l^i_\beta(x)\,\bar{l}^j_\gamma(0) \middle| 0 \right\rangle \gamma^5_{\alpha\beta}\,\gamma^5_{\gamma\delta} + \cdots \tag{1.90}$$

where terms with zero vacuum-expectation-value simply vanish. Using Eqn. (1.70) and the following hermiticity property of the lattice quark propagator

$$Q^\dagger_{\alpha\beta}(x,0;\mathcal{U}) = \gamma^5_{\alpha\gamma}\,Q_{\gamma\delta}(0,x;\mathcal{U})\,\gamma^5_{\delta\beta} \tag{1.91}$$

one obtains the heavy-light pseudoscalar correlator in terms of quark propagators

$$G_P^{(2)}(t,0;\vec{p}\,) = \sum_{\vec{x}} e^{i\frac{2\pi}{L}\vec{p}\cdot\vec{x}} \left\langle \,Tr\Big[\,H^\dagger(x,0;\mathcal{U})\,L(x,0;\mathcal{U})\Big]\, \right\rangle \tag{1.92}$$

where the trace is over both spin and colour, and $\left\langle\cdots\right\rangle$ denotes an average over gauge configurations, $\mathcal{U}$. The 'H'-eavy and 'L'-ight propagators in Eqn. (1.92) are both computed for a fixed origin.

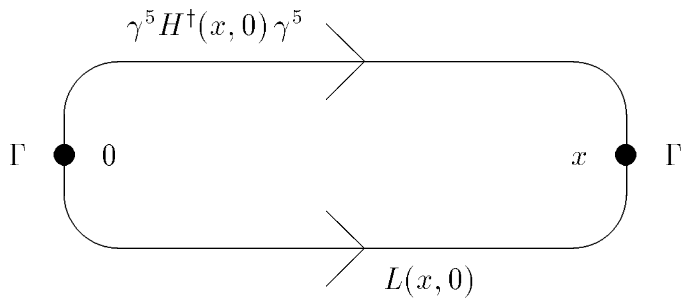

Figure 1.3: The heavy-light meson correlator.

Vector Two-Point Functions

Taking $\Gamma = \gamma^\mu$ in Eqn. (1.83) gives the following vector operators:

$$\hat{V}^\mu(x) = \bar{h}(x)\,\gamma^\mu\, l(x) \tag{1.93}$$
$$\hat{V}^{\mu\dagger}(x) = -\bar{l}(x)\,\gamma^\mu\, h(x)\,. \tag{1.94}$$

Substituting these operators into Eqn. (1.85) one obtains the following heavy-light vector correlator in terms of quark propagators

$$G_V^{(2)\,\mu\nu}(t,0;\vec{p}) = \sum_{\vec{x}} e^{i\frac{2\pi}{L}\vec{p}\cdot\vec{x}} \left\langle Tr\Big[\gamma^\mu\gamma^5\, H^\dagger(x,0;\mathcal{U})\,\gamma^5\gamma^\nu\, L(x,0;\mathcal{U})\Big]\right\rangle \tag{1.95}$$

where the trace is over both spin and colour, and $\langle \cdots \rangle$ denotes an average over gauge configurations, $\mathcal{U}$. The 'H'-eavy and 'L'-ight propagators in Eqn. (1.95) are both computed for a fixed origin. Figure 1.3 shows a heavy-light meson correlator constructed from quark propagators.

1.6 Meson Masses

At large Euclidean times, meson correlation functions have a simple analytic form which can be parameterised by an overall normalisation factor and the mass of the corresponding particle. This section describes the time-dependence of both pseudoscalar and vector meson correlators, given in Section 1.5.

Meson Correlators

Inserting a complete set of states in Eqn. (1.85) gives

$$G_M^{(2)}(t,0;\vec{p}\,) = \frac{1}{L^3}\sum_{\vec{x},\,S,\,\vec{q}} \frac{e^{i\frac{2\pi}{L}\vec{p}\cdot\vec{x}}}{2a\,E_S(\vec{q}\,)} \left\langle 0 \,\middle|\, \Omega_M(x) \,\middle|\, S,\,\vec{q}\,\right\rangle \left\langle S,\,\vec{q} \,\middle|\, \Omega_M^\dagger(0) \,\middle|\, 0 \right\rangle \tag{1.96}$$

with the lattice completeness relation defined as follows:

$$I \equiv \frac{1}{L^3}\sum_{S,\,\vec{p}} \frac{1}{2a\,E_S(\vec{p}\,)} \left|\, S,\,\vec{p}\,\right\rangle \left\langle S,\,\vec{p}\,\right| + \cdots \tag{1.97}$$

where the sum S is over all single-particle states; the omitted terms correspond to multi-particle states.

Under the following symmetry transformation

$$\Omega_M(x) \to \Omega_M'(x) = e^{+\hat{X}(x)}\,\Omega_M(0)\,e^{-\hat{X}(x)} \tag{1.98}$$

with

$$\hat{X} = a\hat{H}t + i\frac{2\pi}{L}\hat{p}\cdot\vec{x} \tag{1.99}$$

where $\hat{H}$ and $\hat{p}$ are the lattice Hamiltonian and the three-momentum operator respectively. These operators act on adjacent states in Eqn. (1.96) to give

$$\begin{aligned} G_M^{(2)}(t,0;\vec{p}\,) \;&=\; \frac{1}{L^3}\sum_{\vec{x},\,S,\,\vec{q}} \frac{e^{i\frac{2\pi}{L}(\vec{p}-\vec{q}\,)\cdot\vec{x}}\,e^{-aE_S(\vec{q}\,)t}}{2a\,E_S(\vec{q}\,)} \\ &\times\; \left\langle 0 \,\middle|\, \Omega_M(0) \,\middle|\, S,\,\vec{q}\,\right\rangle \left\langle S,\,\vec{q} \,\middle|\, \Omega_M^\dagger(0) \,\middle|\, 0 \right\rangle . \end{aligned} \tag{1.100}$$

Finally, using the definition of the lattice delta function

$$\delta(\vec{p},\,\vec{q}\,) \equiv \frac{1}{L^3}\sum_{\vec{x}} e^{i\frac{2\pi}{L}(\vec{p}-\vec{q}\,)\cdot\vec{x}} \tag{1.101}$$

one obtains the following expression for the meson correlator

$$C_M(t;\vec{p}\,) = \sum_S \frac{e^{-aE_S(\vec{p}\,)t}}{2a\,E_S(\vec{p}\,)} \times \left| \left\langle 0 \,\middle|\, \Omega_M(0) \,\middle|\, S,\,\vec{p}\,\right\rangle \right|^2 \tag{1.102}$$

where there is now an explicit time-dependence. The only non-zero contribution to this sum are the ground state meson and its excitations. These higher-energy excitations fall off exponentially compared to the ground state which gives the dominant contribution as $t \to \infty$.

Pseudoscalar Correlator

At large Euclidean times, the pseudoscalar meson correlator is given by

$$C_P(t;\vec{p}\,) \underset{t \to \infty}{\Longrightarrow} \frac{e^{-aE_P(\vec{p}\,)t}}{2a\,E_P(\vec{p}\,)} \times \left| Z_P(\vec{p}\,) \right|^2 \tag{1.103}$$

with

$$Z_P(\vec{p}\,) \equiv \left\langle 0 \left| \hat{P}(0) \right| P,\, \vec{p}\, \right\rangle \tag{1.104}$$

where E_P is the energy of the pseudoscalar meson with lattice three-momentum $\vec{p}$, and Z_P is the corresponding two-point amplitude. This amplitude measures the overlap of the interpolating operator $\hat{P}$ with the pseudoscalar meson state, P.

Vector Correlator

At large Euclidean times, the vector meson correlator is given by

$$\begin{aligned} C_V^{\mu\nu}(t;\vec{p}\,) \underset{t \to \infty}{\Longrightarrow} & \sum_{r=1}^{3} \frac{e^{-aE_V(\vec{p}\,)t}}{2a\,E_V(\vec{p}\,)} \\ & \times \left\langle 0 \left| \hat{V}^\mu(0) \right| V_r,\, \vec{p}\, \right\rangle \left\langle V_r,\, \vec{p} \left| \hat{V}^{\nu\dagger}(0) \right| 0 \right\rangle \end{aligned} \tag{1.105}$$

where E_V is the energy of the vector meson with lattice three-momentum $\vec{p}$. The vector correlator is slightly more complicated than the pseudoscalar case because Eqn (1.105) contains an additional sum over polarisation states, r.

Writing the vector amplitude with an explicit *polarisation vector* as follows:

$$\left\langle 0 \left| \hat{V}^\mu(0) \right| V_r,\, \vec{p}\, \right\rangle \equiv \xi_r^\mu(\vec{p}\,)\, Z_V(\vec{p}\,) \tag{1.106}$$

where Z_V is the vector meson two-point amplitude; and using the following *polarisation sum* identity for a massive vector particle

$$\sum_{r=1}^{3} \xi_r^\mu(\vec{p}\,)\,\xi_r^\nu(\vec{p}\,) \equiv -g^{\mu\nu} + \frac{p^\mu p^\nu}{m^2} \tag{1.107}$$

one obtains the following form for the vector meson correlator

$$C_V^{\mu\nu}(t;\vec{p}\,) = \left(-g^{\mu\nu} + \frac{p^\mu p^\nu}{m^2}\right) \frac{e^{-aE_V(\vec{p}\,)t}}{2a\,E_V(\vec{p}\,)} \times \left|\,Z_V(\vec{p}\,)\,\right|^2. \tag{1.108}$$

Contracting Eqn. (1.108) with the Euclidean metric, and using the *on-shell* condition $p^\mu p_\mu \equiv m^2$, one obtains the *polarisation-averaged* vector meson correlator

$$C_V(t;\vec{p}\,) \underset{t\to\infty}{\Longrightarrow} -3 \times \frac{e^{-aE_V(\vec{p}\,)t}}{2a\,E_V(\vec{p}\,)} \times \left|\,Z_V(\vec{p}\,)\,\right|^2 \tag{1.109}$$

which differs in form from the pseudoscalar correlator, given by Eqn. (1.103), by a simple factor of (minus) 3. This factor corresponds to the three polarisation states of the vector particle.

1.7 Three-Point Functions

On the lattice, matrix elements are extracted by studying the time-dependence of correlation functions. This section describes how to construct three-point functions corresponding to the semi-leptonic decay of both pseudoscalar and vector heavy-light mesons into pseudoscalar mesons.

Three-Point Functions

The three-point function describing the semi-leptonic decay of meson A into meson B is defined as follows:

$$G^{(3)}_{A\to B}(t_y,t_x,0;\vec{p},\vec{q}\,) = \sum_{\vec{x},\vec{y}} e^{i\frac{2\pi}{L}\vec{q}\cdot\vec{x}}\, e^{i\frac{2\pi}{L}\vec{p}\cdot\vec{y}} \left\langle\, 0 \,\middle|\, \hat{T}\left\{B(y)\,J(x)\,A^\dagger(0)\right\} \middle|\, 0 \,\right\rangle \tag{1.110}$$

where $A^\dagger$ and B are the meson creation and annihilation operators respectively, and J is the weak current operator. In Eqn. (1.110) the outgoing meson, B, has lattice three-momentum $\vec{p}$, and $\vec{q}$ is the momentum-recoil from the weak decay. The incoming meson, A, has lattice three-momentum $(\vec{p}+\vec{q}\,)$.

The semi-leptonic decay of a heavy-light meson proceeds as follows: the heavy quark decays into a 'lighter' quark via the weak interaction; and independently of the light quark, l. This suggests the following weak current operator

$$J_W^\mu(x) = \bar{h}'(x)\,\Lambda^\mu\,h(x) \tag{1.111}$$

with

$$\Lambda^\mu = \gamma^\mu\,(1-\gamma^5) \tag{1.112}$$

where h' and h denote two distinct 'heavy' quark flavours. Following Section 1.5, the meson operators are given by

$$A^\dagger(x) \;=\; -\bar{l}(x)\,\Gamma^\nu h'(x) \tag{1.113}$$

$$B(x) \;=\; \bar{h}(x)\,\gamma^5\,l(x) \tag{1.114}$$

where B is the interpolating operator to annihilate a heavy-light pseudoscalar meson. $A^\dagger$ is the interpolating operator to create a pseudoscalar or vector heavy-light meson with $\Gamma^\nu = \gamma^5$ or $\Gamma^\nu = \gamma^\nu$ respectively.

Pseudoscalar-to-Pseudoscalar Decay

For the pseudoscalar decay, taking $\Gamma^\nu = \gamma^5$ in Eqn. (1.110) gives

$$\begin{aligned} G^{(3)\,\mu}_{P\to P}(t_y,t_x,0;\vec{p},\vec{q}\,) \;&=\; -\sum_{\vec{x},\,\vec{y}} e^{i\frac{2\pi}{L}\vec{q}\cdot\vec{x}}\,e^{i\frac{2\pi}{L}\vec{p}\cdot\vec{y}} \\ &\times\;\Big\langle 0\Big|\,\hat{T}\Big\{\,\bar{h}(y)\gamma^5 l(y)\;\bar{h}'(x)\Lambda^\mu h(x)\;\bar{l}(0)\gamma^5 h'(0)\Big\}\Big|0\Big\rangle\,. \end{aligned} \tag{1.115}$$

Applying Wick's theorem, and using Eqns. (1.71) and (1.91), one obtains the pseudoscalar-to-pseudoscalar three-point correlator in terms of quark propagators

$$\begin{aligned} G^{(3)\,\mu}_{P\to P}(t_y,t_x,0;\vec{p},\vec{q}\,) \;&=\; \sum_{\vec{x},\,\vec{y}} e^{i\frac{2\pi}{L}\vec{q}\cdot\vec{x}}\,e^{i\frac{2\pi}{L}\vec{p}\cdot\vec{y}} \\ &\times\;\Big\langle\,Tr_{s,c}\Big[\,H'^\dagger(x,0;\mathcal{U})\,\gamma^5\Lambda^\mu\,H(x,y;\mathcal{U})\,\gamma^5 L(y,0;\mathcal{U})\Big]\Big\rangle \end{aligned} \tag{1.116}$$

where the trace is over both spin and colour, and $\Big\langle\cdots\Big\rangle$ denotes an average over gauge configurations, $\mathcal{U}$.

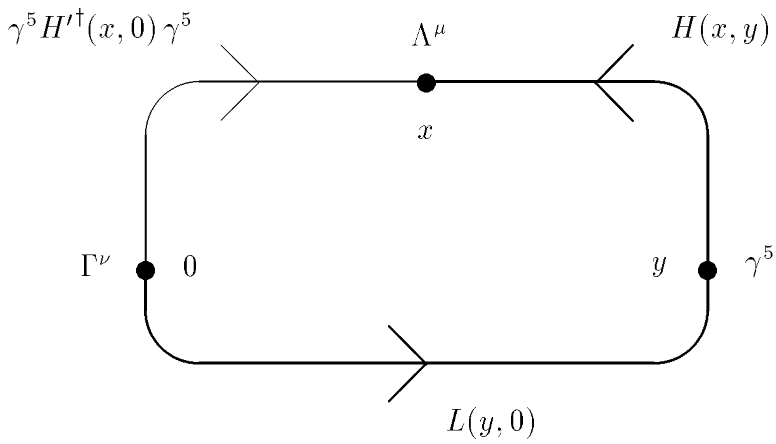

Figure 1.4: The three-point correlator.

Vector-to-Pseudoscalar Decay

Similarly, taking $\Gamma^\nu = \gamma^\nu$ in Eqn. (1.110) one obtains the vector-to-pseudoscalar three-point correlator in terms of quark propagators

$$G^{(3)\,\mu\nu}_{V\to P}(t_y, t_x, 0; \vec{p}, \vec{q}) = \sum_{\vec{x},\vec{y}} e^{i\frac{2\pi}{L}\vec{q}\cdot\vec{x}}\, e^{i\frac{2\pi}{L}\vec{p}\cdot\vec{y}} \times \left\langle Tr_{s,c}\left[\gamma^\nu\gamma^5 H'^{\dagger}(x,0;\mathcal{U})\,\gamma^5\Lambda^\mu\, H(x,y;\mathcal{U})\,\gamma^5 L(y,0;\mathcal{U})\right]\right\rangle \tag{1.117}$$

where the trace is over both spin and colour, and $\left\langle\cdots\right\rangle$ denotes an average over gauge configurations, $\mathcal{U}$. Figure 1.4 shows the three-point correlator constructed from quark propagators.

The heavy quark propagator $H(x,y;\mathcal{U})$, in Eqns. (1.116) and (1.117), requires the inversion of the entire fermion matrix which is computationally prohibitive. Fortunately, three-point correlators can be constructed using an extended quark propagator computed for a fixed origin. In practice, the three-point correlator is computed as a function of t_x with t_y a constant. This corresponds to varying the position of the weak current operator between two fixed mesons.

Extended Quark Propagator

The extended quark propagator is defined as follows:

$$\phi(x,0;t_y;\mathcal{U}) \equiv \sum_{\vec{y}} e^{i\frac{2\pi}{L}\vec{p}\cdot\vec{y}}\, H(x,y;\mathcal{U})\,\gamma^5 L(y,0;\mathcal{U}) \tag{1.118}$$

where the sum is over the spatial dimension, $\vec{y}$. Eqn. (1.118) can be rewritten in the following matrix notation

$$\phi(x,0;t_y;\mathcal{U}) = \delta(t_z,t_y)\, e^{i\frac{2\pi}{L}\vec{p}\cdot\vec{z}}\, H(x,z;\mathcal{U})\,\gamma^5 L(z,0;\mathcal{U}) \tag{1.119}$$

where there is now an implied sum over $(\vec{z}, t_z)$.

Multiplying both sides of Eqn (1.119) by the heavy fermion matrix one obtains

$$H^{-1}(z,x;\mathcal{U})\,\phi(x,0;t_y;\mathcal{U}) = \eta_{SEQ}(z,0) \tag{1.120}$$

with

$$\eta_{SEQ}(z,0) = \delta(t_z,t_y)\, e^{i\frac{2\pi}{L}\vec{p}\cdot\vec{z}}\,\gamma^5\, L(z,0;\mathcal{U}) \tag{1.121}$$

which is in the standard form for fermion matrix inversion, given by Eqn. (1.75). $\eta_{SEQ}(x,0)$ is called the 'sequential' source [44] and is essentially just the t_y-*th* time-slice of the light propagator, $L(x,0;\mathcal{U})$. Thus, three-point correlators can be constructed from quark propagators computed for a fixed origin, and there is no need to invert the entire fermion matrix. The extended propagator is denoted in Figure 1.4 by the bold 'propagator' line.

1.8 Weak Matrix Elements

At large Euclidean times, three-point correlation functions have a simple analytic form which can be parameterised by various two-point quantities (the masses and amplitudes from Section 1.6) and the corresponding matrix element. This section describes the time-dependence of both the pseudoscalar-to-pseudoscalar and vector-to-pseudoscalar three-point correlators, given in Section 1.7.

Three-Point Correlators

Inserting two complete sets of states in Eqn. (1.110) gives

$$
\begin{aligned}
G^{(3)}_{A\to B}(t_y, t_x, 0; \vec{p}, \vec{q}\,) &= \frac{1}{L^3} \sum_{\vec{y},\, S_1,\, \vec{k_1}} \frac{e^{i\frac{2\pi}{L}\vec{p}\cdot\vec{y}}}{2a\, E_{S_1}(\vec{k_1})} \times \frac{1}{L^3} \sum_{\vec{x},\, S_2,\, \vec{k_2}} \frac{e^{i\frac{2\pi}{L}\vec{q}\cdot\vec{x}}}{2a\, E_{S_2}(\vec{k_2})} \\
&\times \Big\langle\, 0 \,\Big|\, B(y) \,\Big|\, S_1,\, \vec{k_1} \,\Big\rangle \Big\langle\, S_1,\, \vec{k_1} \,\Big|\, J^\mu(x) \,\Big|\, S_2,\, \vec{k_2} \,\Big\rangle \\
&\times \Big\langle\, S_2,\, \vec{k_2} \,\Big|\, A^\dagger(0) \,\Big|\, 0 \,\Big\rangle\,. \qquad (1.122)
\end{aligned}
$$

Using translation symmetry, to shift the operators $B(y)$ and $J^\mu(x)$ to the origin, one obtains the following three-point correlator

$$
\begin{aligned}
G^{(3)}_{A\to B}(t_y, t_x, 0; \vec{p}, \vec{q}\,) &= \sum_{S_1} \frac{e^{-aE_{S_1}(\vec{p}\,)\,(t_y - t_x)}}{2a\, E_{S_1}(\vec{p}\,)} \times \sum_{S_2} \frac{e^{-aE_{S_2}(\vec{p}+\vec{q}\,)t_x}}{2a\, E_{S_2}(\vec{p}+\vec{q}\,)} \\
&\times \Big\langle\, 0 \,\Big|\, B(0) \,\Big|\, S_1,\, \vec{p} \,\Big\rangle \Big\langle\, S_1,\, \vec{p} \,\Big|\, J^\mu(0) \,\Big|\, S_2,\, \vec{p}+\vec{q} \,\Big\rangle \\
&\times \Big\langle\, S_2,\, \vec{p}+\vec{q} \,\Big|\, A^\dagger(0) \,\Big|\, 0 \,\Big\rangle \qquad (1.123)
\end{aligned}
$$

where there is now an explicit time-dependence. The only non-zero contribution to this sum are the ground states of the incoming and outgoing mesons, and their excitations. These higher-energy excitations fall off exponentially compared to the ground states which give the dominant contributions as $(t_y - t_x) \to \infty$ and $t_x \to \infty$.

Pseudoscalar-to-Pseudoscalar Time-Dependence

At large Euclidean times, with $t_y = T$ fixed, the pseudoscalar-to-pseudoscalar three-point correlator is given by

$$
\begin{aligned}
C^{(3)}_{P\to P}(t; \vec{p}, \vec{q}; T) &\implies Z^B_P(\vec{p}\,)\, \frac{e^{-aE^B_P(\vec{p}\,)\,(T-t)}}{2a\, E^B_P(\vec{p}\,)} \times Z^A_P(\vec{p}+\vec{q}\,)\, \frac{e^{-aE^A_P(\vec{p}+\vec{q}\,)t}}{2a\, E^A_P(\vec{p}+\vec{q}\,)} \\
&\times \Big\langle\, B_P,\, \vec{p} \,\Big|\, J^\mu(0) \,\Big|\, A_P,\, \vec{p}+\vec{q} \,\Big\rangle \qquad (1.124)
\end{aligned}
$$

where $\left\langle\, B_P,\, \vec{p} \,\middle|\, J^\mu(0) \,\middle|\, A_P,\, \vec{p}+\vec{q} \,\right\rangle$ is the weak matrix element describing the semi-leptonic decay of pseudoscalar meson A into pseudoscalar meson B. E_P and Z_P are the corresponding energies and two-point amplitudes respectively.

Vector to Pseudoscalar Time-Dependence

At large Euclidean times, with $t_y = T$ fixed, the vector-to-pseudoscalar three-point correlator is given by

$$\begin{aligned} C^{(3)\,\mu\nu}_{V\to P}(t;\vec{p},\vec{q};T) \quad \Longrightarrow \quad & Z^B_P(\vec{p}\,)\,\frac{e^{-aE^B_P(\vec{p}\,)\,(T-t)}}{2a\,E^B_P(\vec{p}\,)} \\ \times \quad & Z^A_V(\vec{p}+\vec{q}\,)\,\frac{e^{-aE^A_V(\vec{p}+\vec{q}\,)t}}{2a\,E^A_V(\vec{p}+\vec{q}\,)} \quad \times \quad \mathcal{J}^{\mu\nu} \end{aligned} \tag{1.125}$$

with

$$\mathcal{J}^{\mu\nu} = \sum_{r=1}^{3} \xi^\nu_r(\vec{p}+\vec{q}\,)\,\left\langle\, B_P,\, \vec{p} \,\middle|\, J^\mu(0) \,\middle|\, A^r_V,\, \vec{p}+\vec{q} \,\right\rangle \tag{1.126}$$

where $\mathcal{J}^{\mu\nu}$ is the polarisation-averaged weak matrix element describing the semi-leptonic decay of vector meson A into pseudoscalar meson B. E and Z are the corresponding energies and two-point amplitudes of the pseudoscalar and vector mesons.

Chapter 2

Meson Spectrum

This chapter describes a lattice calculation of the meson spectrum. Lattice results are presented for both the light-light and heavy-light mesons. These results are extrapolated to the physical masses and compared with experiment.

2.1 Simulation Details

The simulation was performed on a 64–node i860 Meiko Computing Surface at the University of Edinburgh by the UKQCD Collaboration. Sixty quenched $SU(3)$ gauge configurations were generated on a $24^3 \times 48$ space-time lattice at $\beta = 6.2$. This corresponds to an inverse lattice spacing $a^{-1} = 2.73 \,^{+5}_{-5}\, GeV$, as determined from the string tension[45]; other physical quantities lead to slightly different values with $a^{-1} = 2.5$–$3.0\ GeV$. This uncertainty in the lattice spacing is taken into account when quoting results for dimensionful quantities. The gauge configurations were generated with periodic boundary conditions using the Hybrid Over-Relaxed algorithm [46].

The quark propagators were calculated using the $O(a)$-improved Sheikholeslami-Wohlert action described in Section 1.3. Light propagators were computed for three values of the quark mass with hopping parameter $\kappa_l = 0.14144$, 0.14226 and 0.14262; heavy quark propagators were generated for four values of the quark mass with $\kappa_h = 0.121$, 0.125, 0.129 and 0.133. The charm quark has a mass equivalent to $\kappa_h = 0.129$ [47] which corresponds to one of the heavy quark propagators. The quark propagators were generated using an Over-Relaxed Minimal Residual (MR) algorithm detailed in [48] with red-black preconditioning and boundary conditions which are periodic in space and anti-periodic in time.

2.2 Statistical Analysis

Recall from Sections 1.6 and 1.8, at large Euclidean times two-point and three-point correlators are described by analytic functions of the meson masses and matrix elements. These parameters can be extracted by fitting correlators to appropriate model functions. Recall from Sections 1.5 and 1.7, correlators are constructed from quark propagators computed for a finite number of gauge configurations. To estimate the error on a fit parameter, the simulation should ideally be repeated (many times) for different gauge configuration samples. In practise, this is prohibitive since both gauge configurations and quark propagators are computationally expensive. The error on a fit parameter can instead be estimated using the Jackknife and Bootstrap methods [49].

Jackknife Error

The jackknife error, σ_P^J, on a quantity P computed from a data set Y with n data elements, $y_1, y_2, \ldots, y_n$, is defined as follows:

$$\sigma_p^J = \sqrt{\frac{(n-1)}{n} \sum_{i=1}^{n} \Big(p_i - \langle\, p_i \,\rangle \Big)^2} \tag{2.1}$$

with

$$\langle\, p_i \,\rangle = \frac{1}{n} \sum_{i=1}^{n} p_i \tag{2.2}$$

where p_i is the quantity P computed from the i–th jackknife sample $(Y - y_i)$ with $(n-1)$ data elements, $y_1, y_2, \ldots, y_{i-1}, y_{i+1}, \ldots, y_n$.

The quantity P and its jackknife error are quoted as follows:

$$P \pm \sigma_p^J. \tag{2.3}$$

The normalisation factor in Eqn. (2.1) is included to make the jackknife give the 'right' answer for the standard deviation, σ; in which case the quantity P is simply the average of the data set. The standard deviation formula of elementary statistical analysis [50] assumes the data is normally distributed. The jackknife method makes no such assumption and is therefore suited to situations in which the distribution of the data is unknown.

Bootstrap Error

The bootstrap error, σ_P^B, on a quantity P computed from a data set Y with n data elements, $y_1, y_2, \ldots, y_n$, is defined as follows:

$$\sigma_P^B = \frac{b^* - a^*}{2} \tag{2.4}$$

with a^* and b^*, the lower and upper bounds respectively, chosen such that

$$\frac{\sharp\,\{\,p_i < a^*\}}{N} = \frac{1-C}{2} \qquad \text{and} \qquad \frac{\sharp\,\{\,p_i < b^*\}}{N} = \frac{1+C}{2} \tag{2.5}$$

where p_i is the quantity P computed from the i–th bootstrap sample, N is the number of bootstrap samples, C is the confidence level in the range $[\,0,1]$, and $\sharp\{\cdots\}$ denotes the number of p_i satisfying the enclosed relation. Each bootstrap sample consists of n data elements selected at random from Y with replacement.

The quantity P and its bootstrap error are quoted as follows:

$$P \,{}^{+}_{-}\, \sigma_P^B. \tag{2.6}$$

Typically, a^* and b^* are computed with a 68% confidence level ($C = 0.68$). For a normal distribution, this is the percentage of measurements which lie within one standard deviation of the mean. The accuracy in the bootstrap estimate of the error increases with the number of bootstrap samples.

Correlator Data

Recall from Section 1.4, quark propagators are computed on a space-time lattice for a fixed number of gauge configurations. And recall from Sections 1.5 and 1.7, correlators are constructed, timeslice by timeslice, by combining quark propagators and averaging (with an appropriate phase factor) over the spatial dimensions of the lattice. Correlator data is stored in an array with the following dimensions:

$$\text{data}[\,c\,][\,n\,][\,t\,] \tag{2.7}$$

where c is the number of correlators, n is the number of gauge configurations and t is the number of timeslice components.

Fit Data

Fit data is obtained by averaging each correlator (over gauge configurations) to obtain observables

$$\mathrm{ave}[\,c\,][\,t\,] = \frac{1}{n}\sum_{i=1}^{n} \mathrm{data}[\,c\,][\,i\,][\,t\,] \tag{2.8}$$

and then computing the following data function

$$d(t) = f\Big(\mathrm{ave}[\,1\,][\,\mathrm{t}\,], \mathrm{ave}[\,2\,][\,\mathrm{t}\,], \ldots, \mathrm{ave}[\,\mathrm{c}\,][\,\mathrm{t}\,]\Big) \tag{2.9}$$

where f is a function of c correlators. The order of these two steps is crucial since the average (over gauge configurations) of a function of c correlators is *not* the same as a function of the correlator averages (the observables).

Covariance Matrix

Following Eqn. (2.1) the jackknife estimate of the covariance matrix is given by

$$C_J(t_i, t_j) = \frac{(n-1)}{n}\sum_{k=1}^{n}\Big[d_k(t_i) - \Big\langle d_k(t_i)\Big\rangle\Big] \times \Big[d_k(t_j) - \Big\langle d_k(t_j)\Big\rangle\Big] \tag{2.10}$$

where $d_k(t)$ is the data function, $d(t)$, computed with the k–*th* jackknife sample. The entries in the covariance matrix correspond as follows: a diagonal entry is the error squared on $d(t_i)$; and an off-diagonal entry is proportional to correlations in the data between timeslices t_i and t_j.

Correlation Matrix

The correlation matrix is defined as follows:

$$C_N(t_i, t_j) = \frac{C_J(t_i, t_j)}{\sqrt{C_J(t_i, t_i)\, C_J(t_j, t_j)}} \tag{2.11}$$

where the correlations between timeslices are now correctly normalised in the range $[-1, +1]$. For uncorrelated data, Eqn. (2.11) reduces to the identity matrix. In practise, Eqn. (2.11) is computed because the correlation matrix is easier to invert numerically.

Fit Procedure

Consider the most general case: fitting an analytic model function, $f(t;\vec{a}\,)$, parameterised by m parameters, $a_i = a_1, a_2, \ldots, a_m$, to a data function, $d(t)$. The fit is performed by minimising the following chi-squared function with respect to the model parameters, $\vec{a}$:

$$\chi^2 = \sum_{t_i,t_j} \Big[f(t_i;\vec{a}\,) - d(t_i) \Big] \times C_J^{-1}(t_i,t_j) \times \Big[f(t_j;\vec{a}\,) - d(t_j) \Big] \tag{2.12}$$

where $C_J^{-1}(t_i,t_j)$ is the inverse of the jackknifed covariance matrix. The minimisation of Eqn. (2.12) is performed numerically using a Marquardt-Levenberg algorithm [51].

Fit Parameter Errors

To estimate the errors on the model parameters, $\vec{a}$, the entire fit procedure is repeated with N bootstrap data sets. For each bootstrap sample, both the data function and the covariance matrix are re-computed using Eqns. (2.8–2.9) and (2.10) respectively. In practice, both the best-fit parameters, $\vec{a}$, and the N bootstrap values are stored. The error on a particular parameter, a_i, is computed (when required) using Eqn. (2.4).

All correlators are computed from the same sixty $SU(3)$ gauge configurations. This data is likely to be highly correlated. Hence, all fit parameters are determined from correlated chi-squared fits. The error quoted on all quantities corresponds to a 68% confidence level, on a distribution obtained from 1000 bootstrap samples. The χ^2/dof is quoted as an indicator of the goodness-of-fit. The number of degrees of freedom (dof) is given by

$$dof = (t - m) \tag{2.13}$$

where m is the number of model parameters and t is the number of timeslices included in the fit. As a rule of thumb a $\chi^2/dof \approx 1$ indicates a good fit to the data.

2.3 Two-Point Correlator Fits

Recall from Section 1.5, the pseudoscalar and the vector meson correlator are constructed from quark propagators using Eqns. (1.92) and (1.95) respectively. And recall from Section 1.6, at large Euclidean times these correlators are given by Eqns. (1.103) and (1.109).

Meson Fit Function

The ground-state energy, E, and the corresponding two-point amplitude, Z, are extracted by fitting the meson correlator to the following fit-function:

$$C(t) = A\left\{e^{-B\,t} + e^{-B\,(T-t)}\right\} \tag{2.14}$$

where the terms $e^{-B\,t}$ and $e^{-B\,(T-t)}$ represent the 'forward' and 'backward' propagating particles respectively[1], and T is the temporal extent of the lattice. The fit parameters A and B are related to the ground state energy and the corresponding two-point amplitude by

$$A = \frac{Z^2}{2\,E} \quad \text{and} \quad B = E. \tag{2.15}$$

For an infinite number of gauge configurations, the meson correlator is exactly mirrored about the mid-point of the lattice. This is a consequence of the boundary conditions and time reversal symmetry. Prior to fitting, the configuration data is 'folded' by averaging the corresponding timeslices from the two halves of the lattice. In this study, $T = 48$ and the data is folded about $t = 24$. This procedure improves statistics by effectively doubling the number of gauge configurations. The vector data is averaged over polarisation states and divided by a factor of 3.

The values of momenta on a lattice of spatial volume L^3, with periodic boundary conditions, are quantised and given by Eqn. (1.26). For $L = 24$, the allowed values of momenta are given by

$$\vec{p} = \frac{\pi}{12\,a}\,(n_x,\, n_y,\, n_z) \tag{2.16}$$

where n_x, n_y and n_z are integers.

[1] For meson correlators these particles are identical.

To increase statistics, the correlator data is averaged over all equivalent momentum channels before fitting. For example, the channels (1,0,0), (0,1,0) and (0,0,1) are equivalent and their average corresponds to a particle with momentum $|\vec{p}\,| = \pi/12\,a$. The UKQCD data set corresponds to particles with the following momenta: $|\vec{p}\,| = 0,\ 1,\ \sqrt{2},\ \sqrt{3}$ and 2, in units of $\pi/12\,a$.

Light-Light Masses

The UKQCD propagator set contains three light quark masses with hopping parameter $\kappa_l = 0.14144$, 0.14226 and 0.14262. These kappa values allow the construction of six independent light-light correlators for both the pseudoscalar and vector mesons. The masses and two-point amplitudes, obtained from fits to zero momentum correlators, are given in Tables 2.1 and 2.2 respectively. For the pseudoscalar channel the fit interval is $t = 14$–22; and for the vector channel $t = 13$–23. These fit ranges were determined in an earlier UKQCD study [45]. The chi-squared values in Table 2.1 indicate a good fit ($\chi^2/dof \approx 1$) for all kappa combinations.

Fits to meson correlators with non-zero momentum were also performed; the corresponding energies and two-point amplitudes are required to extract three-point matrix elements over a range of momentum transfer. The noise in the two-point correlator signal increases rapidly with momentum because the number of gauge configurations is finite. In the pseudoscalar case, a fit to any correlator with lattice momenta greater than $\sqrt{2}$ units of $\pi/12\,a$ either fails or gives an unacceptable chi-squared ($\chi^2/dof \gg 1$).

In Figure 2.1 the pseudoscalar energy is plotted as a function of the momentum squared. This data is fitted to the continuum dispersion relation given by

$$E = \sqrt{m^2 + |\vec{p}\,|^2} \tag{2.17}$$

where only the first three data points are included in each fit. Figure 2.1 shows the dispersion relation is well-satisfied for pseudoscalar meson correlators with momentum $\leq \pi/12\,a$. The fitted masses are also in excellent agreement with the values obtained from the zero-momentum correlators, given in Table 2.1.

κ_{l_1}	κ_{l_2}	Pseudo	χ^2/dof	Vector	χ^2/dof
0.14144	0.14144	$0.298 {}^{+}_{-} {}^{2}_{2}$	1.24	$0.395 {}^{+}_{-} {}^{5}_{4}$	1.82
0.14144	0.14226	$0.259 {}^{+}_{-} {}^{2}_{2}$	0.90	$0.370 {}^{+}_{-} {}^{6}_{5}$	1.35
0.14144	0.14262	$0.241 {}^{+}_{-} {}^{2}_{3}$	0.76	$0.360 {}^{+}_{-} {}^{8}_{6}$	1.01
0.14226	0.14226	$0.214 {}^{+}_{-} {}^{2}_{3}$	0.99	$0.343 {}^{+}_{-} {}^{9}_{7}$	0.86
0.14226	0.14262	$0.192 {}^{+}_{-} {}^{3}_{3}$	0.99	$0.331 {}^{+}_{-} {}^{11}_{10}$	0.60
0.14262	0.14262	$0.167 {}^{+}_{-} {}^{3}_{4}$	1.04	$0.319 {}^{+}_{-} {}^{14}_{13}$	0.44
$0.1418 {}^{+}_{-} {}^{1}_{1}$	$0.14315 {}^{+}_{-} {}^{2}_{2}$	$0.186 {}^{+}_{-} {}^{9}_{7}$	1.37	$0.331 {}^{+}_{-} {}^{13}_{11}$	0.42
$0.14315 {}^{+}_{-} {}^{2}_{2}$	$0.14315 {}^{+}_{-} {}^{2}_{2}$	0	2.30	$0.290 {}^{+}_{-} {}^{13}_{11}$	

Table 2.1: Light-light meson masses in lattice units; for the pseudoscalar channel the fit is over the time interval $t = 14$–22; and for the vector channel the fit is over the time interval $t = 13$–23. The values quoted in the lower half of the table correspond to the pseudoscalar and vector masses extrapolated to $\kappa_c = 0.14315 {}^{+}_{-} {}^{2}_{2}$ and $\kappa_s = 0.1418 {}^{+}_{-} {}^{1}_{1}$.

κ_{l_1}	κ_{l_2}	$Z_P^2(\|p\| = 0)$	$Z_V^2(\|p\| = 0)$
0.14144	0.14144	$0.0081 {}^{+}_{-} {}^{3}_{5}$	$0.0025 {}^{+}_{-} {}^{2}_{1}$
0.14144	0.14226	$0.0067 {}^{+}_{-} {}^{3}_{5}$	$0.0021 {}^{+}_{-} {}^{2}_{2}$
0.14144	0.14262	$0.0062 {}^{+}_{-} {}^{3}_{5}$	$0.0019 {}^{+}_{-} {}^{2}_{2}$
0.14226	0.14226	$0.0056 {}^{+}_{-} {}^{3}_{5}$	$0.0017 {}^{+}_{-} {}^{2}_{2}$
0.14226	0.14262	$0.0052 {}^{+}_{-} {}^{3}_{5}$	$0.0015 {}^{+}_{-} {}^{3}_{3}$

Table 2.2: Light-light meson two-point amplitudes. The fit ranges and χ^2/dof are the same as those in Table 2.1.

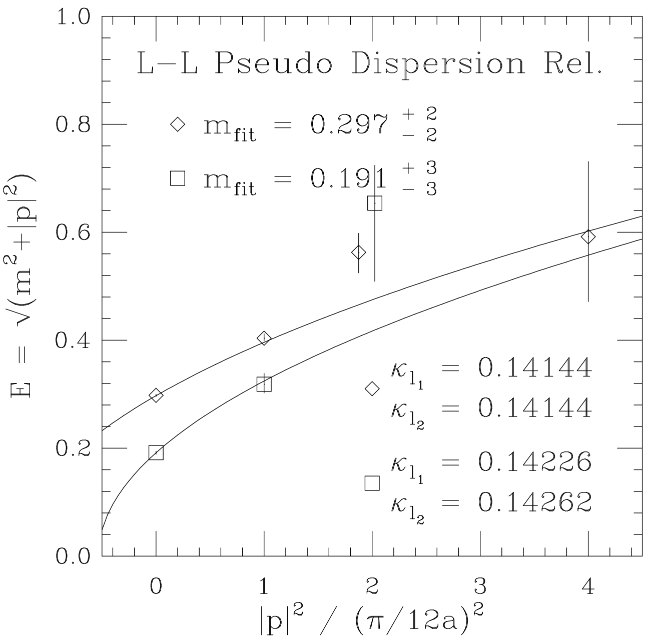

Figure 2.1: Light-light pseudoscalar dispersion relation.

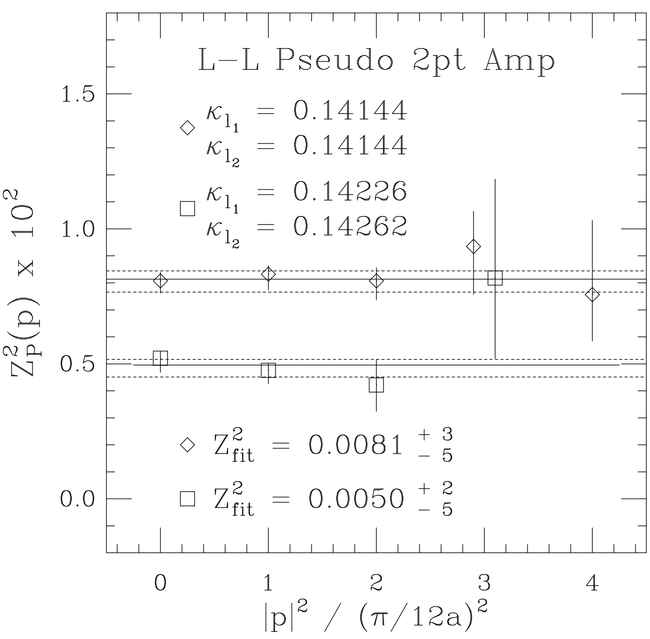

Figure 2.2: Light-light pseudoscalar two-point amplitudes.

In Figure 2.2 the pseudoscalar two-point amplitude is plotted as a function of the momentum squared. This data is fitted to a constant: the two-point amplitude should be independent of momentum for meson correlators constructed from local interpolating operators. The fitted Z^2 are in excellent agreement with the values obtained from the zero-momentum correlators given in Table 2.2.

Heavy-Light Masses

The UKQCD propagator set contains a heavy quark mass with hopping parameter $\kappa_h = 0.129$ corresponding to the mass of the charm quark, and light quark masses with hopping parameter κ_l=0.14144, 0.14226 and 0.14262. These kappa values allow the construction of three independent heavy-light correlators for both the pseudoscalar and vector mesons.

The heavy quark propagator is smeared at both the source and sink using gauge invariant Jacobi smearing described in Section 1.4. Correlators constructed from smeared quark propagators correspond to spatially-extended interpolating operators which help isolate the ground state mass. In the 'static' limit (infinite heavy-quark mass), the use of such operators is essential to obtain any signal.

The masses and two-point amplitudes, obtained from fits to zero-momentum correlators, are given in Tables 2.3 and 2.4 respectively. For both the pseudoscalar and vector channel, the fit interval is t = 11–22. This fit range was determined in an earlier UKQCD study [47]. The chi-squared values in Table 2.3 indicate a good fit ($\chi^2/dof \approx 1$) for all kappa combinations.

In Figure 2.3 the pseudoscalar energy is plotted as a function of the momentum squared. This data is fitted to the continuum dispersion relation given by Eqn. (2.17) where the fit includes all data points. The dispersion relation is well-satisfied for all heavy-light correlators; all data points are within two sigma. The fitted masses are also in excellent agreement with the values obtained from the zero-momentum correlators, given in Table 2.3.

κ_l	Pseudo	χ^2/dof	Vector	χ^2/dof
0.14144	$0.716\,^{+\,3}_{-\,2}$	0.64	$0.745\,^{+\,4}_{-\,2}$	0.71
0.14226	$0.692\,^{+\,4}_{-\,2}$	0.59	$0.722\,^{+\,5}_{-\,3}$	0.72
0.14262	$0.683\,^{+\,5}_{-\,3}$	0.54	$0.713\,^{+\,6}_{-\,5}$	0.61
$0.1418\,^{+\,1}_{-\,1}$	$0.706\,^{+\,6}_{-\,3}$	0.64	$0.736\,^{+\,7}_{-\,3}$	0.16
$0.14315\,^{+\,2}_{-\,2}$	$0.666\,^{+\,6}_{-\,3}$		$0.697\,^{+\,7}_{-\,5}$	

Table 2.3: Heavy-light meson masses in lattice units with $\kappa_h = 0.129$; the fit is over the time interval $t = 11$–22. The values quoted in the lower half of the table correspond to the pseudoscalar and vector masses extrapolated to $\kappa_c = 0.14315\,^{+\,2}_{-\,2}$ and $\kappa_s = 0.1418\,^{+\,1}_{-\,1}$.

κ_l	$Z_P^2(\lvert p\rvert = 0)$	χ^2/dof	$Z_P^2(\lvert p\rvert = 1)$	χ^2/dof
0.14144	$14.5\,^{+\,6}_{-\,5}$	0.64	$10.6\,^{+\,4}_{-\,4}$	0.90
0.14226	$12.7\,^{+\,6}_{-\,5}$	0.59	$9.0\,^{+\,4}_{-\,4}$	0.96
0.14262	$12.0\,^{+\,7}_{-\,6}$	0.54	$8.4\,^{+\,4}_{-\,4}$	0.96

Table 2.4: Heavy-light pseudoscalar meson two-point amplitudes with momentum in units of $\pi/12\,a$ and $\kappa_h = 0.129$. The fit range is the same as in Table 2.3.

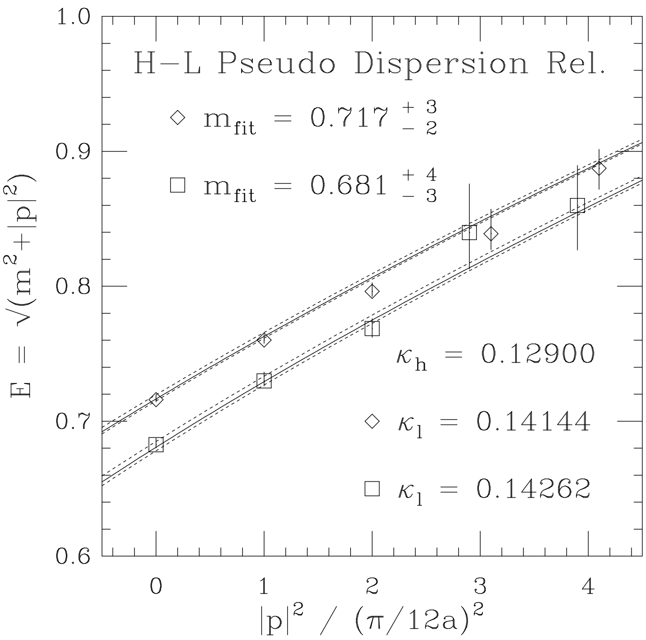

Figure 2.3: Heavy-light pseudoscalar dispersion relation.

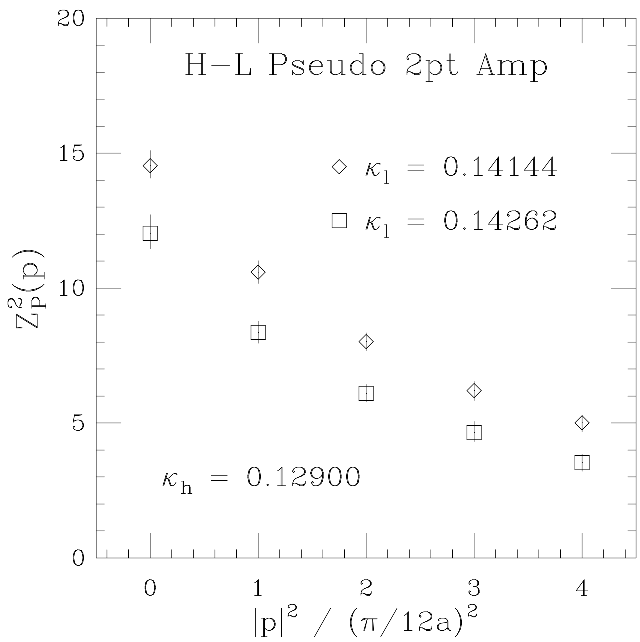

Figure 2.4: Heavy-light pseudoscalar two-point amplitudes.

In Figure 2.4 the pseudoscalar two-point amplitude is plotted as a function of the momentum squared. The momentum dependence of the heavy-light two-point amplitude is a feature of using spatially-extended interpolating operators. The overlap with the ground state decreases with increasing momentum because the volume of the smeared 'wave-function' is Lorentz contracted along the direction of motion.

For non-zero momentum, heavy-light meson correlators are fitted by constraining the two-point energy to values computed from the continuum dispersion relation using the masses in Table 2.3. Thus, a single parameter fit is used to determine the two-point amplitudes for correlators with non-zero momentum. The data in Figure 2.4 is obtained by this method. The two-point amplitudes, obtained from one parameter fits to heavy-light meson correlators with $|\vec{p}| = \pi/12\,a$, are given in Table 2.4.

Three-point correlator fits (discussed in the following chapters) are particularly sensitive to two-point quantities. Thus, two-point energies are computed from the masses quoted in Tables 2.1 and 2.3 using the continuum dispersion relation; light-light two-point amplitudes are constrained to their zero-momentum values, quoted in Table 2.2; and heavy-light two-point amplitudes are obtained from one-parameter fits (described above), quoted in Table 2.4.

2.4 Chiral Extrapolation

This section describes how the physical meson masses are obtained from the lattice light-light and heavy-light data. Recall from Section 1.2, in the Wilson formulation the bare quark mass is given by

$$m = \frac{1}{2}\left(\frac{1}{\kappa} - \frac{1}{\kappa_c}\right) \tag{2.18}$$

where κ_c is the hopping parameter corresponding to zero quark mass. For each quark flavour, a hopping parameter must be found which corresponds to the physical value. The light quarks u and d are assumed to be degenerate in mass (corresponding to an exact isospin symmetry) with $\kappa_u = \kappa_d = \kappa_c$.

Light-Light Pseudoscalar Extrapolation

The light-light pseudoscalar meson obeys the following PCAC [2] relation:

$$m_P^2 \propto m_q \tag{2.19}$$

where m_q is the mass of the constituent light quarks. Using Eqn. (2.18), the mass-dependence of the light-light pseudoscalar data is given by

$$m_P^2\,(\kappa_{l_1},\,\kappa_{l_2}) \;=\; b_P\left(\frac{1}{\kappa_{eff}} - \frac{1}{\kappa_c}\right) \tag{2.20}$$

with

$$\frac{1}{\kappa_{eff}} \;=\; \frac{1}{2}\left(\frac{1}{\kappa_{l_1}} + \frac{1}{\kappa_{l_2}}\right) \;=\; \frac{\kappa_{l_1} + \kappa_{l_2}}{2\,\kappa_{l_1}\kappa_{l_2}} \tag{2.21}$$

where b_P and κ_c are free parameters, and κ_{eff} is an effective kappa corresponding to an average of the constituent quark masses. In this model, κ_c is the hopping parameter for which the pion mass vanishes.

Figure 2.5 shows the light-light pseudoscalar data, quoted in the upper-half of Table 2.1, plotted as a function of the inverse effective-kappa. This data is fitted to Eqn. (2.20) to obtain

$$\kappa_c = 0.14315\,^{+\,2}_{-\,2} \tag{2.22}$$

where the fit chi-squared ($\chi^2/dof \approx 2$), although a little high, is still acceptable. The pion mass, given by Eqn. (2.20) with $\kappa_{l_1} = \kappa_{l_2} = \kappa_c$, is zero by definition. This value and the fit chi-squared are quoted in the lower-half of Table 2.1.

Light-Light Vector Extrapolation

The light-light vector meson is assumed to be linear in the light quark masses

$$m_V(\kappa_{l_1},\,\kappa_{l_2}) = a_V + b_V\left(\frac{1}{\kappa_{eff}} - \frac{1}{\kappa_c}\right) \tag{2.23}$$

where a_V and b_V are free parameters.

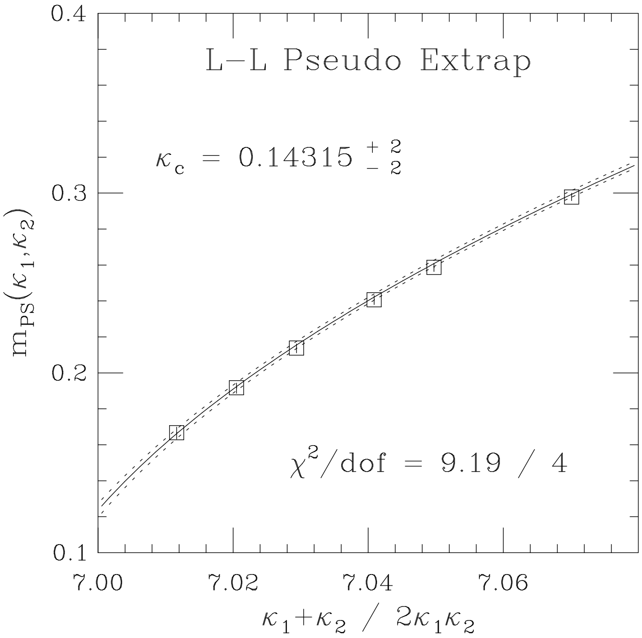

Figure 2.5: Light-light pseudoscalar extrapolation.

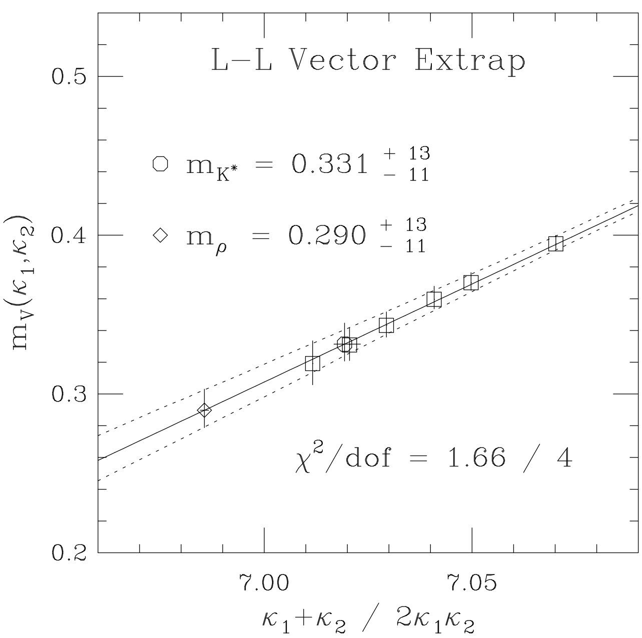

Figure 2.6: Light-light vector extrapolation.

Figure 2.6 shows the light-light vector data, quoted in the upper-half of Table 2.1, plotted as a function of the inverse effective-kappa. This data is fitted to Eqn. (2.23) to obtain

$$m_\rho = 0.290\,^{+\,13}_{-\,11} \tag{2.24}$$

where a_V and b_V are determined by the fit. The chi-squared ($\chi^2/dof \approx 0.4$) indicates a good fit to the data. The rho mass, m_ρ, is computed from Eqn. (2.23) with $\kappa_{l_1} = \kappa_{l_2} = \kappa_c$. This mass and the fit chi-squared are quoted in the lower-half of Table 2.1. Figure 2.6 includes two extra data points corresponding to the mass of the ρ and K^* mesons.

Light-Light Ratio Extrapolation

The hopping parameter κ_s, corresponding to the mass of the strange quark, is required to study the effects of $SU(3)$ symmetry breaking on the meson spectrum. A value for κ_s is determined by fitting the ratio $m_P^2(\kappa_{l_1},\, \kappa_{l_2})\,/\,m_\rho^2$ to some function of the light quark masses; extrapolating κ_{l_1} to κ_c; and using κ_{l_2} to fix the ratio to the experimental value m_K^2/m_ρ^2. The light-quark dependence of $m_P^2(\kappa_{l_1},\, \kappa_{l_2})\,/\,m_\rho^2$ is given by Eqn. (2.20) since m_ρ^2 is just a constant.

The ratio data is computed from the light-light pseudoscalar masses and the light-light vector extrapolated rho mass, quoted in the upper and lower halves of Table 2.1 respectively. Figure 2.7 shows the ratio data plotted as a function of the inverse effective-kappa, and fitted to Eqn. (2.20) to obtain

$$\kappa_s = 0.1418\,^{+\,1}_{-\,1} \qquad \text{with} \qquad \frac{m_K^2}{m_\rho^2} = 0.413 \tag{2.25}$$

where the fit chi-squared ($\chi^2/dof = 1.4$) indicates a fairly good fit to the data. Using Eqns (2.20) and (2.23), to compute the K and K^* meson masses respectively, gives

$$m_K = 0.186\,^{+\,9}_{-\,7} \qquad \text{and} \qquad m_{K^*} = 0.331\,^{+\,13}_{-\,11} \tag{2.26}$$

with $\kappa_{l_1} = \kappa_c$ and $\kappa_{l_2} = \kappa_s$. These masses and the corresponding fit chi-squared are quoted in the lower-half of Table 2.1.

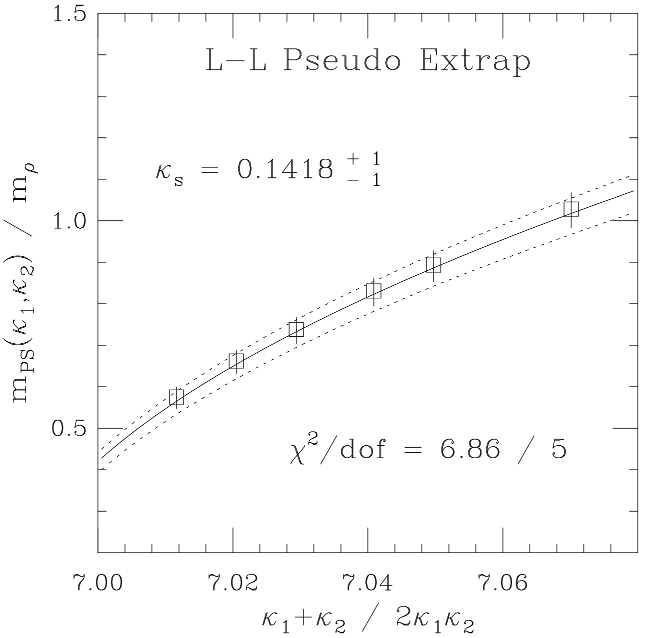

Figure 2.7: Light-light ratio extrapolation.

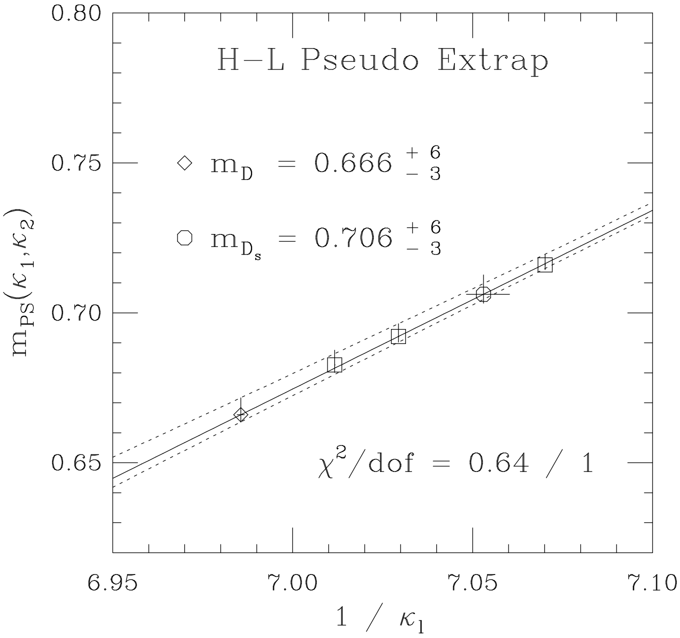

Figure 2.8: Heavy-light pseudoscalar extrapolation.

Heavy-Light Pseudoscalar Extrapolation

Both the pseudoscalar and vector heavy-light mesons are assumed to be linear in the light quark mass

$$m_P(\kappa_l) \equiv m_V(\kappa_l) = a' + b'\left(\frac{1}{\kappa_l} - \frac{1}{\kappa_c}\right) \tag{2.27}$$

where a' and b' are free parameters.

Figure 2.8 shows the heavy-light pseudoscalar data, quoted in the upper-half of Table 2.3, plotted as a function of the inverse light-kappa. This data is fitted to Eqn. (2.27) to obtain

$$m_D = 0.666^{+6}_{-3} \qquad \text{and} \qquad m_{D_s} = 0.706^{+6}_{-3} \tag{2.28}$$

where the fit chi-squared ($\chi^2/dof = 0.6$) indicates a good fit to the data. The D and D_S meson masses are computed from Eqn. (2.27) with $\kappa_l = \kappa_c$ and $\kappa_l = \kappa_s$ respectively. These masses and the fit chi-squared are quoted in the lower-half of Table 2.3.

Heavy-Light Vector Extrapolation

The vector heavy-light data, quoted in the upper-half of Table 2.3, is fitted to Eqn. (2.27) to obtain

$$m_{D^*} = 0.697^{+7}_{-5} \qquad \text{and} \qquad m_{D_S^*} = 0.736^{+7}_{-3} \tag{2.29}$$

where the fit chi-squared ($\chi^2/dof = 0.2$) indicates a good fit to the data. The D^* and D_S^* meson masses are computed from Eqn. (2.27) with $\kappa_l = \kappa_c$ and $\kappa_l = \kappa_s$ respectively. These masses and the fit chi-squared are quoted in the lower-half of Table 2.3. From Eqns. (2.28) and (2.29), it is clear that this lattice calculation is sensitive to $SU(3)$ symmetry breaking effects in the heavy-light meson spectrum.

2.5 Physical Meson Spectrum

The meson masses, up till now, have been quoted in lattice units ($a = 1$). The masses quoted in Table 2.5 are in physical units with $a^{-1} = 2.85 \pm 0.15$ GeV. This value includes an estimate of the error in the determination of the inverse lattice spacing from different quantities. This uncertainty is the largest source of error in the lattice calculation. The experimentally measured masses [52] are quoted in Table 2.5 for comparison.

Figure 2.9 shows the data in Table 2.5 plotted in the form of a histogram. On close inspection, the light-light masses appear to be a little on the high side. This is not unexpected since the choice of inverse lattice spacing is (about 5%) greater than the value determined directly from the rho mass. Nevertheless, all the light-light masses are within one and a half sigma of their experimental values; and the heavy-light masses are within one sigma. In conclusion, the lattice masses quoted in Table 2.5 successfully reproduce the observed pattern in the physical meson spectrum. In the following chapters, these masses are used to extract matrix elements corresponding to weak decays of heavy-light pseudoscalar and vector mesons.

Meson	Experiment	Lattice
$\pi^{\pm}$	139.5679 ± 7	0
π^0	134.9743 ± 8	
ρ	768.1 ± 5	$827 \pm^{57}_{54}$
$K^{\pm}$	493.646 ± 9	$530 \pm^{38}_{34}$
K^0	497.671 ± 31	
$K^{*\pm}$	891.59 ± 24	$943 \pm^{62}_{59}$
K^{*0}	896.10 ± 28	
$D^{\pm}$	1869.3 ± 5	$1898 \pm^{101}_{100}$
D^0	1864.5 ± 5	
$D^{*\pm}$	2010.1 ± 6	$1987 \pm^{106}_{106}$
D^{*0}	2007.1 ± 14	
$D_S{}^{\pm}$	1968.8 ± 7	$2012 \pm^{107}_{106}$
$D_S^{*\pm}$	2110.3 ± 20	$2098 \pm^{112}_{111}$

Table 2.5: Meson masses in MeV.

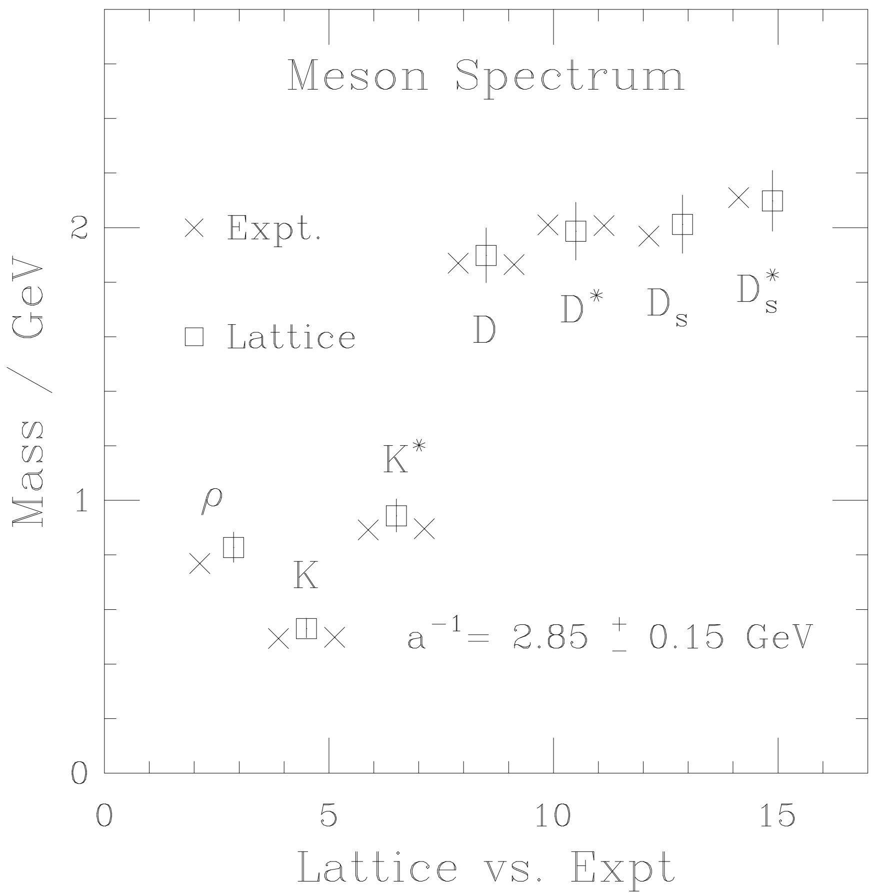

Figure 2.9: Meson mass spectrum.

Chapter 3

Semi-Leptonic D Decays

This chapter describes a lattice calculation of the matrix elements of the vector and axial-vector currents which are relevant to semi-leptonic decays $D \to K, K^*$ and $D \to \pi, \rho$. This calculation is performed using an O(a)-improved fermionic action in an attempt to reduce discretisation errors due to the lattice spacing, a.

3.1 Phenomenology

Using Lorentz, parity and time-reversal invariance, the $D \to K, K^*$ weak matrix elements can be parametrized in terms of six form factors. In the helicity basis, these form factors are defined (in Minkowski space) as follows [73, 74]:

$$\begin{aligned} \left\langle K \middle| (V-A)_\mu \middle| D \right\rangle &= \left(P - \frac{m_D^2 - m_K^2}{q^2}\, q \right)_\mu f^+(q^2) \\ &+ \frac{m_D^2 - m_K^2}{q^2}\, q_\mu\, f^0(q^2) \end{aligned} \tag{3.1}$$

$$\left\langle K_r^* \middle| (V-A)_\mu \middle| D \right\rangle = \xi_r^\beta\, T_{\mu\beta} \tag{3.2}$$

with

$$\begin{aligned} T_{\mu\beta} &= \frac{2\,V(q^2)}{m_D + m_{K^*}}\, \varepsilon_{\mu\gamma\delta\beta}\, p_D^\gamma\, p_{K^*}^\delta + i \left(m_D + m_{K^*} \right) A^1(q^2)\, g_{\mu\beta} \\ &- i\, \frac{A^2(q^2)}{m_D + m_{K^*}}\, P_\mu\, q_\beta + i\, \frac{2\,A(q^2)\, m_{K^*}}{q^2}\, q_\mu\, P_\beta \end{aligned} \tag{3.3}$$

where f^+, f^0, V, A^1, A^2 and A are form factors, ξ_r^β is the polarisation vector of the K^* meson with helicity $r = [0, +, -]$, $P = p_D + p_{K^{(*)}}$ and $q = p_D - p_{K^{(*)}}$ is the four-momentum transfer.

The form factors are dimensionless functions of the scalar quantity q^2 which has the following kinematically allowed range:

$$0 < q^2 \leq q^2_{max} \tag{3.4}$$

where $q_{max} = m_D - m_{K^{(*)}}$ is the maximum momentum transfer. In the limit of zero lepton masses, terms proportional to $q = p_e + p_\nu$ in Eqns. (3.1) and (3.3) do not contribute to the transition amplitudes and hence the decay rates.

The physical interpretation of the different form factors can be understood by writing the matrix elements, of the vector current ($V_\mu = \bar{s}\gamma_\mu c$) and the axial current ($A_\mu = \bar{s}\gamma_\mu\gamma_5 c$), in the centre of mass frame of the lepton pair. In this frame, the matrix elements are given by [73]

$$\left\langle K \middle| V^0 \middle| D \right\rangle = \frac{m_D^2 - m_K^2}{\sqrt{q^2}} f^0(q^2)\,, \tag{3.5}$$

$$\left\langle K \middle| V^i \middle| D \right\rangle = 2\, p_D^i\, f^+(q^2)\,, \tag{3.6}$$

$$\left\langle K_r^* \middle| V^0 \middle| D \right\rangle = 0\,, \tag{3.7}$$

$$\left\langle K_r^* \middle| V^i \middle| D \right\rangle = i\, \frac{2\sqrt{q^2}}{m_D + m_{K^*}} \left(\vec{\xi}_r \times \vec{p}_{K^*}\right)^i V(q^2)\,, \tag{3.8}$$

$$\left\langle K_r^* \middle| A^0 \middle| D \right\rangle = i\, \frac{2\, m_{K^*}}{\sqrt{q^2}} \left(\vec{\xi}_r \cdot \vec{q}\right)^i A^0(q^2)\,, \tag{3.9}$$

$$\begin{aligned} \left\langle K_r^* \middle| A^i \middle| D \right\rangle &= i\left(m_D + m_{K^*}\right) \xi_r^i\, A^1(q^2) \\ &\quad - i\, \frac{2\,\vec{p}_D}{m_D + m_{K^*}} \left(\vec{\xi}_r \cdot \vec{q}\right)^i A^2(q^2)\,. \end{aligned} \tag{3.10}$$

In the helicity basis, f^0 and f^+ are associated with the transition amplitudes corresponding to the exchange of scalar (0^+) and vector (1^-) states respectively. Similarly, the form factors V, $A^{1,2}$ and A^0 are associated with the exchange of vector (1^-), axial (1^+) and pseudoscalar (0^-) states respectively. The axial component of the weak current between two pseudoscalar states is zero.

Furthermore, Eqn. (3.1) can be parameterised as follows:

$$\left\langle K \left| (V-A)^{\mu} \right| D \right\rangle = \left(p_D + p_K\right)^{\mu} f^{+}(q^2) \, + \, \left(p_D - p_K\right)^{\mu} f^{-}(q^2) \qquad (3.11)$$

where the relation between the different form factors is given by

$$\left(m_D^2 - m_K^2\right) f^{0}(q^2) = \left(m_D^2 - m_K^2\right) f^{+}(q^2) + q^2 f^{-}(q^2) \qquad (3.12)$$

with $f^{0}(0) = f^{+}(0)$. Finally, A can be written as follows:

$$A(q^2) = A^0(q^2) - A^3(q^2) \qquad (3.13)$$

where

$$A^3(q^2) = \frac{m_D + m_{K^*}}{2\, m_{K^*}} A^1(q^2) \; - \; \frac{m_D - m_{K^*}}{2\, m_{K^*}} A^2(q^2) \qquad (3.14)$$

with $A^0(0) = A^3(0)$.

Pole Dominance

In the pole dominance model [77] the form factors are dominated by the pole of the corresponding resonance. This suggests the following behaviour with q^2:

$$f^{+}(q^2) \;=\; \frac{f^{+}(0)}{1 - q^2/m_{1^-}^2}, \qquad f^{0}(q^2) \;=\; \frac{f^{0}(0)}{1 - q^2/m_{0^+}^2}, \qquad (3.15)$$

$$V(q^2) \;=\; \frac{V(0)}{1 - q^2/m_{1^-}^2}, \qquad A^0(q^2) \;=\; \frac{A^0(0)}{1 - q^2/m_{0^-}^2}, \qquad (3.16)$$

$$A^i(q^2) \;=\; \frac{A^i(0)}{1 - q^2/m_{1^+}^2}, \qquad i \;=\; 1,\, 2,\, 3 \qquad (3.17)$$

where m_{J^P} denotes the mass of the $\bar{s}c$ meson with spin J and parity P. This model has certain limitations: the pole-dominated form factor varies rapidly with q^2 near the end point, and the resonances associated with the form factors f^{0}, A^1, A^2 and A^3 are not well-determined experimentally. On the lattice, the form factors can be computed as a function of q^2 and assumptions such as pole dominance can be tested from first principles.

Decay Rates

The decay rates, computed from Eqns. (3.1–3.3), are given by [43]

$$\Gamma\left(D \to K\, l^+ \nu_l\right) \;=\; \frac{G_F^2\, |V_{cs}|^2}{192\,\pi^3\, m_D^3} \int_0^{q^2_{max}} dq^2\, \left[\lambda(q^2)\right]^{\frac{3}{2}} \times\, \left|f^+(q^2)\right|^2 \qquad (3.18)$$

$$\begin{aligned}\Gamma\left(D \to K^* l^+ \nu_l\right) \;&=\; \frac{G_F^2\, |V_{cs}|^2}{192\,\pi^3\, m_D^3} \int_0^{q^2_{max}} dq^2\, q^2 \left[\lambda(q^2)\right]^{\frac{1}{2}} \qquad (3.19)\\ &\times\; \left\{ \left|H^0(q^2)\right|^2 + \left|H^+(q^2)\right|^2 + \left|H^-(q^2)\right|^2 \right\}\end{aligned}$$

with

$$\lambda(q^2) = \left(m_D^2 + m_{K^{(*)}}^2 - q^2\right)^2 - 4\, m_D^2\, m_{K^{(*)}}^2 \qquad (3.20)$$

where $q_{max} = m_D - m_{K^{(*)}}$ is the maximum momentum transfer. The longitudinal and transverse contributions, H^0 and $H^{\pm}$ respectively, are given by [79]

$$\begin{aligned}H^0(q^2) \;&=\; \frac{1}{2\, m_{K^*}\sqrt{q^2}} \left\{ \frac{4\, m_D^2\, |\vec{p}_{K^*}|^2}{m_D + m_{K^*}}\, A^2(q^2) \right. \qquad (3.21)\\ &-\; \left. \left(m_D^2 - m_{K^*}^2 - q^2\right) (\, m_D + m_{K^*})\, A^1(q^2) \right\}\end{aligned}$$

$$H^{\pm}(q^2) \;=\; (\, m_D + m_{K^*})\, A^1(q^2) \pm \frac{2\, m_D\, |\vec{p}_{K^*}|}{m_D + m_{K^*}}\, V(q^2) \qquad (3.22)$$

where $\vec{p}_{K^*}$ is the momentum of the K^* in the D meson rest frame.

Branching Ratios

The branching ratio for a particular decay mode, A, is defined as follows:

$$B_A = \frac{\Gamma_A}{\Gamma_{total}} \qquad (3.23)$$

where Γ_{total} is the total decay width. The particle lifetime is given by

$$\tau = \frac{1}{\Gamma_{total}} = \frac{B_A}{\Gamma_A}\,. \qquad (3.24)$$

3.2 Experimental Results

This section gives a brief overview of the experimental data on semi-leptonic D decays. Following the recent review articles by Bellini [68] and Witherell [69], experimental results are quoted for both the $D \to K, K^*$ and $D \to \pi, \rho$ decay rates. The form factors, parameterising these decays, are also quoted where the experimental data is available.

Pseudoscalar to Pseudoscalar Decays

The largest and best measured semi-leptonic decay is $D \to K\, l^+\nu_l$. Several experiments [53]–[56] have measured the branching ratios $B(D^0 \to K^- l^+\nu_l)$ and $B(D^+ \to \bar{K}^0\, l^+\nu_l)$. From these experiments and measurements of the D^0 and D^+ total lifetimes, the semi-leptonic decay rates can be computed using Eqn. (3.24). The decay rates $\Gamma(D^0 \to K^- l^+\nu_l)$ and $\Gamma(D^+ \to \bar{K}^0\, l^+\nu_l)$ should coincide by isospin symmetry. The world-average value [68] is

$$\Gamma(D \to K\, l^+\nu_l) = (7.1 \pm 0.6) \times 10^{10}\, s^{-1}. \tag{3.25}$$

However, taking just the (larger) $D^0 \to K^- l^+\nu_l$ sample, and assuming isospin symmetry, a different world average is obtained [69] with $\Gamma(D \to K\, l^+\nu_l) = (9.0 \pm 0.5) \times 10^{10}\, s^{-1}$ where this value includes new data from CLEO [57].

The form factor $f^+(q^2)$ describes the increasing overlap of the D and K wave-functions, as the energy of the K meson decreases: at $q^2 = 0$ the form factor is at a minimum; at $q^2_{max} = (m_D - m_K)^2$ the K meson is at rest (in the D meson rest frame), the overlap is as large as possible and the form factor is at a maximum. The CLEO Collaboration [57] have measured this distribution with the largest $D^0 \to K^- l^+\nu_l$ sample. Assuming pole dominance, the data is fitted to Eqn. (3.15) to obtain

$$m_{1^-} = 2.00 \pm 0.12 \pm 0.18\, GeV \tag{3.26}$$

which is in excellent agreement with the mass of the D_S^* meson, given in Table 2.5; this is the closest resonance with the correct quantum numbers.

The form factor normalisation $f^+(0)$ is obtained by integrating the semi-leptonic width, given by Eqn. (3.18), over q^2; assuming pole dominance and a value for $|V_{cs}|$. The world-average value [68] is

$$f^+(0) = 0.70 \pm 0.03 \tag{3.27}$$

which is consistent with the value $f^+(0) = 0.77 \pm 0.04$ obtained from just the $D^0 \to K^- l^+ \nu_l$ sample [69].

The Cabibbo-suppressed semi-leptonic decay $D \to \pi\, l^+ \nu_l$ has also been observed. A measurement of the branching ratio $B(D \to \pi\, l^+\nu_l)\,/\,B(D \to K\, l^+\nu_l)$ allows a determination of $f_\pi^+(0)\,/\,f_K^+(0)$ since $|V_{cd}\,/V_{cs}|$ is known from unitarity. This ratio is predicted to lie in the range 0.7–1.4 . The Mark III Collaboration [58] found $B(D^0 \to \pi^- l^+ \nu_l) = 0.39\,^{+\,0.23}_{-\,0.11} \pm 0.04$ which corresponds to the ratio $f_\pi^+(0)\,/\,f_K^+(0) = 1.0\,^{+\,0.6}_{-\,0.3} \pm 0.1$ [69]. More recently, the CLEO Collaboration [59] obtained

$$\frac{f_\pi^+(0)}{f_K^+(0)} = 1.29 \pm 0.21 \pm 0.11 \tag{3.28}$$

where the errors in this ratio are still very large. Finally, the total decay rate $D \to \pi\, l^+ \nu_l$ quoted in [69] is

$$\Gamma(D \to \pi\, l^+ \nu_l) = (1.2 \pm 0.3) \times 10^{10}\, s^{-1}. \tag{3.29}$$

Pseudoscalar to Vector Decays

The semi-leptonic decay $D \to K^*\, l^+ \nu_l$ has also been observed. The branching ratios $B(D^0 \to K^{*-} l^+ \nu_l)$ and $B(D^+ \to \bar{K}^{*0}\, l^+ \nu_l)$ have been measured by a number of experiments [57, 60]–[63]. From these experiments, and measurements of the D^0 and D^+ total lifetimes, the semi-leptonic decay rates can be computed using Eqn. (3.24). The decay rates $\Gamma(D^0 \to K^{*-} l^+ \nu_l)$ and $\Gamma(D^+ \to \bar{K}^{*0}\, l^+ \nu_l)$ should, once again, coincide by isospin symmetry. The world-average value [69] is

$$\Gamma(D \to K^*\, l^+ \nu_l) = (5.1 \pm 0.5) \times 10^{10}\, s^{-1}. \tag{3.30}$$

The world-average values [69] for the vector and axial form factors are as follows:

$$V(0) = 1.16 \pm 0.16 \tag{3.31}$$

$$A^1(0) = 0.61 \pm 0.05 \tag{3.32}$$

$$A^2(0) = 0.45 \pm 0.09 \tag{3.33}$$

where the decay rate is dominated by the A^1 form factor. Thus experiments have concentrated on the following form factor ratios: $R_V = V(0)\,/A^1(0)$ and $R_2 = A^2(0)\,/A^1(0)$ which are obtained by fitting the angular distributions. The world-average values [68] are as follows:

$$R_V = 1.9 \pm 0.2 \qquad \text{and} \qquad R_2 = 0.74 \pm 0.14 \tag{3.34}$$

with

$$\frac{\Gamma_L}{\Gamma_T} = 1.2 \pm 0.1 \tag{3.35}$$

where the decay rate ratio $\Gamma_L\,/\,\Gamma_T$ is computed from the longitudinal and transverse contributions corresponding to the terms H^0 and H^{+}_{-} respectively, given in Eqn. (3.19). For the Cabibbo-suppressed decay $D \to \rho\ l^+\nu_l$ there exists only an upper-limit on the branching ratio: $B(D \to \rho\ l^+\nu_l) < 0.37$ with a 90% confidence-level [55].

3.3 Three-Point Correlator Fits

Recall from Section 1.7, weak matrix elements are extracted by studying the time-dependence of three-point functions. This section describes the construction of three-point functions corresponding to the semi-leptonic decays $D \to K,\ K^*$. These correlators are computed over a range of momentum transfer. Results are presented for the form factors parameterising these decays. The form factors are obtained from three-point correlator fits which are described in detail.

Three-Point Functions

The weak matrix elements describing the semi-leptonic decays $D \to K$ and $D \to K^*$ are obtained from the following three-point functions:

$$
\begin{aligned}
G^{(3)\,\mu}_{K\to D}(t_y, t_x, 0; \vec{p}, \vec{q}\,) &= \sum_{\vec{x},\vec{y}} e^{i\frac{2\pi}{L}\vec{q}\cdot\vec{x}}\, e^{i\frac{2\pi}{L}\vec{p}\cdot\vec{y}} \\
&\times \left\langle 0 \,\middle|\, \Omega_D(y)\, J^\mu_W(x)\, \Omega^\dagger_K(0) \,\middle|\, 0 \right\rangle
\end{aligned}
\tag{3.36}
$$

$$
\begin{aligned}
G^{(3)\,\mu\nu}_{K^*\to D}(t_y, t_x, 0; \vec{p}, \vec{q}\,) &= \sum_{\vec{x},\vec{y}} e^{i\frac{2\pi}{L}\vec{q}\cdot\vec{x}}\, e^{i\frac{2\pi}{L}\vec{p}\cdot\vec{y}} \\
&\times \left\langle 0 \,\middle|\, \Omega_D(y)\, J^\mu_W(x)\, \Omega^{\nu\dagger}_{K^*}(0) \,\middle|\, 0 \right\rangle
\end{aligned}
\tag{3.37}
$$

where Ω_D is the interpolating operator to annihilate the pseudoscalar D meson; $\Omega^\dagger_K$ and $\Omega^{\nu\dagger}_{K^*}$ are the interpolating operators to create the pseudoscalar K meson and the vector K^* meson respectively; and J^μ_W is the $O(a)$-improved lattice operator corresponding to the continuum weak current $\bar{s}\,\gamma^\mu(1-\gamma^5)\,c$. The vector current $V^\mu = \bar{s}\,\gamma^\mu c$ and the axial current $A^\mu = \bar{s}\,\gamma^\mu\gamma^5 c$ are related to the continuum ones by renormalisation constants Z_V and Z_A respectively.

Recall from Section 1.7, the pseudoscalar-to-pseudoscalar and vector-to-pseudoscalar three-point correlators can be constructed from quark propagators using Eqns. (1.116) and (1.117). The quark propagators were computed on a $24^3 \times 48$ space-time lattice, as detailed in Section 2.1. The heavy-light component of the three-point correlator is computed as an extended quark propagator using a light quark source which is Jacobi smeared at the sink. In this study, the D meson is fixed at the mid-point of the lattice where temporal boundary conditions allow the correlators to be symmeterised about $t_y = 24$ using Euclidean time-reversal symmetry.

Figure 3.1 shows the $D \to K$, K^* three-point correlator constructed from quark propagators where $\Gamma^\nu = \gamma^5$ and $\Gamma^\nu = \gamma^\nu$ correspond to the K and K^* mesons respectively and $\Lambda^\mu = \gamma^\mu(1-\gamma^5)$ corresponds to the weak current operator. The bold 'propagator' line denotes the extended quark propagator.

Three-Point Fit Function

Following Eqns. (1.124) and (1.125), the time-dependence of the $D \to K,\, K^*$ three-point correlators is given by

$$C(t; \vec{p}_D, \vec{q}\,) = Q\, e^{-R(24-t)}\, e^{-St} \tag{3.38}$$

with

$$R = E_D(\vec{p}_D) \qquad \text{and} \qquad S = E_{K^{(*)}}(\vec{p}_D + \vec{q}\,) \tag{3.39}$$

where the fit parameters R and S are just the energies of the D and $K^{(*)}$ mesons respectively. For the decay $D \to K$, the fit parameter Q is related to the matrix element in Eqn. (3.1) by

$$\begin{aligned} Q^\mu &= \Delta(\mu) \times \frac{Z_D(\vec{p}_D)\, Z_K(\vec{p}_D + \vec{q}\,)}{4\, E_D(\vec{p}_D)\, E_K(\vec{p}_D + \vec{q}\,)} \\ &\times \left\langle K,\, \vec{p}_D + \vec{q} \,\middle|\, V^\mu \,\middle|\, D,\, \vec{p}_D \right\rangle \end{aligned} \tag{3.40}$$

with

$$\Delta(\sigma = 0) = -1 \quad \text{and} \quad \Delta(\sigma = 1, 2, 3) = 1\,. \tag{3.41}$$

Similarly, for the decay $D \to K^*$, Q is related to the matrix element in Eqn. (3.2) by

$$\begin{aligned} Q^{\mu\nu} &= \Delta(\mu)\, \Delta(\nu) \times \frac{Z_D(\vec{p}_D)\, Z_{K^*}(\vec{p}_D + \vec{q}\,)}{4\, E_D(\vec{p}_D)\, E_{K^*}(\vec{p}_D + \vec{q}\,)} \\ &\times \sum_{r=1}^{3} \xi_r^\nu(\vec{p}_D + \vec{q}\,) \left\langle K_r^*,\, \vec{p}_D + \vec{q} \,\middle|\, (V - A)^\mu \,\middle|\, D,\, \vec{p}_D \right\rangle \end{aligned} \tag{3.42}$$

where the matrix element in Eqn. (3.42) is averaged over the three polarisation states of the K^* meson. $\Delta(\mu)$ relates the matrix elements computed, using Eqns. (3.36) and (3.37), to the $D \to K,\, K^*$ matrix elements of interest. On the lattice, the time-reversed matrix elements are computed because the extended heavy quark propagator is computationally less expensive than the extended light quark propagator required to compute the $D \to K,\, K^*$ matrix elements directly.

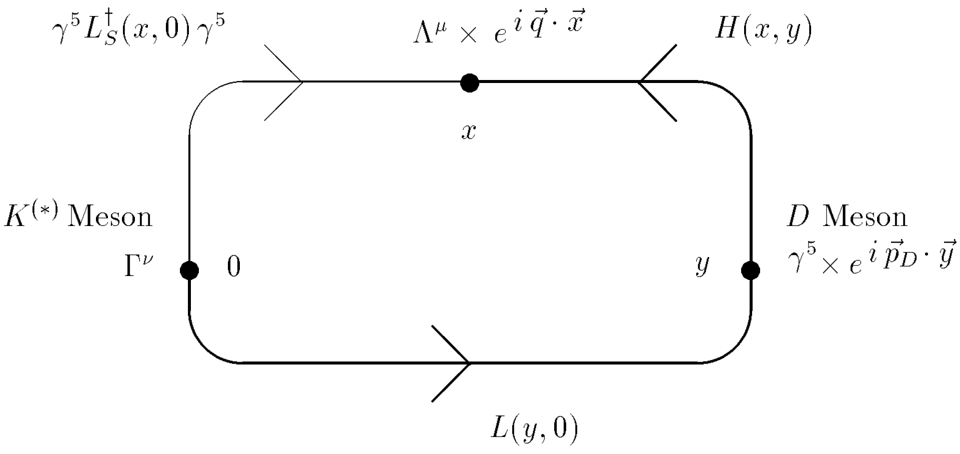

Figure 3.1: The $D \to K$, K^* three-point correlator.

Three-Point Correlators

Following Eqns. (3.36) and (3.37), the three-point correlators $C^{\mu}_{K\to D}(t;\vec{p}_D,\vec{q}\,)$ and $C^{\mu\nu}_{K^*\to D}(t;\vec{p}_D,\vec{q}\,)$ were computed for all values of the Lorentz indices μ and ν. Table 3.1 shows the Lorentz channels computed; channels 1–4 correspond to the pseudoscalar-to-pseudoscalar correlators; channels 5–36 correspond to the vector-to-pseudoscalar correlators; and channels 37–60 were computed for a UKQCD study of the decay $b \to s\gamma$ [18]. These correlators were computed for two values of the D meson momentum with $\vec{p}_D = (0,0,0)$ and $(1,0,0)$ in units of $\pi/12\,a$, and for all values of the momentum transfer with $|\vec{q}\,| \leq \pi/6\,a$. Table 3.2 and Table 3.3 show the values of momentum transfer computed, with the corresponding momentum of the $K^{(*)}$ meson, for $\vec{p}_D = (0,0,0)$ and $(1,0,0)$ respectively.

In practice, results corresponding to momentum channels with $|\,\vec{p}_{K^{(*)}}\,| > \pi/12\,a$ are not quoted since fits to three-point correlators with 'high' momentum either fail or give an unacceptable chi-squared ($\chi^2/dof \gg 1$). Recall from Section 2.3, the noise in the two-point signal increases rapidly with momentum because the number of gauge configurations is finite. For three-point correlators, this signal-to-noise problem is complicated by the finite separation of the D and $K^{(*)}$ mesons. In many cases, the three-point signal fails to 'plateau' which indicates that the temporal extent of the lattice is too short.

Chan	Γ^ν	Λ^μ	Chan	Γ^ν	Λ^μ	Chan	Γ^ν	Λ^μ
1	γ^5	γ^1	21	γ^1	$\gamma^1\gamma^5$	41	γ^1	σ_{13}
2	γ^5	γ^2	22	γ^1	$\gamma^2\gamma^5$	42	γ^1	σ_{12}
3	γ^5	γ^3	23	γ^1	$\gamma^3\gamma^5$	43	γ^2	σ_{34}
4	γ^5	γ^4	24	γ^1	$\gamma^4\gamma^5$	44	γ^2	σ_{24}
5	γ^1	γ^1	25	γ^2	$\gamma^1\gamma^5$	45	γ^2	σ_{23}
6	γ^1	γ^2	26	γ^2	$\gamma^2\gamma^5$	46	γ^2	σ_{14}
7	γ^1	γ^3	27	γ^2	$\gamma^3\gamma^5$	47	γ^2	σ_{13}
8	γ^1	γ^4	28	γ^2	$\gamma^4\gamma^5$	48	γ^2	σ_{12}
9	γ^2	γ^1	29	γ^3	$\gamma^1\gamma^5$	49	γ^3	σ_{34}
10	γ^2	γ^2	30	γ^3	$\gamma^2\gamma^5$	50	γ^3	σ_{24}
11	γ^2	γ^3	31	γ^3	$\gamma^3\gamma^5$	51	γ^3	σ_{23}
12	γ^2	γ^4	32	γ^3	$\gamma^4\gamma^5$	52	γ^3	σ_{14}
13	γ^3	γ^1	33	γ^4	$\gamma^1\gamma^5$	53	γ^3	σ_{13}
14	γ^3	γ^2	34	γ^4	$\gamma^2\gamma^5$	54	γ^3	σ_{12}
15	γ^3	γ^3	35	γ^4	$\gamma^3\gamma^5$	55	γ^4	σ_{34}
16	γ^3	γ^4	36	γ^4	$\gamma^4\gamma^5$	56	γ^4	σ_{24}
17	γ^4	γ^1	37	γ^1	σ_{34}	57	γ^4	σ_{23}
18	γ^4	γ^2	38	γ^1	σ_{24}	58	γ^4	σ_{14}
19	γ^4	γ^3	39	γ^1	σ_{23}	59	γ^4	σ_{13}
20	γ^4	γ^4	40	γ^1	σ_{14}	60	γ^4	σ_{12}

Table 3.1: Lorentz channels for three-point correlators.

Chan	$\vec{p}_K$	$\vec{q}$	Chan	$\vec{p}_K$	$\vec{q}$
1	(0,0,0)	(0,0,0)	10	(0,1,-1)	(0,1,-1)
2	(1,0,0)	(1,0,0)	11	(1,1,1)	(1,1,1)
3	(0,1,0)	(0,1,0)	12	(1,1,-1)	(1,1,-1)
4	(0,0,1)	(0,0,1)	13	(1,-1,1)	(1,-1,1)
5	(1,1,0)	(1,1,0)	14	(-1,1,1)	(-1,1,1)
6	(1,0,1)	(1,0,1)	15	(2,0,0)	(2,0,0)
7	(0,1,1)	(0,1,1)	16	(0,2,0)	(0,2,0)
8	(1,-1,0)	(1,-1,0)	17	(0,0,2)	(0,0,2)
9	(-1,0,1)	(-1,0,1)	18	N/A	N/A

Table 3.2: Momentum channels for correlators with $\vec{p}_D = (0, 0, 0)$, in units $\pi/12\,a$.

Chan	$\vec{p}_K$	$\vec{q}$	Chan	$\vec{p}_K$	$\vec{q}$
1	(0,0,0)	(-1,0,0)	11	(1,0,-1)	(0,0,-1)
2	(1,0,0)	(0,0,0)	12	(0,1,1)	(-1,1,1)
3	(-1,0,0)	(-2,0,0)	13	(0,1,-1)	(-1,1,-1)
4	(0,1,0)	(-1,1,0)	14	(0,-1,1)	(-1,-1,1)
5	(0,-1,0)	(-1,-1,0)	15	(0,-1,-1)	(-1,-1,-1)
6	(0,0,1)	(-1,0,1)	16	(1,1,1)	(0,1,1)
7	(0,0,-1)	(-1,0,-1)	17	(1,-1,1)	(0,-1,1)
8	(1,1,0)	(0,1,0)	18	(1,1,-1)	(0,1,-1)
9	(1,0,1)	(0,0,1)	19	(1,-1,-1)	(0,-1,-1)
10	(1,-1,0)	(0,-1,0)	20	(2,0,0)	(1,0,0)

Table 3.3: Momentum channels for correlators with $\vec{p}_D = (1, 0, 0)$, in units $\pi/12\,a$.

Three-Point Correlator Data

Three-point correlators were computed for a fixed charm quark mass with hopping parameter $\kappa_h = 0.129$; for two values of the strange quark mass with $\kappa_s = 0.14144$ and 0.14226; and for three values of the light quark mass with $\kappa_l = 0.14144$, 0.14226, and 0.14262. These hopping parameter values correspond to six kappa-independent three-point correlators.

For each kappa combination, the correlator data consists of 2220 (37 momentum $\times$ 60 Lorentz) channels per timeslice. To reduce storage overheads only timeslices t = 7–16 and t = 32–41 are saved; these intervals corresponds to the 'forward' and 'backward' correlator components respectively which are well separated in Euclidean time. Prior to fitting, the configuration data is folded by averaging the corresponding timeslices from the two halves of the lattice.

To increase statistics, the correlator data is averaged over all equivalent momentum channels; and over all Lorentz channels corresponding to the same matrix element. For example, when $\vec{p}_D = (0, 0, 0)$ the momentum channels with $\vec{p}_{K^{(*)}} = (1, 0, 0)$, (0,1,0) and (0,0,1), in units of $\pi/12\,a$, are equivalent and their average corresponds to a decay with momentum transfer $|\vec{q}\,| = \pi/12\,a$.

The $D \to K$, K^* form factors are obtained by performing simultaneous fits to all Lorentz-independent three-point correlators. The energies and the corresponding two-point amplitudes in Eqns. (3.38)–(3.41) are constrained to the values obtained from two-point correlator fits, as detailed in Chapter 2. In the following section, the 'time-independent' correlators are defined as three-point correlators with these two-point factors removed. Thus, each Lorentz-independent correlator component is fitted (simultaneously) to a constant or 'plateau'. The masses and energies corresponding to the form factor parameterisation are also constrained to values obtained from two-point correlator fits.

Correlated chi-squared fits are performed but only correlations between timeslices corresponding to the same matrix element are kept since different matrix elements may have different systematic errors. For each correlator component, the fit interval is t=11–13; for t=12 the weak current operator is equidistant from both the D and $K^{(*)}$ mesons.

Pseudoscalar-to-Pseudoscalar Fits

For each momentum channel, the form factors f^+ and f^0 are obtained by performing a simultaneous fit to all Lorentz-independent pseudoscalar-to-pseudoscalar three-point correlators. Using the (second) form factor parameterisation, given by Eqn. (3.11), the time-independent correlators can be written as follows:

$$Z_V \times \left\langle K \middle| \gamma^0 \middle| D \right\rangle = (E_D + E_K) f^+ + (E_D - E_K) f^- \tag{3.43}$$

$$Z_V \times \left\langle K \middle| \gamma^i \middle| D \right\rangle = (p_D + p_K)^i f^+ + (p_D - p_K)^i f^- \tag{3.44}$$

where $\left\langle K \middle| \gamma^0 \middle| D \right\rangle$ and $\left\langle K \middle| \gamma^i \middle| D \right\rangle$ denote the temporal and spatial correlator components respectively, and Z_V is the renormalisation constant corresponding to the lattice vector current. Thus, in general there are (at least) two Lorentz-independent pseudoscalar-to-pseudoscalar three-point correlators.

However, for the momentum channel $(0,0,0) \to (0,0,0)$ there is only one non-zero component. Using the (first) form factor parameterisation, given by Eqn. (3.1), the temporal component is given by

$$Z_V \times \left\langle K \middle| \gamma^0 \middle| D \right\rangle = (m_D + m_K) f^0 \tag{3.45}$$

where the momentum of both the D and K mesons is zero. Thus, for this channel the form factor f^0 is obtained from a one-parameter fit; there is no determination of the form factor f^+. For the momentum channel $(1,0,0) \to (0,1,0)$ there are three Lorentz-independent correlator components: one temporal and two spatial. Thus, the form factors f^+ and f^0 are obtained from a two-parameter fit which is over-determined.

The form factors f^+ and f^0, obtained from simultaneous fits to pseudoscalar-to-pseudoscalar correlators, are given in Table 3.4 with the corresponding q^2 values computed from the meson masses, given in Tables 2.1 and 2.3. In general, the chi-squared values indicate a good fit to the data for all kappa combinations. However, for the channel $(1,0,0) \to (-1,0,0)$ the fit chi-squared are on the high side which suggests that one of the correlator components has not plateaued within the fit window.

$\vec{p}_D$	$\vec{p}_K$	κ_l	κ_{l_s}	$a^2\,q^2$	f^+/Z_V	χ^2/dof	f^0/Z_V
(0,0,0)	(0,0,0)	0.14144	0.14144	$0.175\,^{+\,3}_{-\,1}$	N/A	0.8	$1.03\,^{+\,6}_{-\,3}$
			0.14226	$0.209\,^{+\,3}_{-\,2}$	N/A	1.5	$0.99\,^{+\,7}_{-\,3}$
		0.14226	0.14144	$0.188\,^{+\,4}_{-\,2}$	N/A	1.1	$1.04\,^{+\,7}_{-\,4}$
			0.14226	$0.229\,^{+\,5}_{-\,2}$	N/A	1.9	$1.00\,^{+\,9}_{-\,3}$
		0.14262	0.14144	$0.195\,^{+\,4}_{-\,2}$	N/A	0.8	$1.05\,^{+\,7}_{-\,4}$
			0.14226	$0.241\,^{+\,6}_{-\,3}$	N/A	1.6	$1.02\,^{+\,9}_{-\,4}$
(0,0,0)	(1,0,0)	0.14144	0.14144	$0.034\,^{+\,2}_{-\,1}$	$0.91\,^{+\,5}_{-\,2}$	0.7	$0.87\,^{+\,4}_{-\,2}$
			0.14226	$0.053\,^{+\,2}_{-\,1}$	$0.88\,^{+\,5}_{-\,2}$	0.8	$0.81\,^{+\,4}_{-\,2}$
		0.14226	0.14144	$0.037\,^{+\,3}_{-\,1}$	$0.90\,^{+\,5}_{-\,3}$	0.6	$0.85\,^{+\,5}_{-\,2}$
			0.14226	$0.057\,^{+\,3}_{-\,1}$	$0.86\,^{+\,6}_{-\,3}$	0.7	$0.78\,^{+\,5}_{-\,3}$
		0.14262	0.14144	$0.038\,^{+\,3}_{-\,1}$	$0.88\,^{+\,5}_{-\,3}$	0.5	$0.83\,^{+\,5}_{-\,3}$
			0.14226	$0.060\,^{+\,3}_{-\,2}$	$0.84\,^{+\,6}_{-\,4}$	0.6	$0.75\,^{+\,6}_{-\,3}$
(1,0,0)	(0,0,0)	0.14144	0.14144	$0.147\,^{+\,3}_{-\,2}$	$1.25\,^{+\,8}_{-\,6}$	1.2	$0.98\,^{+\,6}_{-\,5}$
			0.14226	$0.185\,^{+\,3}_{-\,2}$	$1.33\,^{+\,10}_{-\,7}$	1.1	$0.96\,^{+\,7}_{-\,5}$
		0.14226	0.14144	$0.163\,^{+\,4}_{-\,2}$	$1.27\,^{+\,9}_{-\,7}$	0.6	$0.99\,^{+\,6}_{-\,5}$
			0.14226	$0.208\,^{+\,5}_{-\,2}$	$1.40\,^{+\,12}_{-\,10}$	0.2	$1.00\,^{+\,8}_{-\,6}$
		0.14262	0.14144	$0.172\,^{+\,5}_{-\,2}$	$1.26\,^{+\,9}_{-\,9}$	0.9	$0.99\,^{+\,6}_{-\,6}$
			0.14226	$0.222\,^{+\,6}_{-\,3}$	$1.42\,^{+\,13}_{-\,14}$	0.5	$1.01\,^{+\,7}_{-\,7}$

Table 3.4: The $D \to K$ form factors with momentum in units of $\pi/12\,a$ and $\kappa_h = 0.129$.

$\vec{p}_D$	$\vec{p}_K$	κ_l	κ_{l_s}	$a^2\,q^2$	f^+/Z_V	χ^2/dof	f^0/Z_V
(1,0,0)	(1,0,0)	0.14144	0.14144	$0.134\,^{+2}_{-1}$	$1.13\,^{+9}_{-6}$	0.1	$0.91\,^{+8}_{-6}$
			0.14226	$0.155\,^{+3}_{-1}$	$1.12\,^{+11}_{-8}$	0.3	$0.82\,^{+9}_{-7}$
		0.14226	0.14144	$0.138\,^{+3}_{-1}$	$1.08\,^{+13}_{-10}$	0.6	$0.78\,^{+14}_{-11}$
			0.14226	$0.162\,^{+3}_{-1}$	$1.07\,^{+17}_{-13}$	0.6	$0.64\,^{+15}_{-12}$
		0.14262	0.14144	$0.141\,^{+3}_{-2}$	$0.99\,^{+17}_{-15}$	1.0	$0.59\,^{+18}_{-19}$
			0.14226	$0.165\,^{+4}_{-2}$	$0.94\,^{+24}_{-20}$	0.8	$0.41\,^{+21}_{-20}$
(1,0,0)	(−1,0,0)	0.14144	0.14144	$-0.140\,^{+2}_{-1}$	$0.60\,^{+4}_{-2}$	2.2	$0.72\,^{+5}_{-3}$
			0.14226	$-0.119\,^{+3}_{-1}$	$0.58\,^{+4}_{-3}$	1.8	$0.69\,^{+5}_{-4}$
		0.14226	0.14144	$-0.136\,^{+3}_{-1}$	$0.60\,^{+5}_{-3}$	3.4	$0.71\,^{+6}_{-4}$
			0.14226	$-0.113\,^{+3}_{-1}$	$0.59\,^{+7}_{-4}$	2.8	$0.69\,^{+8}_{-5}$
		0.14262	0.14144	$-0.133\,^{+3}_{-2}$	$0.58\,^{+8}_{-5}$	3.8	$0.70\,^{+9}_{-6}$
			0.14226	$-0.109\,^{+4}_{-2}$	$0.58\,^{+10}_{-7}$	3.5	$0.68\,^{+12}_{-9}$
(1,0,0)	(0,1,0)	0.14144	0.14144	$-0.003\,^{+2}_{-1}$	$0.78\,^{+4}_{-3}$	1.2	$0.78\,^{+4}_{-3}$
			0.14226	$0.018\,^{+3}_{-1}$	$0.75\,^{+5}_{-3}$	1.1	$0.73\,^{+4}_{-3}$
		0.14226	0.14144	$0.001\,^{+3}_{-1}$	$0.76\,^{+5}_{-4}$	0.5	$0.76\,^{+5}_{-4}$
			0.14226	$0.025\,^{+3}_{-1}$	$0.73\,^{+6}_{-5}$	0.3	$0.70\,^{+5}_{-4}$
		0.14262	0.14144	$0.004\,^{+3}_{-2}$	$0.74\,^{+6}_{-5}$	0.2	$0.74\,^{+6}_{-5}$
			0.14226	$0.028\,^{+4}_{-2}$	$0.71\,^{+8}_{-6}$	0.1	$0.68\,^{+7}_{-6}$

Table 3.4: (Cont.)

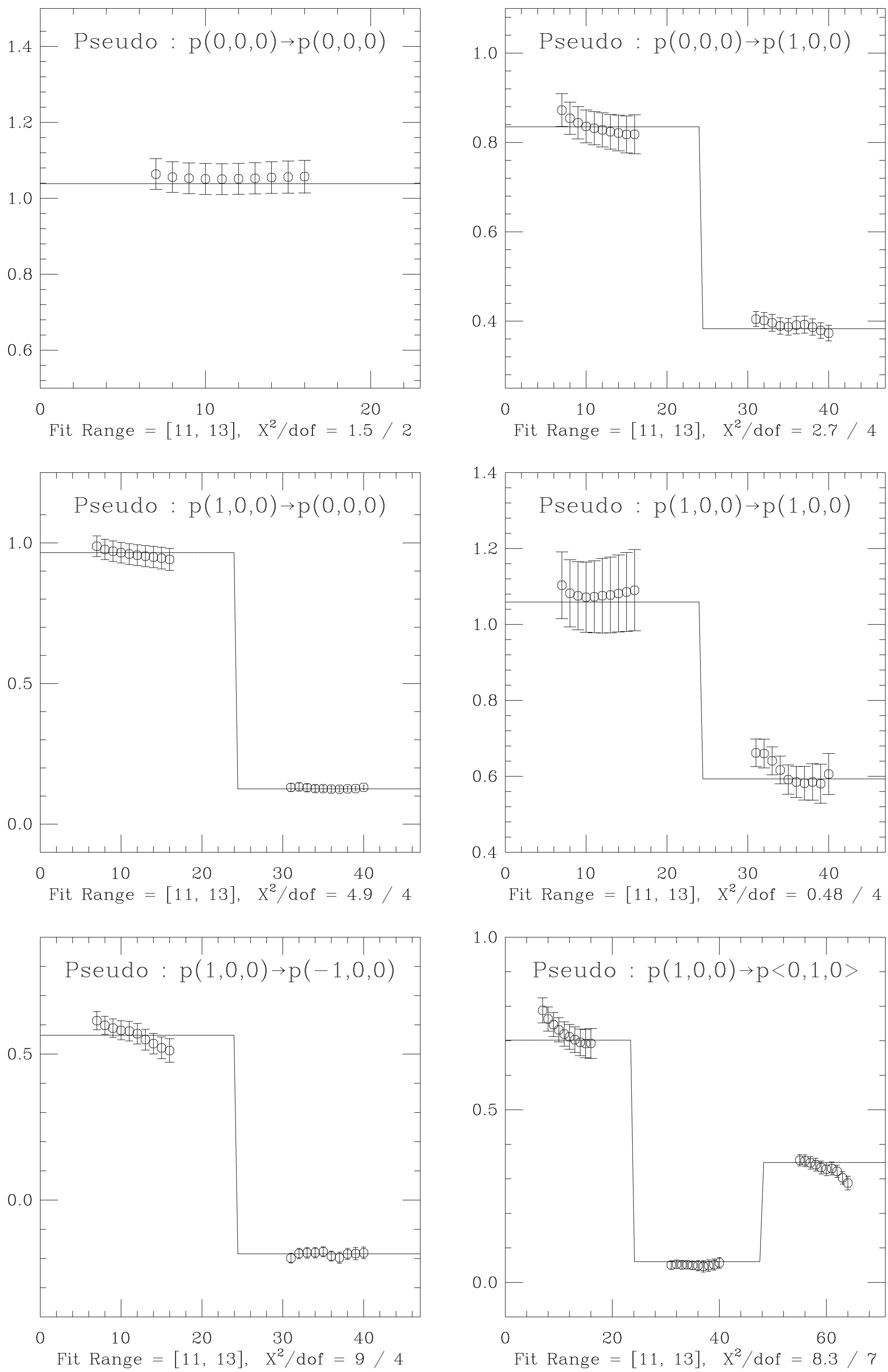

Figure 3.2: Pseudoscalar-to-Pseudoscalar plateau plots with $\kappa_l = \kappa_{l_s} = 0.14144$ and $\kappa_h = 0.129$. Momentum in units of $\pi/12\,a$.

Figure 3.2 shows six 'plateau' plots, one for each momentum channel, corresponding to the simultaneous fit of Eqns. (3.43) and (3.44) to the temporal and spatial correlator components respectively. The plateau plot shows each Lorentz-independent component fitted (simultaneously) to a constant; the time-dependence has been removed by multiplying by the appropriate two-point factor. These plots serve as a guide to the 'quality' of the plateau in the three-point data.

Vector-to-Pseudoscalar Vector Fits

For each momentum channel, the vector form factor is obtained by performing a simultaneous fit to all Lorentz-independent three-point correlators. Multiplying both sides of Eqn. (3.2) by a 'dummy' polarisation vector, summing over polarisation states of the vector K^* meson, and using the polarisation sum identity, given in Eqn. (1.107), one obtains the form factor parameterisation corresponding to the polarisation-averaged vector three-point correlator:

$$Z_V \times V^{\mu\nu} = \left(\frac{p_{K^*}^{\beta} p_{K^*}^{\nu}}{m_{K^*}^2} - g^{\beta\nu} \right) \times \frac{2\,V}{m_D + m_{K^*}} \, \varepsilon_{\mu\gamma\delta\beta} \, p_D^{\gamma} \, p_{K^*}^{\delta} \tag{3.46}$$

with

$$V^{\mu\nu} = \sum_{r=1}^{3} \xi_r^{\nu} \left\langle K_r^* \middle| V^{\mu} \middle| D \right\rangle \tag{3.47}$$

where $V^{\mu\nu}$ is the time-independent three-point correlator data, and Z_V is the renormalisation constant corresponding to the lattice vector current.

The form factor V, obtained from simultaneous fits to vector-to-pseudoscalar vector correlators, is given in Table 3.5 with the corresponding q^2 values computed from the meson masses, given in Tables 2.1 and 2.3. For the momentum channel $(0,0,0) \to (0,0,0)$ all Lorentz components are zero and there is no determination of the vector form factor. In general, there is only one Lorentz-independent component and V is obtained from a one-parameter fit. However, for the momentum channel $(1,0,0) \to (0,1,0)$ there are three Lorentz-independent correlators: a mixed temporal and spatial component, and two spatial components corresponding to the longitudinal and transverse contributions with respect to the momentum of the D meson. Thus, for this channel V is obtained from a one-parameter fit which is over-determined.

$\vec{p}_D$	$\vec{p}_K$	κ_l	κ_{l_s}	$a^2\, q^2$	V/Z_V	χ^2/dof
(0,0,0)	(0,0,0)	0.14144	0.14144	$0.103\,^{+\,3}_{-\,3}$	N/A	N/A
			0.14226	$0.120\,^{+\,4}_{-\,4}$	N/A	N/A
		0.14226	0.14144	$0.104\,^{+\,4}_{-\,4}$	N/A	N/A
			0.14226	$0.122\,^{+\,6}_{-\,5}$	N/A	N/A
		0.14262	0.14144	$0.104\,^{+\,5}_{-\,4}$	N/A	N/A
			0.14226	$0.124\,^{+\,8}_{-\,7}$	N/A	N/A
(0,0,0)	(1,0,0)	0.14144	0.14144	$-0.010\,^{+\,2}_{-\,2}$	$1.49\,^{+\,8}_{-\,5}$	0.17
			0.14226	$0.000\,^{+\,3}_{-\,2}$	$1.47\,^{+\,10}_{-\,5}$	0.55
		0.14226	0.14144	$-0.012\,^{+\,3}_{-\,2}$	$1.45\,^{+\,11}_{-\,7}$	0.74
			0.14226	$-0.001\,^{+\,4}_{-\,3}$	$1.41\,^{+\,14}_{-\,10}$	1.94
		0.14262	0.14144	$-0.012\,^{+\,3}_{-\,3}$	$1.43\,^{+\,16}_{-\,12}$	0.96
			0.14226	$-0.001\,^{+\,5}_{-\,4}$	$1.36\,^{+\,20}_{-\,16}$	1.69
(1,0,0)	(0,0,0)	0.14144	0.14144	$0.067\,^{+\,3}_{-\,3}$	$1.46\,^{+\,13}_{-\,8}$	0.01
			0.14226	$0.085\,^{+\,4}_{-\,4}$	$1.38\,^{+\,18}_{-\,12}$	0.30
		0.14226	0.14144	$0.068\,^{+\,4}_{-\,4}$	$1.35\,^{+\,22}_{-\,16}$	0.20
			0.14226	$0.089\,^{+\,7}_{-\,6}$	$1.28\,^{+\,30}_{-\,23}$	0.32
		0.14262	0.14144	$0.069\,^{+\,6}_{-\,5}$	$1.40\,^{+\,33}_{-\,30}$	0.38
			0.14226	$0.092\,^{+\,9}_{-\,8}$	$1.39\,^{+\,46}_{-\,40}$	0.37

Table 3.5: The $D \to K^*$ vector form factor with momentum in units of $\pi/12\,a$ and $\kappa_h = 0.129$.

$\vec{p}_D$	$\vec{p}_K$	κ_l	κ_{l_s}	$a^2\,q^2$	V/Z_V	χ^2/dof
(1,0,0)	(1,0,0)	0.14144	0.14144	$0.083\,^{+\,2}_{-\,2}$	$2.7\,^{+\,5}_{-\,4}$	0.71
			0.14226	$0.096\,^{+\,3}_{-\,3}$	$3.0\,^{+\,6}_{-\,5}$	1.33
		0.14226	0.14144	$0.082\,^{+\,3}_{-\,3}$	$3.4\,^{+\,8}_{-\,6}$	3.15
			0.14226	$0.095\,^{+\,4}_{-\,4}$	$4.1\,^{+\,10}_{-\,9}$	6.35
		0.14262	0.14144	$0.082\,^{+\,4}_{-\,3}$	$3.7\,^{+\,12}_{-\,10}$	5.65
			0.14226	$0.096\,^{+\,6}_{-\,5}$	$5.2\,^{+\,15}_{-\,13}$	8.75
(1,0,0)	(–1,0,0)	0.14144	0.14144	$-0.191\,^{+\,2}_{-\,2}$	$0.90\,^{+\,9}_{-\,5}$	0.08
			0.14226	$-0.179\,^{+\,3}_{-\,3}$	$0.90\,^{+\,11}_{-\,7}$	0.06
		0.14226	0.14144	$-0.192\,^{+\,3}_{-\,3}$	$0.85\,^{+\,13}_{-\,11}$	0.04
			0.14226	$-0.179\,^{+\,4}_{-\,4}$	$0.87\,^{+\,17}_{-\,14}$	0.01
		0.14262	0.14144	$-0.192\,^{+\,4}_{-\,3}$	$0.80\,^{+\,21}_{-\,18}$	0.02
			0.14226	$-0.179\,^{+\,6}_{-\,5}$	$0.81\,^{+\,28}_{-\,25}$	0.07
(1,0,0)	(0,1,0)	0.14144	0.14144	$-0.054\,^{+\,2}_{-\,2}$	$1.22\,^{+\,8}_{-\,6}$	1.15
			0.14226	$-0.042\,^{+\,3}_{-\,3}$	$1.18\,^{+\,10}_{-\,7}$	1.40
		0.14226	0.14144	$-0.055\,^{+\,3}_{-\,3}$	$1.11\,^{+\,12}_{-\,10}$	1.20
			0.14226	$-0.042\,^{+\,4}_{-\,4}$	$1.06\,^{+\,15}_{-\,12}$	1.38
		0.14262	0.14144	$-0.055\,^{+\,4}_{-\,3}$	$1.00\,^{+\,19}_{-\,19}$	1.19
			0.14226	$-0.042\,^{+\,6}_{-\,5}$	$0.90\,^{+\,23}_{-\,23}$	1.18

Table 3.5: (Cont.)

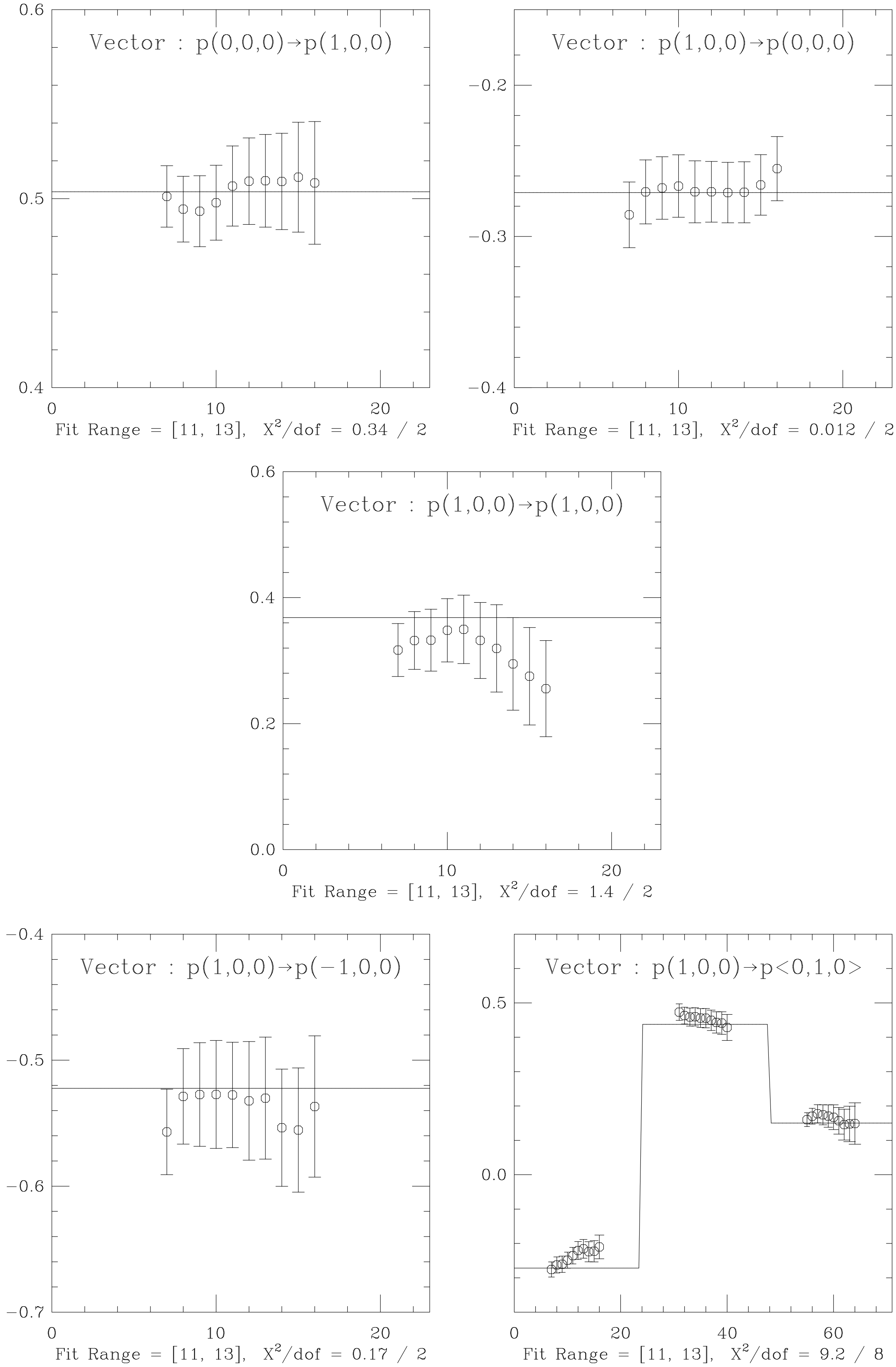

Figure 3.3: Vector-to-pseudoscalar vector plateau plots with $\kappa_l = \kappa_{l_s} = 0.14144$ and $\kappa_h = 0.129$. Momentum in units of $\pi/12\,a$.

In general, the chi-squared values quoted in Table 3.5 indicate a good fit to the correlator data for all kappa combinations. However, for the momentum channel $(1,0,0) \to (1,0,0)$ the fit chi-squared are on the high side which suggests that the time-independent correlator data is not plateauing within the fit window. Figure 3.3 shows six plateau plots, one for each momentum channel, corresponding to the simultaneous fit of Eqn. (3.46) to the Lorentz-independent vector-to-pseudo-scalar vector correlator components.

Vector-to-Pseudoscalar Axial Fits

For each momentum channel, the axial form factors are obtained by performing a simultaneous fit to all Lorentz-independent vector-to-pseudoscalar three-point correlators. Multiplying both sides of Eqn. (3.2) by a 'dummy' polarisation vector one obtains the form factor parameterisation corresponding to the polarisation-averaged axial three-point correlator:

$$\begin{aligned} Z_A \times A^{\mu\nu} &= \left(g^{\mu\nu} - \frac{p^{\mu}_{K^*} p^{\nu}_{K^*}}{m^2_{K^*}} \right) (m_D + m_{K^*})\, A_1 - \left(p_D - \frac{p_D \cdot p_{K^*}}{m^2_{K^*}}\, p_{K^*} \right)^{\nu} \\ &\times \left\{ \frac{A_2}{(m_D + m_{K^*})} (p_D + p_{K^*})^{\mu} - \frac{2\, A\, m_{K^*}}{q^2} (p_D - p_{K^*})^{\mu} \right\} \end{aligned} \qquad (3.48)$$

with

$$A^{\mu\nu} = \sum_{r=1}^{3} \xi^{\nu}_r \left\langle K^*_r \,\middle|\, A^{\mu} \,\middle|\, D \right\rangle \qquad (3.49)$$

where $A^{\mu\nu}$ is the time-independent three-point correlator data, and Z_A is the renormalisation constant corresponding to the lattice axial current.

The form factors A^1, A^2 and A^0, obtained from simultaneous fits to vector-to-pseudoscalar axial correlators, are given in Table 3.6 with the corresponding q^2 values given in Table 3.5. For the momentum channel $(0,0,0) \to (0,0,0)$ the form factor parameterisation, given by Eqn. (3.48), reduces as follows:

$$Z_A \times A^{ij} = -\,(m_D + m_{K^*})\, A_1\,; \qquad i = j \qquad (3.50)$$

$$A^{ij} = 0\,; \qquad i \neq j \qquad (3.51)$$

where the temporal component A^{00} is zero. Thus, the form factor A_1 is obtained from a one-parameter fit; there is no determination of the form factors A_2 and A_0.

$\vec{p}_D$	$\vec{p}_K$	κ_l	κ_{l_s}	A^1/Z_A	A^2/Z_A	A^0/Z_A	χ^2/dof
(0,0,0)	(0,0,0)	0.14144	0.14144	$0.74 {}^{+4}_{-1}$	N/A	N/A	2.0
			0.14226	$0.70 {}^{+4}_{-2}$	N/A	N/A	1.6
		0.14226	0.14144	$0.76 {}^{+5}_{-2}$	N/A	N/A	0.9
			0.14226	$0.72 {}^{+6}_{-3}$	N/A	N/A	0.5
		0.14262	0.14144	$0.78 {}^{+6}_{-3}$	N/A	N/A	0.6
			0.14226	$0.73 {}^{+7}_{-4}$	N/A	N/A	0.2
(0,0,0)	(1,0,0)	0.14144	0.14144	$0.70 {}^{+4}_{-2}$	$0.59 {}^{+8}_{-6}$	$0.73 {}^{+3}_{-2}$	1.2
			0.14226	$0.65 {}^{+4}_{-2}$	$0.51 {}^{+8}_{-7}$	$0.72 {}^{+4}_{-2}$	0.6
		0.14226	0.14144	$0.71 {}^{+5}_{-3}$	$0.62 {}^{+11}_{-8}$	$0.73 {}^{+5}_{-2}$	0.8
			0.14226	$0.66 {}^{+5}_{-3}$	$0.53 {}^{+12}_{-10}$	$0.72 {}^{+6}_{-3}$	0.6
		0.14262	0.14144	$0.71 {}^{+6}_{-4}$	$0.61 {}^{+15}_{-12}$	$0.73 {}^{+6}_{-4}$	0.8
			0.14226	$0.64 {}^{+8}_{-5}$	$0.50 {}^{+19}_{-17}$	$0.72 {}^{+8}_{-5}$	0.8
(1,0,0)	(0,0,0)	0.14144	0.14144	$0.69 {}^{+4}_{-2}$	$0.66 {}^{+45}_{-34}$	$0.88 {}^{+8}_{-7}$	1.0
			0.14226	$0.66 {}^{+5}_{-2}$	$0.93 {}^{+58}_{-41}$	$0.88 {}^{+10}_{-10}$	0.8
		0.14226	0.14144	$0.69 {}^{+5}_{-3}$	$0.58 {}^{+72}_{-44}$	$0.92 {}^{+10}_{-11}$	0.9
			0.14226	$0.65 {}^{+6}_{-4}$	$0.91 {}^{+94}_{-63}$	$0.92 {}^{+16}_{-16}$	0.8
		0.14262	0.14144	$0.69 {}^{+7}_{-4}$	$0.39 {}^{+90}_{-59}$	$0.98 {}^{+14}_{-15}$	0.6
			0.14226	$0.65 {}^{+8}_{-6}$	$0.75 {}^{+121}_{-90}$	$1.00 {}^{+21}_{-21}$	0.6

Table 3.6: The $D \to K^*$ axial form factors with momentum in units of $\pi/12\,a$; the corresponding q^2 values are given in Table 3.5.

$\vec{p}_D$	$\vec{p}_K$	κ_l	κ_{l_s}	A^1/Z_A	A^2/Z_A	A^0/Z_A	χ^2/dof
(1,0,0)	(1,0,0)	0.14144	0.14144	$0.75 {}^{+9}_{-6}$	$1.4 {}^{+12}_{-11}$	$0.93 {}^{+13}_{-11}$	0.6
			0.14226	$0.71 {}^{+11}_{-7}$	$1.4 {}^{+13}_{-12}$	$0.96 {}^{+18}_{-14}$	0.8
		0.14226	0.14144	$0.65 {}^{+15}_{-13}$	$0.6 {}^{+19}_{-20}$	$0.75 {}^{+23}_{-20}$	0.9
			0.14226	$0.59 {}^{+18}_{-16}$	$0.6 {}^{+21}_{-20}$	$0.78 {}^{+30}_{-25}$	1.0
		0.14262	0.14144	$0.49 {}^{+24}_{-21}$	$-0.7 {}^{+30}_{-29}$	$0.53 {}^{+33}_{-35}$	1.1
			0.14226	$0.41 {}^{+30}_{-27}$	$-0.9 {}^{+32}_{-31}$	$0.57 {}^{+41}_{-42}$	1.0
(1,0,0)	(-1,0,0)	0.14144	0.14144	$0.57 {}^{+5}_{-3}$	$0.36 {}^{+8}_{-7}$	$0.44 {}^{+4}_{-3}$	1.4
			0.14226	$0.53 {}^{+6}_{-4}$	$0.30 {}^{+10}_{-8}$	$0.44 {}^{+5}_{-4}$	1.1
		0.14226	0.14144	$0.59 {}^{+9}_{-7}$	$0.37 {}^{+14}_{-12}$	$0.45 {}^{+5}_{-4}$	1.0
			0.14226	$0.56 {}^{+10}_{-9}$	$0.31 {}^{+17}_{-15}$	$0.47 {}^{+6}_{-6}$	0.7
		0.14262	0.14144	$0.58 {}^{+14}_{-12}$	$0.34 {}^{+20}_{-20}$	$0.46 {}^{+8}_{-8}$	0.8
			0.14226	$0.58 {}^{+15}_{-16}$	$0.30 {}^{+24}_{-24}$	$0.50 {}^{+9}_{-10}$	0.6
(1,0,0)	(0,1,0)	0.14144	0.14144	$0.61 {}^{+3}_{-2}$	$0.41 {}^{+7}_{-6}$	$0.62 {}^{+4}_{-2}$	1.4
			0.14226	$0.56 {}^{+4}_{-2}$	$0.35 {}^{+9}_{-8}$	$0.60 {}^{+4}_{-2}$	1.1
		0.14226	0.14144	$0.59 {}^{+5}_{-4}$	$0.35 {}^{+11}_{-10}$	$0.63 {}^{+5}_{-3}$	1.3
			0.14226	$0.53 {}^{+6}_{-4}$	$0.29 {}^{+14}_{-13}$	$0.60 {}^{+6}_{-3}$	1.0
		0.14262	0.14144	$0.54 {}^{+8}_{-6}$	$0.23 {}^{+20}_{-16}$	$0.63 {}^{+8}_{-6}$	1.3
			0.14226	$0.48 {}^{+10}_{-7}$	$0.19 {}^{+21}_{-22}$	$0.61 {}^{+10}_{-7}$	1.0

Table 3.6: (Cont.)

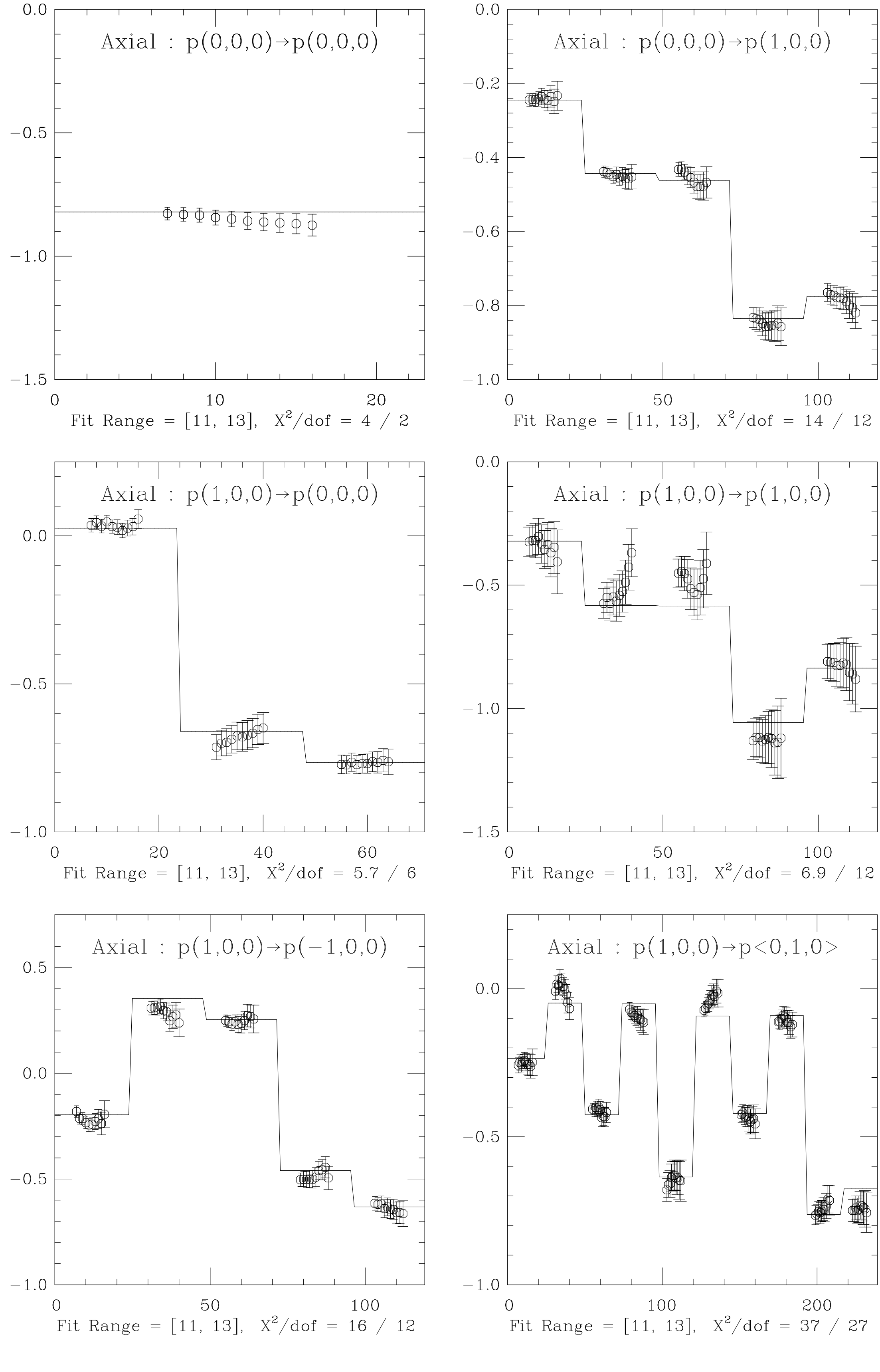

Figure 3.4: Vector-to-pseudoscalar axial plateau plots with $\kappa_l = \kappa_{l_s} = 0.14144$ and $\kappa_h = 0.129$. Momentum in units of $\pi/12\,a$.

In general, there are three or more Lorentz-independent correlators and the form factors A^1, A^2 and A_0 are obtained from a three-parameter fit which (in most cases) is over-determined. The chi-squared values, quoted in Table 3.6 indicate a good fit to the data for all kappa combinations. Figure 3.4 shows six plateau plots, one for each momentum channel, corresponding to the simultaneous fit of Eqn. (3.48) to the Lorentz-independent vector-to-pseudoscalar axial correlator components.

3.4 Form Factor Extrapolations

Recall from Section 3.3, the form factors describing the $D \to K$, K^* decays were obtained from simultaneous fits to three-point correlators computed for six kappa combinations. In this section, the form factors are extrapolated to the physical quark masses: the strange and light quark masses, determined in Section 2.4, corresponding to $\kappa_s = 0.1418\,^{+\,1}_{-\,1}$ and $\kappa_c = 0.14315\,^{+\,2}_{-\,2}$ respectively. The form factors describing the related decays $D \to \pi$, ρ are also computed.

Form Factor Mass Dependence

Recall from Section 3.1, in the pole dominance model the q^2 dependence of the form factors is given by

$$F(q^2) = \frac{F(0)}{1 - q^2/m_{pole}^2} \tag{3.52}$$

where F is a generic form factor and m_{pole} is the mass of the corresponding resonance. In this study, the form factors are assumed to have the following dependence on the light quark masses:

$$F(\kappa_{l_s}, \kappa_l) = a + b\,\frac{\Delta m_D(\kappa_l)}{m_D(\kappa_c)} + c\,\frac{\Delta m_{K^{(*)}}(\kappa_{l_s}, \kappa_l)}{m_{K^{(*)}}(\kappa_s, \kappa_c)} + d\left(\frac{\Delta m_{K^{(*)}}(\kappa_{l_s}, \kappa_l)}{m_{K^{(*)}}(\kappa_s, \kappa_c)}\right)^2 \tag{3.53}$$

with $\Delta m_D(\kappa_l)$ and $\Delta m_{K^{(*)}}(\kappa_{l_s}, \kappa_l)$ defined as follows:

$$\Delta m_D(\kappa_l) = m_D(\kappa_l) - m_D(\kappa_c) \tag{3.54}$$

$$\Delta m_{K^{(*)}}(\kappa_{l_s}, \kappa_l) = m_{K^{(*)}}(\kappa_{l_s}, \kappa_l) - m_{K^{(*)}}(\kappa_s, \kappa_c) \tag{3.55}$$

where $m_D(\kappa_l)$ is given by Eqn. (2.27), and $m_K(\kappa_{l_s}, \kappa_l)$ and $m_{K^*}(\kappa_{l_s}, \kappa_l)$ are given by Eqns. (2.20) and (2.23) respectively.

The form of Eqn. (3.53) is motivated by the results of a Taylor expansion of $q^2(\kappa_{l_s}, \kappa_l)$ about $q^2(\kappa_s, \kappa_c)$, and the following expansion:

$$F(\kappa_{l_s}, \kappa_l) = \left\{1 + \frac{q^2(\kappa_{l_s}, \kappa_l)}{m^2_{pole}} + \cdots\right\} F(0) \tag{3.56}$$

which is valid for all $|q^2| \ll 1$.

For the heavy-light masses, given in Table 2.3, the heaviest kappa combination (with $\kappa_h = 0.129$ and $\kappa_l = 0.14144$) gives $\Delta m_D(\kappa_l) \,/\, m_D(\kappa_c) \approx 0.01$. Thus, higher-order terms in Eqn. (3.53) are not required. However, for the light-light masses, given in Table 2.1, the heaviest kappa combination (with $\kappa_{l_1} = \kappa_{l_2} = 0.14144$) gives $\Delta m_K(\kappa_{l_s}, \kappa_l) \,/\, m_K(\kappa_s, \kappa_c) \approx 0.6$ and $\Delta m_{K^*}(\kappa_{l_s}, \kappa_l) \,/\, m_{K^*}(\kappa_s, \kappa_c) \approx 0.2$. This suggests that the quadratic term in Eqn. (3.53) is important for the $D \to K$ form factor extrapolations.

Pseudoscalar-to-Pseudoscalar Extrapolations

For each momentum channel, the form factors f^+ and f^0 are extrapolated (independently) to the physical quark masses by fitting the six kappa-independent values, given in Table 3.4, to the following fit function:

$$\begin{aligned} F(\kappa_{l_s}, \kappa_l) &= \alpha + \beta\left(\frac{1}{\kappa_l} - \frac{1}{\kappa_c}\right) + \gamma\left(\frac{1}{\kappa_{l_s}} + \frac{1}{\kappa_l} - \frac{2}{\kappa_c}\right)^{\frac{1}{2}} \\ &+ \delta\left(\frac{1}{\kappa_{l_s}} + \frac{1}{\kappa_l} - \frac{2}{\kappa_c}\right) \end{aligned} \tag{3.57}$$

where α, β, γ and δ are free parameters determined by the fit.

The $D \to K$ form factors f_K^+ and f_K^0, computed from Eqn. (3.57) with $\kappa_{l_s} = \kappa_s$ and $\kappa_l = \kappa_c$, are given in Table 3.7; the corresponding q^2 values were computed from the physical meson masses, given in the lower halves of Tables 2.1 and 2.3. In general, the chi-squared values quoted in Table 3.7 indicate a good fit to the data, for all momentum channels. However, for the $(1,0,0) \to (1,0,0)$ channel the chi-squared corresponding to the f^0 extrapolation suggests a bad fit to the data ($\chi^2/dof \gg 1$). Thus, this result is excluded from the following analysis of the form factor q^2 dependence.

$\vec{p}_D$	$\vec{p}_K$	$a^2\,q^2$	f_K^+/Z_V	χ^2/dof	f_K^0/Z_V	χ^2/dof
(0,0,0)	(0,0,0)	$0.230\,^{+\,8}_{-\,7}$	N/A	N/A	$1.04\,^{+\,10}_{-\,5}$	0.43
(0,0,0)	(1,0,0)	$0.050\,^{+\,4}_{-\,3}$	$0.86\,^{+\,7}_{-\,4}$	0.52	$0.77\,^{+\,7}_{-\,3}$	0.92
(1,0,0)	(0,0,0)	$0.212\,^{+\,9}_{-\,8}$	$1.41\,^{+\,13}_{-\,16}$	0.32	$1.03\,^{+\,8}_{-\,7}$	0.14
(1,0,0)	(1,0,0)	$0.156\,^{+\,5}_{-\,3}$	$1.16\,^{+\,21}_{-\,17}$	1.40	$0.77\,^{+\,22}_{-\,13}$	2.82
(1,0,0)	(−1,0,0)	$-0.119\,^{+\,5}_{-\,3}$	$0.62\,^{+\,9}_{-\,5}$	0.13	$0.73\,^{+\,10}_{-\,6}$	0.09
(1,0,0)	(0,1,0)	$0.018\,^{+\,5}_{-\,3}$	$0.75\,^{+\,7}_{-\,5}$	0.24	$0.72\,^{+\,7}_{-\,5}$	0.24

Table 3.7: The $D \to K$ form factors with momentum in units of $\pi/12\,a$.

$\vec{p}_D$	$\vec{p}_K$	$a^2\,q^2$	f_π^+/Z_V	f_π^0/Z_V
(0,0,0)	(0,0,0)	$0.380\,^{+\,7}_{-\,3}$	N/A	$1.00\,^{+\,31}_{-\,12}$
(0,0,0)	(1,0,0)	$0.091\,^{+\,5}_{-\,2}$	$0.76\,^{+\,14}_{-\,10}$	$0.56\,^{+\,14}_{-\,8}$
(1,0,0)	(0,0,0)	$0.375\,^{+\,7}_{-\,3}$	$2.07\,^{+\,36}_{-\,47}$	$1.25\,^{+\,18}_{-\,20}$
(1,0,0)	(1,0,0)	$0.202\,^{+\,5}_{-\,2}$	$1.30\,^{+\,52}_{-\,46}$	$0.11\,^{+\,47}_{-\,32}$
(1,0,0)	(−1,0,0)	$-0.073\,^{+\,5}_{-\,2}$	$0.73\,^{+\,25}_{-\,15}$	$0.84\,^{+\,31}_{-\,20}$
(1,0,0)	(0,1,0)	$0.065\,^{+\,5}_{-\,2}$	$0.72\,^{+\,17}_{-\,15}$	$0.61\,^{+\,15}_{-\,13}$

Table 3.8: The $D \to \pi$ form factors with momentum in units of $\pi/12\,a$; the fit chi-squared are the same as those in Table 3.7.

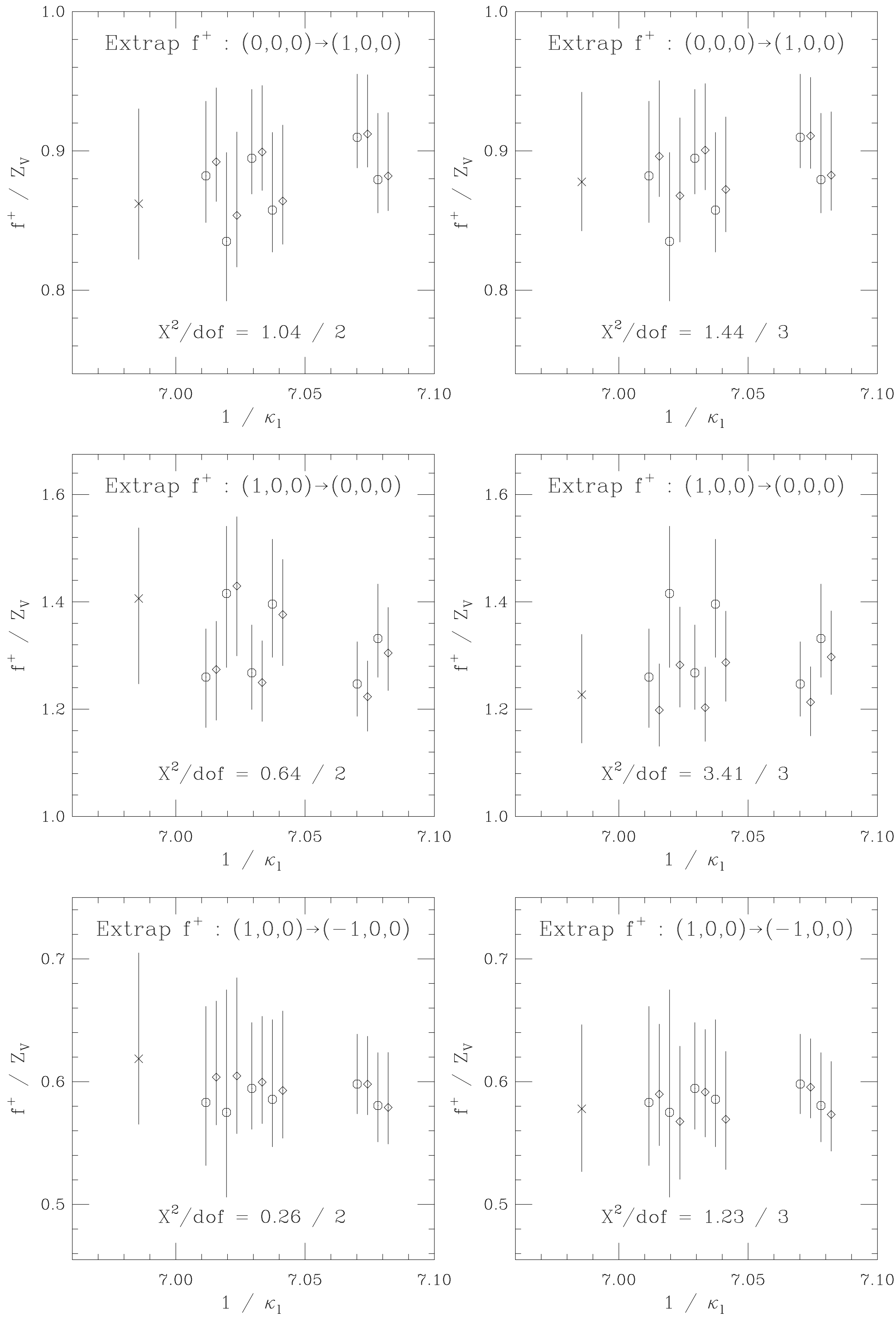

Figure 3.5: Extrapolation plots for the f^+ form factor.

Recall from Section 2.4, the lattice pion mass computed using Eqn. (2.20) with $\kappa_{l_1} = \kappa_{l_2} = \kappa_c$ is zero by definition. However, in order to compute the $D \to \pi$ form factors, and the corresponding q^2 values, a non-zero estimate of the light quark mass is required. Fixing the light-light pseudoscalar mass $m_P = 0.05$ in Eqn. (2.20) gives

$$\kappa_u = \kappa_d = 0.14310\,^{+\,2}_{-\,2} \tag{3.58}$$

which corresponds to a physical pion mass with $m_\pi \approx 140\ MeV$. In practice, the use of massless u and d quarks has no effect on the determination of κ_s, or m_ρ which is used to set the lattice spacing. The $D \to \pi$ form factors f_π^+ and f_π^0, computed from Eqn. (3.57) with $\kappa_{l_s} = \kappa_l = \kappa_u$, are given in Table 3.8; the corresponding q^2 values were computed using $m_\pi = 0.05$ and the physical D meson mass, given in the lower-half of Table 2.3.

Figure 3.5 shows the f^+ form factor data, given in Table 3.4, plotted as a function of the inverse light-kappa, κ_l, for three different momentum channels. This data, denoted by 'circles', is fitted to Eqn. (3.57) as follows: the left-hand plots correspond to four-parameter fits; the right-hand plots correspond to three-parameter fits with the δ parameter constrained to zero. The 'diamonds' correspond to the form factor f^+ computed using Eqn. (3.57), for each of the six kappa combinations; the extrapolated form factor f_K^+ is denoted by a cross. Note, the data lies in two distinct planes which correspond to the two values of the strange kappa, κ_{l_s}. For small δ, the f_K^+ form factor will lie on a plane bisecting these two data planes.

The 'extrapolation' plot gives an indication of how well the fit function is modelling the data: a good fit function will reproduce the data, i.e. the circles and diamonds will overlap. From Figure 3.5 it is clear that the quadratic term in Eqn. (3.57) is important: for the momentum channel $(1,0,0) \to (0,0,0)$ the extrapolated results differ by as much as 15% between the two fit methods. In general, the four-parameter fit gives a smaller chi-squared and the corresponding extrapolation plot has a better 'overlap'. However, this method gives slightly larger errors on the extrapolated form factor. The $D \to K$ and $D \to \pi$ form factors quoted in Tables 3.7 and 3.8 were obtained using the four-parameter fit method.

$\vec{p}_D$	$\vec{p}_K$	$a^2\, q^2$	V_{K^*}/Z_V	χ^2/dof
(0,0,0)	(0,0,0)	$0.112 \,^{+\,8}_{-\,8}$	N/A	N/A
(0,0,0)	(1,0,0)	$-0.009 \,^{+\,5}_{-\,5}$	$1.4 \,^{+\,2}_{-\,1}$	0.12
(1,0,0)	(0,0,0)	$0.079 \,^{+\,9}_{-\,9}$	$1.0 \,^{+\,3}_{-\,1}$	0.76
(1,0,0)	(1,0,0)	$0.086 \,^{+\,6}_{-\,5}$	$3.8 \,^{+\,12}_{-\,9}$	1.85
(1,0,0)	(−1,0,0)	$-0.188 \,^{+\,6}_{-\,5}$	$0.8 \,^{+\,2}_{-\,1}$	0.37
(1,0,0)	(0,1,0)	$-0.051 \,^{+\,6}_{-\,5}$	$1.1 \,^{+\,2}_{-\,1}$	0.61

Table 3.9: The $D \to K^*$ vector form factor with momentum in units of $\pi/12\,a$.

$\vec{p}_D$	$\vec{p}_K$	$a^2\, q^2$	V_ρ/Z_V
(0,0,0)	(0,0,0)	$0.142 \,^{+\,9}_{-\,9}$	N/A
(0,0,0)	(1,0,0)	$0.007 \,^{+\,5}_{-\,5}$	$1.4 \,^{+\,2}_{-\,1}$
(1,0,0)	(0,0,0)	$0.113 \,^{+\,10}_{-\,10}$	$1.0 \,^{+\,3}_{-\,2}$
(1,0,0)	(1,0,0)	$0.106 \,^{+\,6}_{-\,6}$	$4.0 \,^{+\,15}_{-\,10}$
(1,0,0)	(−1,0,0)	$-0.168 \,^{+\,6}_{-\,6}$	$0.8 \,^{+\,2}_{-\,1}$
(1,0,0)	(0,1,0)	$-0.031 \,^{+\,6}_{-\,6}$	$1.0 \,^{+\,2}_{-\,1}$

Table 3.10: The $D \to \rho$ vector form factor with momentum in units of $\pi/12\,a$; the fit chi-squared are the same as those in Table 3.9.

$\vec{p}_D$	$\vec{p}_K$	$A^1_{K^*}/Z_A$	χ^2/dof	$A^2_{K^*}/Z_A$	χ^2/dof	$A^0_{K^*}/Z_A$	χ^2/dof
(0,0,0)	(0,0,0)	$0.76 {+ 7 \atop - 3}$	0.25	N/A	N/A	N/A	N/A
(0,0,0)	(1,0,0)	$0.71 {+ 7 \atop - 4}$	0.17	$0.7 {+ 1 \atop - 1}$	0.11	$0.72 {+ 6 \atop - 3}$	0.09
(1,0,0)	(0,0,0)	$0.67 {+ 7 \atop - 4}$	0.03	$0.5 {+ 9 \atop - 6}$	0.15	$0.92 {+ 14 \atop - 15}$	0.26
(1,0,0)	(1,0,0)	$0.68 {+ 17 \atop - 16}$	0.61	$1.4 {+ 26 \atop - 27}$	0.38	$0.75 {+ 35 \atop - 22}$	0.41
(1,0,0)	(−1,0,0)	$0.59 {+ 12 \atop - 6}$	0.44	$0.4 {+ 2 \atop - 1}$	0.21	$0.44 {+ 7 \atop - 6}$	0.69
(1,0,0)	(0,1,0)	$0.58 {+ 7 \atop - 5}$	0.84	$0.4 {+ 2 \atop - 1}$	0.63	$0.59 {+ 8 \atop - 5}$	0.16

Table 3.11: The $D \to K^*$ axial form factors with momentum in units $\pi/12\,a$. The corresponding q^2 values are given in Table 3.9.

$\vec{p}_D$	$\vec{p}_K$	A^1_ρ/Z_A	A^2_ρ/Z_A	A^0_ρ/Z_A
(0,0,0)	(0,0,0)	$0.69 {+ 8 \atop - 4}$	N/A	N/A
(0,0,0)	(1,0,0)	$0.64 {+ 7 \atop - 4}$	$0.5 {+ 1 \atop - 1}$	$0.71 {+ 7 \atop - 3}$
(1,0,0)	(0,0,0)	$0.61 {+ 9 \atop - 5}$	$0.9 {+ 10 \atop - 7}$	$0.90 {+ 18 \atop - 17}$
(1,0,0)	(1,0,0)	$0.62 {+ 19 \atop - 18}$	$1.5 {+ 29 \atop - 28}$	$0.81 {+ 43 \atop - 23}$
(1,0,0)	(−1,0,0)	$0.52 {+ 14 \atop - 7}$	$0.3 {+ 2 \atop - 2}$	$0.43 {+ 9 \atop - 7}$
(1,0,0)	(0,1,0)	$0.50 {+ 7 \atop - 6}$	$0.3 {+ 2 \atop - 2}$	$0.56 {+ 8 \atop - 6}$

Table 3.12: The $D \to \rho$ axial form factors with momentum in units $\pi/12\,a$; the fit chi-squared are the same as those in Table 3.11. The corresponding q^2 values are given in Table 3.10.

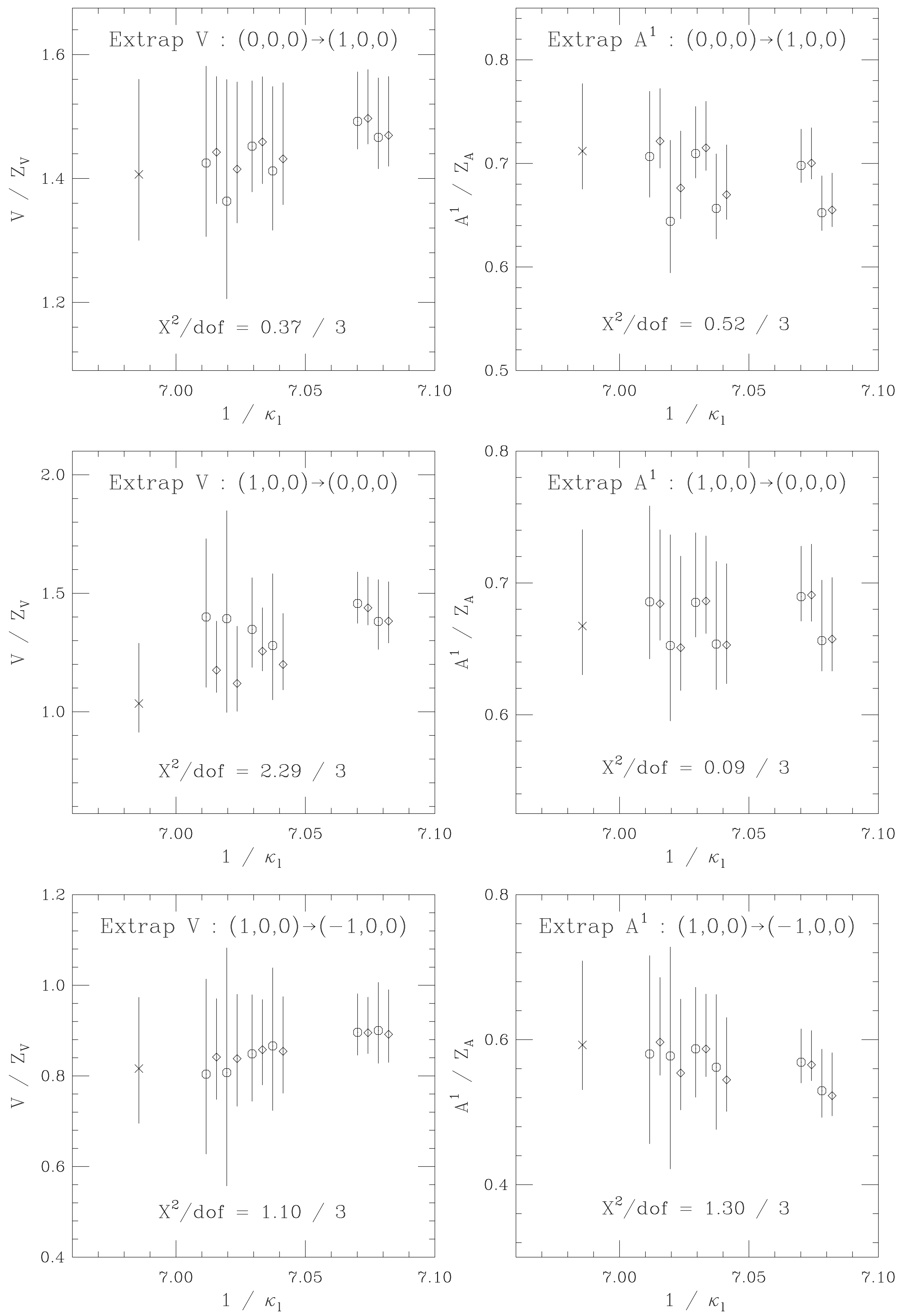

Figure 3.6: Extrapolation plots for the V and A^1 form factors.

Pseudoscalar-to-Vector Extrapolations

For each momentum channel, the vector and axial form factors are extrapolated (independently) to the physical quark masses by fitting the six kappa-independent values, given in Tables 3.5 and 3.6 respectively, to the following fit function:

$$F(\kappa_{l_s}, \kappa_l) = \alpha + \beta\left(\frac{1}{\kappa_l} - \frac{1}{\kappa_c}\right) + \gamma\left(\frac{1}{\kappa_{l_s}} + \frac{1}{\kappa_l} - \frac{2}{\kappa_c}\right)^{\frac{1}{2}} \tag{3.59}$$

where α, β, and γ are free parameters determined by the fit.

The $D \to K^*$ vector and axial form factors, computed from Eqn. (3.59) with $\kappa_{l_s} = \kappa_s$ and $\kappa_l = \kappa_c$, are given in Tables 3.9 and 3.11 respectively; the corresponding q^2 values were computed from the physical meson masses, given in the lower halves of Tables 2.1 and 2.3. In general, the chi-squared values indicate a good fit to the data, for all momentum channels. However, for the $(1,0,0) \to (1,0,0)$ channel the chi-squared corresponding to the V extrapolation ($\chi^2/dof = 1.85$) suggests a bad fit to the data. Similarly, a large error on A^2 corresponds to a poor determination of the form factor for this momentum channel. Thus, these results are excluded from the following analysis of the form factor q^2 dependence.

The $D \to \rho$ form factors were also computed: the vector and axial form factors, computed from Eqn. (3.59) with $\kappa_{l_s} = \kappa_l = \kappa_u$, are given in Tables 3.10 and 3.12 respectively. Figure 3.6 shows extrapolation plots for three different momentum channels: the left-hand and right-hand plots correspond to the V and A^1 form factor data, given in Tables 3.5 and 3.6 respectively, fitted to Eqn. (3.59). In general, the three-parameter fit gives an excellent description of the data. Thus, additional (quadratic) terms in Eqn. (3.59) are not required.

3.5 Pole Dominance Fits

In Section 3.4, the $D \to K$, K^* and $D \to \pi$, ρ form factors were extrapolated to their physical values, for a range of q^2. This data could be used to test the pole dominance relations, given by Eqns. (3.15)–(3.17), from first principles. The q^2 dependence of the form factors is required to determine the decay rates. However, the scalar (0^+) and axial (1^+) pole masses are poorly determined. Thus, in this Section, the form factor data is fitted to the pole dominance model.

Pseudoscalar-to-Pseudoscalar Form Factors

Figures 3.7 and 3.9 show the f_K^+ and f_π^+ form factor data, given in Tables 3.7 and 3.8 respectively, plotted as a function of q^2. The f_K^+ and f_π^+ data is fitted to the pole dominance model, given by Eqn. (3.52), as follows: the left-hand plots correspond to a two-parameter fit; the right-hand plots correspond to a one-parameter fit with the pole mass constrained to the mass of the associated resonance, $m_{D_s^*}$ and m_{D^*} respectively. In the pole dominance plot, the solid 'fit' line corresponds to the kinematically allowed region, given by Eqn. (3.4), and the 'cross' denotes the extrapolated form factor, $F(0)$.

For the f_K^+ data the two fit methods give a consistent determination of $f_K^+(0)$; the two-parameter fit yields

$$\frac{f_K^+(0)}{Z_V} = 0.76\,^{+\,6}_{-\,3}; \qquad m_{1^-}^{c\bar{s}} = 0.68\,^{+\,7}_{-\,3} \tag{3.60}$$

where the pole mass agrees (within errors) with both the lattice value $0.736\,^{+\,7}_{-\,3}$, given in Table 2.3, and with the experimental value $2.00 \pm 0.12 \pm 0.18\,GeV$, quoted in Section 3.2. The chi-squared ($\chi^2/dof = 0.37$) indicates an excellent fit to the data; all data points lie within one sigma, for both fit methods. Thus, pole dominance gives a good description of the f_K^+ form factor. Recall from Section 3.1, the $D \to K$ decay rate, given in Eqn. (3.18), is proportional to an integral over q^2 which is a function of f_K^+. Assuming pole dominance (with confidence) this integral can be performed analytically.

Figure 3.8 shows the f_K^0 form factor data, given in Table 3.7, plotted as a function of q^2. A two-parameter fit, using Eqn. (3.52), gives

$$\frac{f_K^0(0)}{Z_V} = 0.73\,^{+\,6}_{-\,4}; \qquad m_{0^+}^{c\bar{s}} = 0.89\,^{+\,12}_{-\,7} \tag{3.61}$$

where the pole mass is consistent with the lattice value $2.3 \pm 0.2\,GeV$ [75]; the scalar 0^+ meson is experimentally undetermined. The chi-squared ($\chi^2/dof = 0.82$) indicates an excellent fit to the data; all data points (in the kinematically allowed region) lie within one sigma. Thus, pole dominance gives a good description of the f_K^0 form factor. Furthermore, Eqn. (3.60) and (3.61) are consistent with the kinematic constraint $f_K^+(0) = f_K^0(0)$, given in Section 3.1.

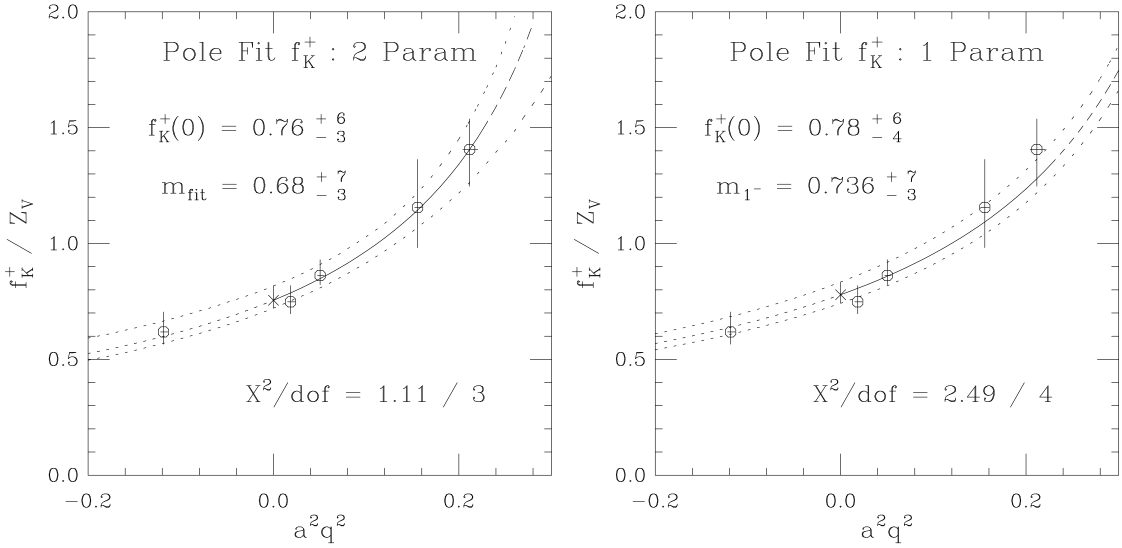

Figure 3.7: Pole dominance plots for the f_K^+ form factor.

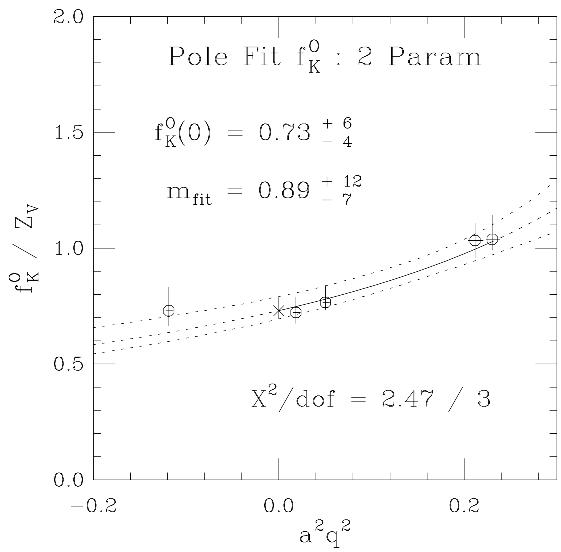

Figure 3.8: Pole dominance plot for the f_K^0 form factor.

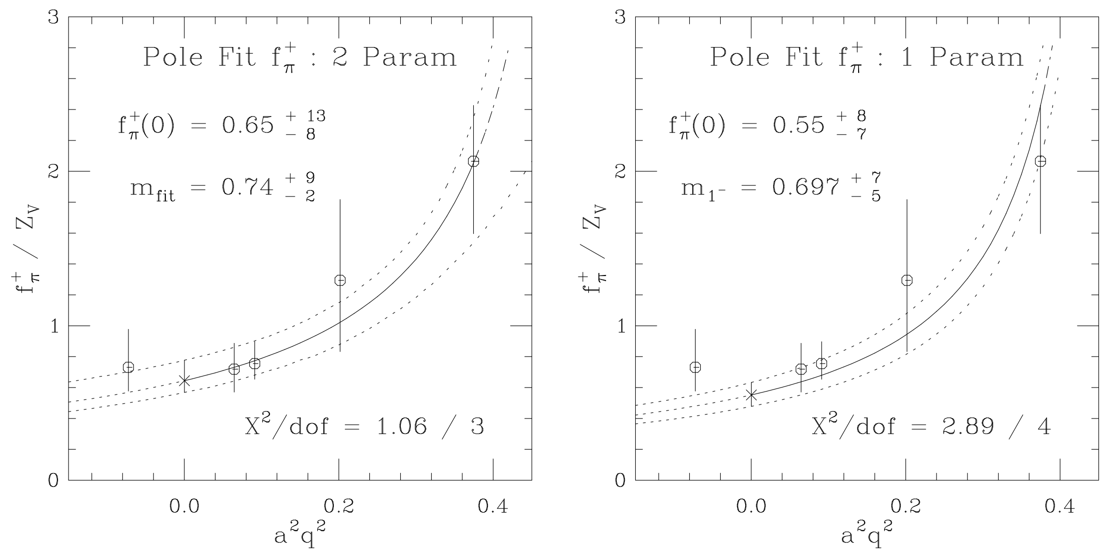

Figure 3.9: Pole dominance plots for f_π^+ form factor.

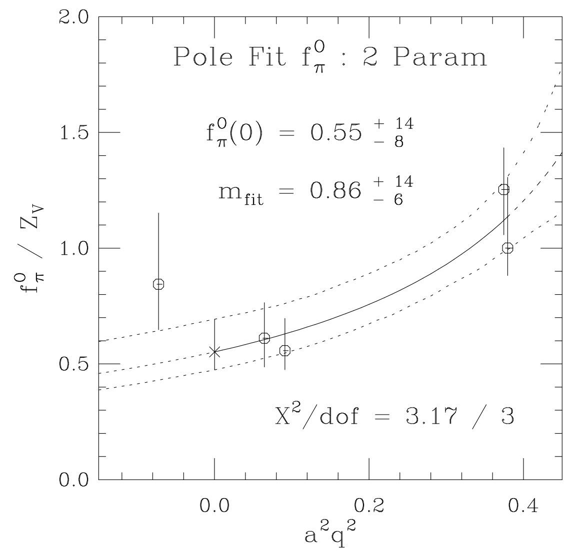

Figure 3.10: Pole dominance plot for f_π^0 form factor.

Similarly, for the f_π^+ data the two fit methods give a consistent determination of $f_\pi^+(0)$ (within errors); the two-parameter fit yields

$$\frac{f_\pi^+(0)}{Z_V} = 0.65\,^{+\,13}_{-\,8}\,; \qquad m_{1^-}^{c\bar{d}} = 0.74\,^{+\,9}_{-\,2} \tag{3.62}$$

where the pole mass is high compared to the lattice value $0.697\,^{+\,7}_{-\,5}$, given in Table 2.3. However, these masses still agree within two sigma. The chi-squared ($\chi^2/dof = 0.35$) indicates an excellent fit to the data; all data points (in the kinematically allowed region) lie within one sigma, for both fit methods. Thus, pole dominance gives a good description of the f_π^+ form factor. In practice, the discrepancy in the pole mass has only a small effect (less than 10%) on the $D \to \pi$ decay rate.

Figure 3.10 shows the f_π^0 form factor data, given in Table 3.8, plotted as a function of q^2. A two-parameter fit, using Eqn. (3.52), gives

$$\frac{f_\pi^0(0)}{Z_V} = 0.55\,^{+\,14}_{-\,8}\,; \qquad m_{0^+}^{c\bar{d}} = 0.86\,^{+\,14}_{-\,6} \tag{3.63}$$

where the pole mass corresponding to the scalar 0^+ meson is experimentally undetermined. The chi-squared ($\chi^2/dof = 1.06$) indicates a good fit to the data; all data points (in the kinematically allowed region) lie within one sigma. However, the data point corresponding to the momentum channel $(1,0,0) \to (-1,0,0)$ is on the high side but still within two sigma. Thus, pole dominance gives a fairly good description of the f_π^0 form factor. Furthermore, Eqn. (3.62) and (3.63) are consistent (within errors) with the kinematic constraint $f_\pi^+(0) = f_\pi^0(0)$.

Recall from Section 3.2, the form factor ratio $f_\pi^+(0)/f_K^+(0)$ has been measured experimentally. Using the lattice values, in Eqns. (3.60) and (3.62), gives

$$\frac{f_\pi^+(0)}{f_K^+(0)} = 0.85\,^{+\,12}_{-\,9} \tag{3.64}$$

where any deviation from unity is evidence of $SU(3)$ symmetry breaking. However, the errors in both the theoretical and experimental measurements are still too large to make any firm predictions.

Pseudoscalar-to-Vector Vector Form Factors

Figures 3.11 and 3.12 show the V_{K^*} and V_ρ form factor data, given in Tables 3.9 and 3.10 respectively, plotted as a function of q^2. The V_{K^*} and V_ρ data is fitted to the pole dominance model, given by Eqn. (3.52), as follows: the left-hand plots correspond to a two-parameter fit; the right-hand plots correspond to a one-parameter fit with the pole mass constrained to the mass of the associated resonance, $m_{D_s^*}$ and m_{D^*} respectively.

For the V_{K^*} data the two fit methods give a consistent determination of $V_{K^*}(0)$; the two-parameter fit yields

$$\frac{V_{K^*}(0)}{Z_V} = 1.15\,^{+\,13}_{-\,6}\,; \qquad m_{1^-}^{c\bar{s}} = 0.8\,^{+\,2}_{-\,1} \tag{3.65}$$

where the pole mass agrees (within errors) with both the lattice value $0.736\,^{+\,7}_{-\,3}$, given in Table 2.3, and with the experimental value $2.00 \pm 0.12 \pm 0.18\,GeV$, quoted in Section 3.2. The chi-squared ($\chi^2/dof \gg 1$) indicates a bad fit to the data.

Similarly, for the V_ρ data the two fit methods give a consistent determination of $V_\rho(0)$; the two-parameter fit yields

$$\frac{V_\rho(0)}{Z_V} = 1.09\,^{+\,12}_{-\,7}\,; \qquad m_{1^-}^{c\bar{d}} = 0.9\,^{+\,3}_{-\,1} \tag{3.66}$$

where the pole mass is high compared to the lattice value $0.697\,^{+\,7}_{-\,5}$, given in Table 2.3. However, these masses still agree within two sigma. The chi-squared ($\chi^2/dof \gg 1$) indicates a bad fit to the data. Thus, pole dominance appears to give a poor description of the V_{K^*} and V_ρ form factors.

In Figure 3.11 the data point closest to $q^2 = 0$ is high (more than two sigma), in both plots. This point corresponds to the momentum channel $(0,0,0) \to (1,0,0)$ with $p_D = (0,0,0)$; the other three data points correspond to momentum channels with $p_D = (1,0,0)$. The difference in these two data sets is probably statistical but it may also be due to systematic effects, discussed in Section 3.6. A two-parameter fit to the data points with $p_D = (1,0,0)$ only gives an acceptable chi-squared but the pole mass is poorly determined (huge errors).

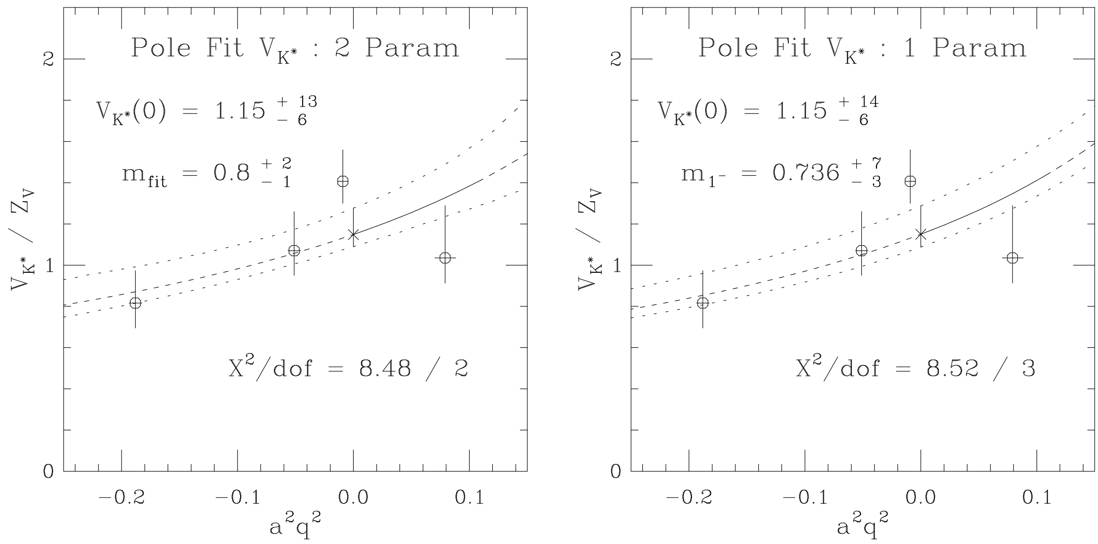

Figure 3.11: Pole dominance plots for the V_{K^*} form factor.

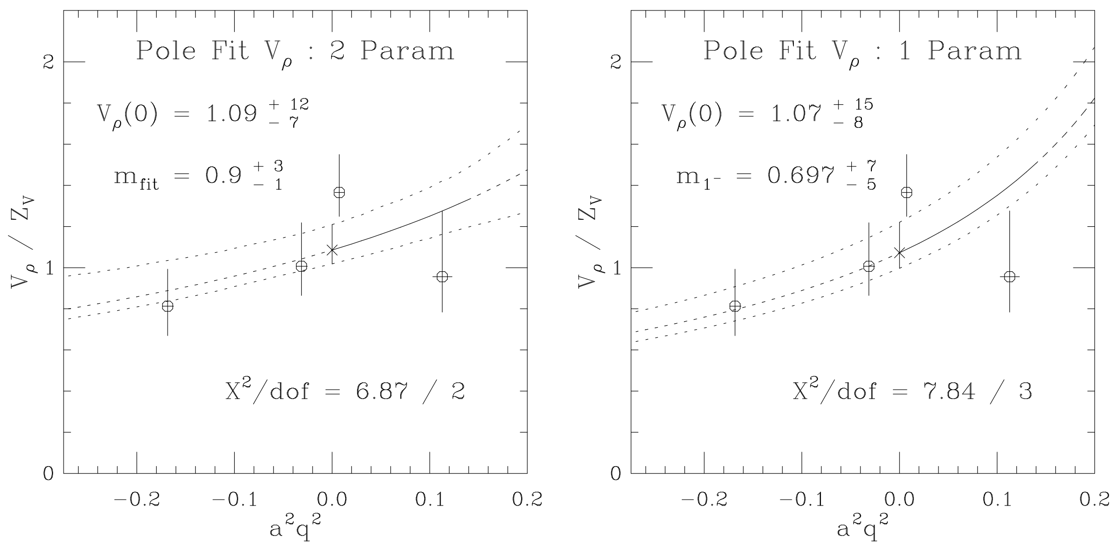

Figure 3.12: Pole dominance plots for the V_ρ form factor.

As described above, the form factors at $q^2 = 0$ have been extracted by fitting the chiral-extrapolated form factor data to the pole dominance model. However, the choice of momentum channels includes some data points close to $q^2 = 0$. An alternative way to obtain $F(0)$ is to assume pole dominance and to extrapolate the point closest to $q^2 = 0$; constraining the pole mass to the mass of the corresponding resonance. This method has the advantage that the extrapolation in q^2 is small; the disadvantage is that a single data point only is used.

For the f_K^+ and f_π^+ data, the form factors at $q^2 = 0$ obtained by extrapolating the corresponding data point closest to $q^2 = 0$ agree (within errors) with the values quoted in Eqns. (3.60) and (3.62). However, for the V_{K^*} and V_ρ data this is not the case: the two-parameter fit 'favours' the data points with $p_D = (1, 0, 0)$ but the data point closest to $q^2 = 0$ corresponds to $p_D = (0, 0, 0)$. The 'difference' in these two data sets leads to different estimates for the form factors at zero recoil.

Thus, the final 'results' for the V_{K^*} and V_ρ form factors are as follows:

$$\frac{V_{K^*}(0)}{Z_V} = 1.15\,^{+\,28}_{-\;\,6}\,; \qquad m_{1^-}^{c\bar{s}} = 0.8\,^{+\,2}_{-\,1} \tag{3.67}$$

$$\frac{V_\rho(0)}{Z_V} = 1.09\,^{+\,25}_{-\;\,7}\,; \qquad m_{1^-}^{c\bar{d}} = 0.9\,^{+\,3}_{-\,1} \tag{3.68}$$

where the upper errors in Eqns. (3.65) and (3.66) have been increased to include the form factor results obtained by extrapolating the corresponding data point closest to $q^2 = 0$.

Pseudoscalar-to-Vector Axial Form Factors

Figures 3.13 and 3.15 show the $A_{K^*}^1$ and $A_{K^*}^2$ form factor data, given in Table 3.11, plotted as a function of q^2. The $A_{K^*}^1$ and $A_{K^*}^2$ data is fitted to the pole dominance model, given by Eqn. (3.52), as follows: the left-hand plots correspond to a two-parameter fit; the right-hand plots correspond to a one-parameter fit with the pole mass constrained to the value 0.9. This value corresponds to the mass of the D_{S1} meson ($\approx 2.5\ GeV$), used to extract the form factors in Ref. [63]; the quantum numbers of this resonance require confirmation [52].

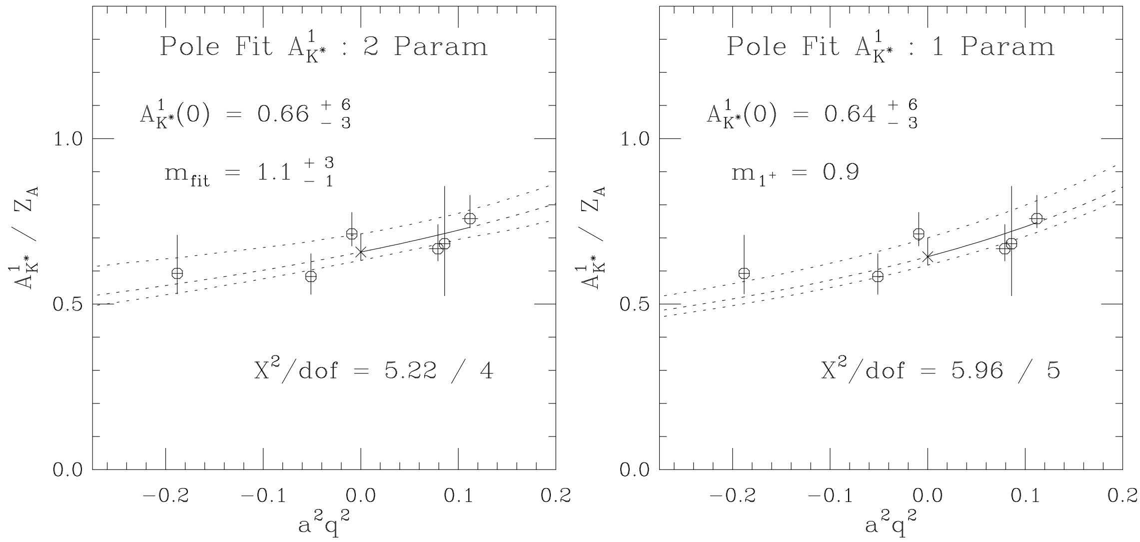

Figure 3.13: Pole dominance plots for the $A^1_{K^*}$ form factor.

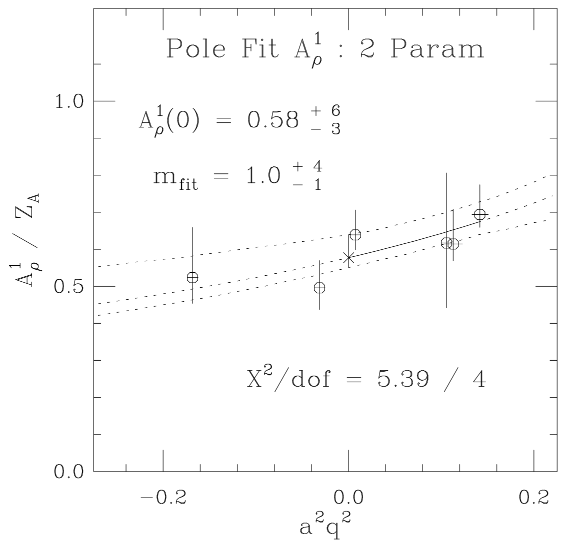

Figure 3.14: Pole dominance plot for the A^1_ρ form factor.

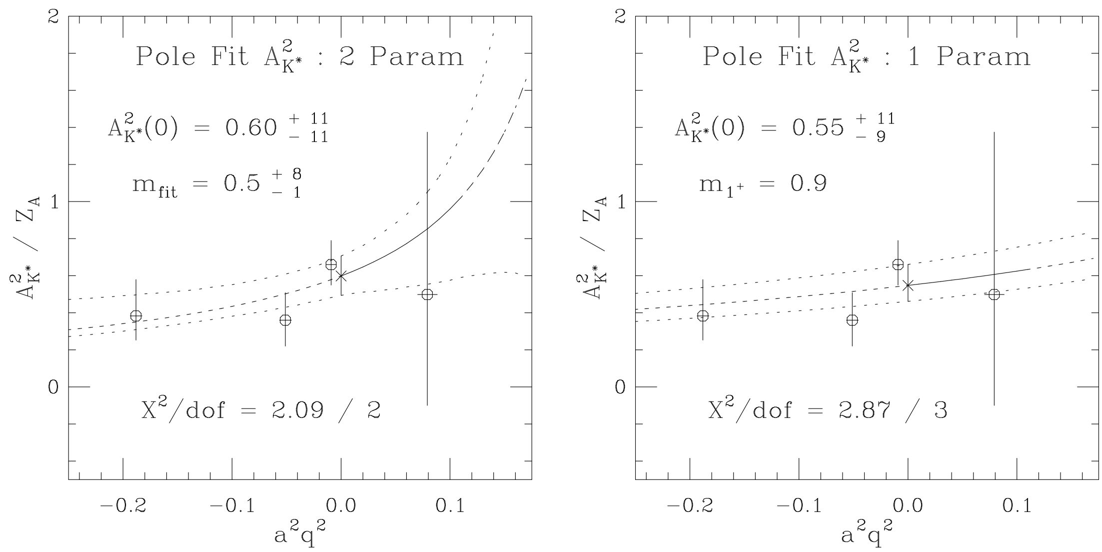

Figure 3.15: Pole dominance plots for the $A^2_{K^*}$ form factor.

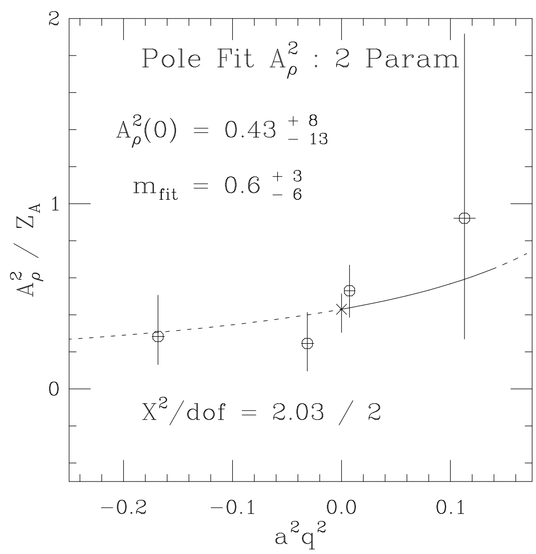

Figure 3.16: Pole dominance plot for the A^2_ρ form factor.

For the $A^1_{K^*}$ and $A^2_{K^*}$ data the two fit methods give a consistent determination of $A^1_{K^*}(0)$ and $A^2_{K^*}(0)$; the two-parameter fit yields

$$\frac{A^1_{K^*}(0)}{Z_A} = 0.66\,^{+\,6}_{-\,3}\,; \qquad m^{c\bar{s}}_{1^+} = 1.1\,^{+\,3}_{-\,1} \tag{3.69}$$

$$\frac{A^2_{K^*}(0)}{Z_A} = 0.60\,^{+\,11}_{-\,11}\,; \qquad m^{c\bar{s}}_{1^+} = 0.5\,^{+\,8}_{-\,1} \tag{3.70}$$

where the pole masses agree (within errors) with the experimental value $0.9\,^{+\,1}_{-\,1}$; the quoted error in the experimental measurement is due to the uncertainty in the lattice spacing. However, the $A^2_{K^*}$ pole mass is poorly determined (large errors). The chi-squared ($\chi^2/dof \approx 1$) indicate a good fit to the data for both form factors. Thus, pole dominance gives a good description of the $A^1_{K^*}$ form factor but the q^2 dependence of the $A^2_{K^*}$ form factor (within the kinematic region) is not well-determined.

Figures 3.14 and 3.16 show the A^1_ρ and A^2_ρ form factor data, given in Table 3.12, plotted as a function of q^2. Two-parameter fits, using Eqn. (3.52), give

$$\frac{A^1_\rho(0)}{Z_A} = 0.58\,^{+\,6}_{-\,3}\,; \qquad m^{c\bar{d}}_{1^+} = 1.0\,^{+\,4}_{-\,1} \tag{3.71}$$

$$\frac{A^2_\rho(0)}{Z_A} = 0.43\,^{+\,8}_{-\,13}\,; \qquad m^{c\bar{d}}_{1^+} = 0.6\,^{+\,3}_{-\,6} \tag{3.72}$$

where both pole masses agree (within two sigma) with the mass of the D_1 meson ($\approx 2.4\ GeV$); the quantum numbers of this resonance require confirmation [52]. The chi-squared ($\chi^2/dof \approx 1$) indicate a good fit to the data, for both form factors. Thus, pole dominance gives a good description of the A^1_ρ and A^2_ρ form factors.

Figures 3.17 and 3.18 show the $A^0_{K^*}$ and A^0_ρ form factor data, given in Table 3.11 and Table 3.12 respectively, plotted as a function of q^2. The $A^0_{K^*}$ and A^0_ρ data is fitted to the pole dominance model, given by Eqn. (3.52), as follows: the left-hand plots correspond to a two-parameter fit; the right-hand plots correspond to a one-parameter fit with the pole mass constrained to the mass of the associated resonance, m_{D_s} and m_D respectively.

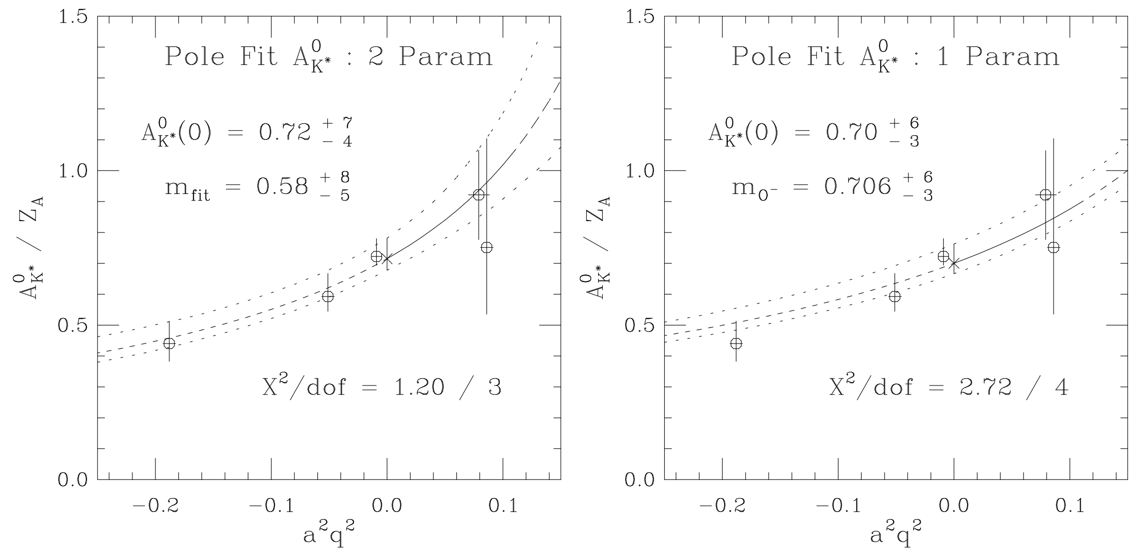

Figure 3.17: Pole dominance plots for the $A^0_{K^*}$ form factor.

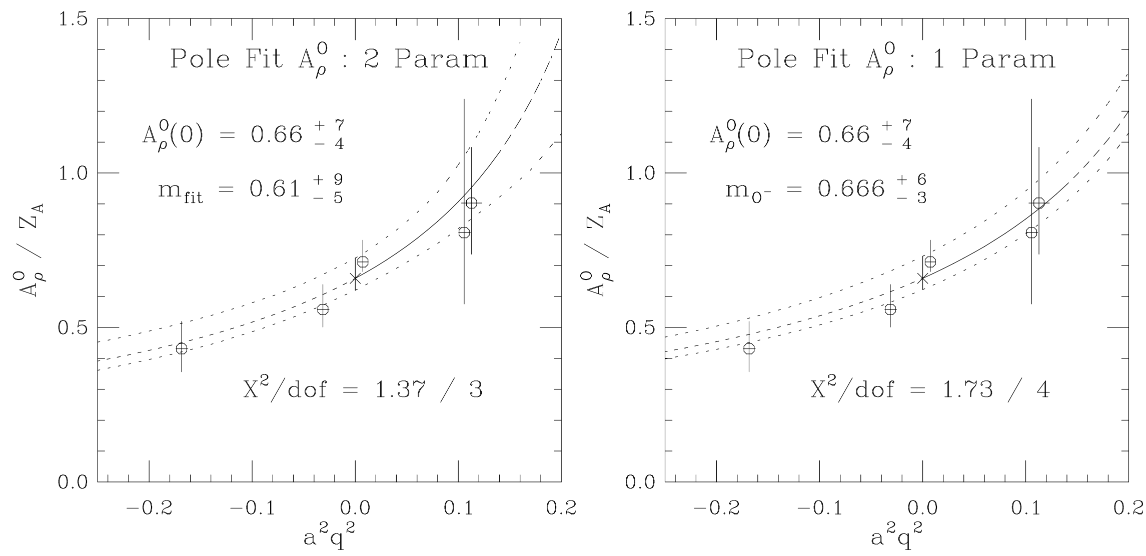

Figure 3.18: Pole dominance plots for the A^0_ρ form factor.

For the $A^0_{K^*}$ data the two fit methods give a consistent determination of $A^0_{K^*}(0)$; the two-parameter fit yields

$$\frac{A^0_{K^*}(0)}{Z_A} = 0.72\,^{+\,7}_{-\,4}; \qquad m^{c\bar{s}}_{0^-} = 0.58\,^{+\,8}_{-\,5} \tag{3.73}$$

where the pole mass is low compared to the lattice value $0.706\,^{+\,6}_{-\,3}$, given in Table 2.3. However, these masses still agree within two sigma. The fit chi-squared ($\chi^2/dof = 0.40$) indicates an excellent fit to the data; all data points lie within one sigma, for both fit methods. Thus, pole dominance gives a good determination of $A^0_{K^*}(0)$ but the q^2 dependence of the $A^0_{K^*}$ form factor (within the kinematic region) is not well-determined.

Similarly, for the A^0_ρ data the two fit methods give a consistent determination of $A^0_\rho(0)$; the two-parameter fit yields

$$\frac{A^0_\rho(0)}{Z_A} = 0.66\,^{+\,7}_{-\,4}; \qquad m^{c\bar{d}}_{0^-} = 0.61\,^{+\,9}_{-\,5} \tag{3.74}$$

where the pole mass agrees (within errors) with the lattice value $0.666\,^{+\,6}_{-\,3}$, given in Table 2.3. The fit chi-squared ($\chi^2/dof = 0.46$) indicates an excellent fit to the data; all data points lie within one sigma, for both fit methods. Thus, pole dominance gives a good description of the A^0_ρ form factor.

Recall from Section 3.1, the $D \to K^*$, ρ decay rates, given by Eqn. (3.19), are proportional to an integral over q^2 which is a function of V, A^1 and A^2. For the vector and axial form factor data, given in Tables 3.9–3.12, pole dominance gives a good description of the $A^1_{K^*}$ and A^1_ρ form factors. However, the q^2 dependence of the V_{K^*}, V_ρ, $A^2_{K^*}$ and A^2_ρ form factors is not well-determined. Fortunately, the decay rate is dominated by the A^1 form factor; the V and A^2 contributions are small and only important in the region $q^2 = 0$ where they are reasonably well-determined. For example, the discrepancy in the $A^2_{K^*}$ pole-mass (a factor of two) has only a small effect (less than 5%) on the $D \to K^*$ decay rate. Thus, the form factor results quoted in this Section can be used to compute (with some confidence) the total decay rates.

3.6 Renormalisation Constants

In this section, the problem of determining the $D \to K$, K^* and $D \to \pi$, ρ form factors due to discretisation errors is discussed. In this study, discretisation errors are substantially reduced by the use of the $O(a)$-improved SW action. However, for currently accessible lattice spacings these errors lead to an uncertainty of order 10% in the form factors.

Renormalisation Constant Definition

The lattice currents V_L^μ and A_L^μ used in this study are related to the physical ones (V^μ and A^μ) by renormalisation constants Z_V and Z_A as follows:

$$Z_V\, V_L^\mu = V^\mu \tag{3.75}$$

$$Z_A\, A_L^\mu = A^\mu \tag{3.76}$$

where $V_L^\mu = \bar{q}\,\gamma^\mu \mathrm{Q}$ and $A_L^\mu = \bar{q}\,\gamma^\mu\gamma^5 Q$ are the vector and axial heavy-light currents respectively.

Light-Light Current

A UKQCD study [64] of the light-light current $\bar{q}\,\gamma^\mu q$ for the SW action at $\beta = 6.2$ (using chiral Ward identities) obtained

$$Z_V = 0.817 \pm 2 \pm 8 \tag{3.77}$$

where the first error is statistical, the second is due to the mass dependence of Z_V corresponding to $\kappa_l = 0.14144$, 0.14226 and 0.14262; Z_V increases linearly with increasing light quark mass. This result is in good agreement with the one-loop perturbative value 0.83 [65]–[66] computed using a 'boosted' coupling constant [67]. Similarly, a study of the light-light current $\bar{q}\,\gamma^\mu\gamma^5 q$ obtained

$$Z_A = 1.05 \pm 1 \tag{3.78}$$

which is higher than the perturbative value 0.97. However, no dependence on the light quark mass was observed. Thus, when both quarks are light the discretisation errors are small.

Heavy-Light Current

A UKQCD study [19] of the heavy-heavy vector current $\bar{Q}\gamma^\mu Q$ was performed by defining an effective Z_V as follows:

$$Z_V^{eff} = \frac{G_P^{(2)}(t_y, 0; \vec{p}\,)\, p^\mu}{G_{P\to P}^{(3)\mu}(t_y, t_x, 0; \vec{p}\,)\, E} \tag{3.79}$$

with

$$G_P^{(2)}(t_y, 0; \vec{p}\,) = \sum_{\vec{x}} e^{i\frac{2\pi}{L}\vec{p}\cdot\vec{y}} \left\langle 0 \left| \hat{T} \left\{ \hat{P}(y)\, \hat{P}^\dagger(0) \right\} \right| 0 \right\rangle \tag{3.80}$$

$$G_{P\to P}^{(3)\mu}(t_y, t_x, 0; \vec{p}\,) = \sum_{\vec{x},\vec{y}} e^{i\frac{2\pi}{L}\vec{p}\cdot\vec{y}} \left\langle 0 \left| \hat{T} \left\{ \hat{P}(y)\, V^\mu(x)\, \hat{P}^\dagger(0) \right\} \right| 0 \right\rangle \tag{3.81}$$

where $\hat{P}^\dagger$ and $\hat{P}$ are interpolating operators to create and annihilate a heavy-light pseudoscalar meson respectively.

For degenerate heavy quarks with $\kappa_h = 0.129$, and using correlation functions with $\vec{p} = 0$ and $\mu = 4$, gives

$$Z_V^{eff} = 0.9177 \,^{+\,3}_{-\,2} \tag{3.82}$$

which differs by about 10% from the value 0.83 determined using light quarks. This difference is a measure of the size of the discretisation errors for the SW action which are of $O(\alpha_s ma)$ and $O(m^2a^2)$. For the Wilson action the discretisation errors are much larger, $O(ma)$.

Furthermore, it is important to realise that discretisation errors of $O(\alpha_s ma)$ and $O(m^2a^2)$ are, in general, different for matrix elements with different Lorentz indices and between different states. Thus, these errors cannot be absorbed into universal (effective) Z_V and Z_A. Fortunately, hypercubic group invariance ensures there are no discretisation errors of $O(\alpha_s ma)$ which affect spatial components differently from temporal components, for each q^2 value. However, even if $O(m^2a^2)$ corrections are neglected (in which case discretisation errors are independent of the Lorentz current) these errors could be different for different form factors, and they could have a different q^2 dependence than the form factors themselves.

Effective Renormalisation Constants

In this study, the discretisation errors are modelled by using effective (mass-dependent) renormalisation constants, Z_V^{eff} and Z_A^{eff}, in an attempt to absorb at least part of the error. For the vector current an approximate average of the perturbative value 0.83 (obtained using light quarks) and the non-perturbative value 0.92 (obtained using heavy quarks) gives

$$Z_V^{eff} = 0.88\,^{+\,4}_{-\,5}. \tag{3.83}$$

For the light-light axial current the perturbative and non-perturbative determinations of Z_A do not agree. Thus, the 'best' estimate for the axial renormalisation constant is

$$Z_A^{eff} = 1.05\,^{+\,1}_{-\,8} \tag{3.84}$$

which corresponds to the non-perturbative result but with the lower error increased to include the perturbative value.

3.7 Comparison with Experiment

In Section 3.5, the $D \to K$, K^* and $D \to \pi$, ρ form factor data was fitted to the pole dominance form, given by Eqn. (3.52), to obtain the form factors at $q^2 = 0$ and the corresponding pole masses. In this section, the form factors are compared with experiment and other theoretical calculations. In order to make this comparison, values for the renormalisation constants Z_V and Z_A must be specified. The $D \to K$, K^* and $D \to \pi$, ρ decay rates, given by Eqns. (3.18) and (3.19), are also computed; the integrals (over q^2) were performed analytically by assuming pole-dominance for the form factors.

Physical Form Factors

The $D \to K$, K^* and $D \to \pi$, ρ form factors at $q^2 = 0$, obtained from pole dominance fits in Section 3.5, are given in Tables 3.13 and 3.14 respectively, using effective renormalisation constants $Z_V^{eff} = 0.88\,^{+\,4}_{-\,5}$ and $Z_A^{eff} = 1.05\,^{+\,1}_{-\,8}$, as detailed in Section 3.6. The experimental world average, and other theoretical results are quoted for comparison.

Source	Reference	$f_K^+(0)$	$V_{K^*}(0)$
Exp't	World Ave. [68]	0.70 ± 0.03	N/A
	World Ave. [69]	0.77 ± 0.04	1.16 ± 0.16
Lattice Clover	This Work	$0.67\,^{+\,0.05}_{-\,0.03}\,^{+\,0.03}_{-\,0.04}$	$1.01\,^{+\,0.25}_{-\,0.05}\,^{+\,0.05}_{-\,0.06}$
	APE [70]	0.78 ± 0.08	1.08 ± 0.22
Lattice Wilson	LANL [71]	0.71 ± 0.04	1.28 ± 0.07
	Wuppertal [72]	$0.71 \pm 0.12\,^{+\,0.10}_{-\,0.07}$	$1.34 \pm 0.24\,^{+\,0.19}_{-\,0.14}$
	LMMS [73]	0.63 ± 0.08	0.86 ± 0.10
	BKS [74]	$0.90 \pm 0.08 \pm 0.21$	$1.43 \pm 0.45\,^{+\,0.48}_{-\,0.49}$
	ELC [75]	$0.60 \pm 0.15 \pm 0.07$	0.86 ± 0.24
Quark Models	ISGW [76]	0.76–0.82	1.1
	WSB [77]	0.76	1.27
	KS [78]	0.76	0.8
	GS [79]	0.69	1.5
Sum Rules	BBD [80]	$0.60\,^{+\,0.15}_{-\,0.10}$	1.10 ± 0.25
	AEK [81]	0.60 ± 0.15	N/A
	DP [81]	0.75 ± 0.05	N/A

Table 3.13: $D \to K$, K^* form factors: Theory vs. Experiment.

Source	Reference	$A^1_{K^*}(0)$	$A^2_{K^*}(0)$
Exp't	World Ave. [69]	0.61 ± 0.05	0.45 ± 0.09
Lattice Clover	This Work	$0.69 {}^{+0.06}_{-0.03} {}^{+0.01}_{-0.05}$	$0.63 \pm 0.12 {}^{+0.01}_{-0.05}$
	APE [70]	0.67 ± 0.11	0.49 ± 0.34
Lattice Wilson	LANL [71]	0.72 ± 0.03	0.49 ± 0.09
	Wuppertal [72]	$0.61 \pm 0.06 {}^{+0.09}_{-0.07}$	$0.83 \pm 0.20 {}^{+0.12}_{-0.08}$
	LMMS [73]	0.53 ± 0.03	0.19 ± 0.21
	BKS [74]	$0.83 \pm 0.14 \pm 0.28$	$0.59 \pm 0.14 {}^{+0.24}_{-0.23}$
	ELC [75]	0.64 ± 0.16	$0.40 \pm 0.28 \pm 0.04$
Quark Models	ISGW [76]	0.8	0.8
	WSB [77]	0.88	1.15
	KS [78]	0.82	0.8
	GS [79]	0.73	0.55
Sum Rules	BBD [80]	0.50 ± 0.15	0.60 ± 0.15

Table 3.13: (Cont.)

Source	Reference	$V_{K^*}(0)/A^1_{K^*}(0)$	$A^2_{K^*}(0)/A^1_{K^*}(0)$
Exp't	World Ave. [69]	1.90 ± 0.25	0.74 ± 0.15
Lattice Clover	This Work	$1.47 {}^{+0.45}_{-0.12} \pm 0.05$	$0.9 \pm 0.1 \pm 0.1$
	APE [70]	1.6 ± 0.3	0.7 ± 0.4
Lattice Wilson	LANL [71]	1.78 ± 0.07	0.68 ± 0.11
	LMMS [73]	1.6 ± 0.2	0.4 ± 0.4
	BKS [74]	$1.99 \pm 0.22 {}^{+0.31}_{-0.35}$	$0.70 \pm 0.16 {}^{+0.20}_{-0.15}$
	ELC [75]	1.3 ± 0.2	0.6 ± 0.3
Quark Models	ISGW [76]	1.4 ± 0.4	1.0 ± 0.3
	WSB [77]	1.4	1.3
	KS [78]	1.0	1.0
	GS [79]	2.0	0.8
Sum Rules	BBD [80]	2.2 ± 0.2	1.2 ± 0.2

Table 3.13: (Cont.)

Source	Reference	$f_\pi^+(0)$	$V_\rho(0)$
Clover	This Work	$0.57 \begin{smallmatrix}+0.11\\-0.07\end{smallmatrix} \pm 0.03$	$0.96 \begin{smallmatrix}+0.22\\-0.06\end{smallmatrix} \begin{smallmatrix}+0.04\\-0.06\end{smallmatrix}$
Lattice Wilson	Wuppertal [72]	$0.68 \pm 0.13 \begin{smallmatrix}+0.10\\-0.07\end{smallmatrix}$	$1.31 \pm 0.25 \begin{smallmatrix}+0.18\\-0.13\end{smallmatrix}$
	LMMS [73]	0.58 ± 0.09	0.77 ± 0.09
	BKS [74]	$0.84 \pm 0.12 \pm 0.35$	$1.07 \pm 0.49 \pm 0.35$
Quark Models	ISGW [76]	0.51	N/A
	WSB [77]	0.69	1.23
	KS [78]	0.69	1.23
Sum Rules	AEK, DP [81]	0.6–0.75	N/A

Source	Reference	$A_\rho^1(0)$	$A_\rho^2(0)$
Clover	This Work	$0.61 \begin{smallmatrix}+0.06\\-0.03\end{smallmatrix} \begin{smallmatrix}+0.01\\-0.05\end{smallmatrix}$	$0.45 \begin{smallmatrix}+0.08\\-0.14\end{smallmatrix} \begin{smallmatrix}+0.01\\-0.03\end{smallmatrix}$
Lattice Wilson	Wuppertal [72]	$0.59 \pm 0.07 \begin{smallmatrix}+0.08\\-0.06\end{smallmatrix}$	$0.83 \pm 0.20 \begin{smallmatrix}+0.12\\-0.08\end{smallmatrix}$
	LMMS [73]	0.47 ± 0.07	-0.07 ± 0.42
	BKS [74]	$0.65 \pm 0.15 \begin{smallmatrix}+0.24\\-0.23\end{smallmatrix}$	$0.59 \begin{smallmatrix}+0.28\\-0.25\end{smallmatrix}$
Quark Models	WSB [77]	0.78	0.92
	KS [78]	0.78	0.92

Table 3.14: $D \to \pi$, ρ form factors.

The errors quoted for 'This Work', in Tables 3.13 and 3.14, correspond as follows: the first set are statistical, the second are due to the uncertainty in the effective renormalisation constants, computed using the extreme values of Z_V^{eff} and Z_A^{eff}. However, the systematic error for the ratio $A^2_{K^*}(0)/A^1_{K^*}(0)$ corresponds to an estimate of the uncertainty in Z_A^{eff} for different form factors. Recall from Section 3.6, different form factors could have different discretisation errors. Thus, the effective renormalisation constant Z_A^{eff} may be different for A^1 than for A^2; this leads to an additional ambiguity of 10% for this ratio. The errors quoted for 'Other Work' correspond as follows: the first error is statistical, the second is an estimate of the systematic error.

The $D \to K$, K^* form factors obtained in this study are in good agreement with experimental measurements (all results agree within 1.5 sigma), and with the most recent lattice simulations using $O(a)$-improved SW [70] and Wilson [71, 72] actions. The values reported in Refs. [73, 75] and [74] (obtained in the pioneering lattice studies using Wilson fermions) are also in agreement but the former are, in general, lower and the latter higher than the predictions made in this study. In principle, discretisation errors are larger for Wilson than for $O(a)$-improved SW actions. However, part of the discrepancy in the lattice results is due to the different values used in the literature for the effective renormalisation constants, Z_V^{eff} and Z_A^{eff}. The lattice results are also in agreement with quark-model and sum-rule predictions.

The $D \to \pi$, ρ form factors obtained in this study are in excellent agreement with other lattice results, and with quark-model and sum-rule predictions. However, there are no experimental measurements available for these form factors. Thus, the lattice is the only source of quantitative results for the $D \to \pi$, ρ form factors.

Decay Rates

The $D \to K$, K^* and $D \to \pi$, ρ decay rates, computed using lattice masses with $|V_{cs}| = 0.975$ and $|V_{cd}| = 0.222$ [52], are given in Table 3.15. The experimental world average, and other theoretical results are quoted for comparison. Ref [69] gives $\Gamma(D \to \pi) = 1.2 \pm 0.3\ 10^{10}\ s^{-1}$. Assuming isospin symmetry, one obtains the decay rate $\Gamma(D \to \pi^{\pm}) = 0.60 \pm 0.15\ 10^{10}\ s^{-1}$, quoted in Table 3.15, with charged pions in the final state.

Source	Reference	$\Gamma(D \to K)$	$\Gamma(D \to K^*)$
Exp't	World Ave. [68]	7.1 ± 0.6	4.5 ± 0.5
	World Ave. [69]	9.0 ± 0.5	5.1 ± 0.5
Lattice Clover	This Work	$7.1 ^{+1.2}_{-0.6} {}^{+0.7}_{-0.8} {}^{+2.1}_{-1.7}$	$5.7 ^{+1.2}_{-0.5} {}^{+0.1}_{-0.8} {}^{+1.7}_{-1.3}$
	APE [70]	9.1 ± 2.0	6.9 ± 1.8
Lattice Wilson	LMMS [73]	5.8 ± 1.5	5.0 ± 0.9
	ELC [75]	$5.4 \pm 3.0 \pm 1.4$	6.4 ± 2.8
Quark Models	ISGW [76]	8.5	9.1 ± 0.25
	WSB [77]	8.26	N/A
	GS [79]	7.1	N/A
Sum Rules	BBD [80]	6.4 ± 1.4	3.2 ± 1.3
	AEK [81]	5.1 ± 1.7	N/A
	DP [81]	8.2 ± 1.1	N/A

Source	Reference	$\Gamma(D \to \pi^\pm)$	$\Gamma(D \to \rho^\pm)$
Exp't	World Ave. [69]	0.60 ± 0.15	N/A
Lattice Clover	This Work	$0.50 ^{+0.18}_{-0.11} {}^{+0.05}_{-0.06} {}^{+0.15}_{-0.12}$	$0.41 ^{+0.09}_{-0.03} {}^{+0.01}_{-0.06} {}^{+0.12}_{-0.10}$
	APE [70]	0.8 ± 0.2	0.6 ± 0.2
Lattice Wilson	LMMS [73]	0.5 ± 0.2	0.40 ± 0.09
	ELC [75]	$0.5 \pm 0.3 \pm 0.1$	$0.6 \pm 0.3 \pm 0.1$
Sum Rules	DP [81]	0.76 ± 0.24	N/A

Table 3.15: $D \to K$, K^*, π, ρ decay rates: Theory vs. Exp't. Units in $10^{10}\ s^{-1}$.

Source	Reference	$\frac{\Gamma(D\to K^*)}{\Gamma(D\to K)}$	$\frac{\Gamma_L(D\to K^*)}{\Gamma_T(D\to K^*)}$
Exp't	World Ave. [68]	0.55 ± 0.07	1.2 ± 0.1
Lattice	This Work	$0.80 {}^{+0.17}_{-0.10} \pm 0.05$	$1.12 {}^{+0.17}_{-0.11} \pm 0.01$
Clover	APE [70]	0.8 ± 0.3	1.2 ± 0.3
Lattice	LMMS [73]	0.86 ± 0.22	1.51 ± 0.27
Wilson	ELC [75]	$1.1 \pm 0.6 \pm 0.3$	1.4 ± 0.3
	ISGW [76]	1.1	1.1 ± 0.2
Quark	WSB [77]	1.15	0.9
Models	KS [78]	0.95	1.1
	GS [79]	1.4	1.2
Sum Rules	BBD [80]	0.50 ± 0.15	0.86 ± 0.06

Table 3.15: (Cont.)

For the pseudoscalar-to-pseudoscalar decay, Z_V^{eff} is an overall factor in the decay rate, given by Eqns. (3.18). Therefore, this result could be quoted in terms of $\Gamma(D \to K)/(Z_V^{eff})^2$. However, for the pseudoscalar-to-vector decay such a factorisation is not possible; the H_-^+ form factors mix the vector and axial contributions, given by Eqn. (3.19). Therefore, both decay rates are computed using effective renormalisation constants $Z_V^{eff} = 0.88\,^{+\,4}_{-\,5}$ and $Z_A^{eff} = 1.05\,^{+\,1}_{-\,8}$, as detailed in Section 3.6.

The errors quoted for 'This Work', in Table 3.15, correspond as follows: the first set are statistical; the second are due to the uncertainty in the effective renormalisation constants Z_V and Z_A; the third are due to the uncertainty in the inverse lattice spacing, computed using the extreme values of $a^{-1} = 2.85 \pm 0.15$ GeV. The errors quoted for 'Other Work' correspond as follows: the first error is statistical, and the second is an estimate of the systematic error.

The $D \to K$, K^* and $D \to \pi$, ρ decay rates obtained in this study are in excellent agreement with experimental measurements, other lattice results, and quark-model and sum-rule predictions. For the decay $D \to \rho$, the lattice provides the only quantitative result for the decay rate. In this study, the uncertainty in the inverse lattice spacing is the largest source of error in determining the decay rates.

Summary and Conclusions

This thesis describes a lattice calculation of the matrix elements of the vector and axial-vector currents which are relevant for the semi-leptonic decays $D \to K$ and $D \to K^*$. The simulation was performed in the quenched approximation to lattice QCD on a $24^3 \times 48$ space-time lattice at $\beta = 6.2$, using the $O(a)$-improved Sheikholeslami-Wohlert (SW) action.

In the limit of zero lepton masses the $D \to K$ and $D \to K^*$ decays are described by four form factors: f_K^+, V_{K^*}, $A^1_{K^*}$ and $A^2_{K^*}$ which are dimensionless functions of q^2, where q^μ is the four-momentum transfer. The $D \to K$ and $D \to K^*$ form factors were determined for different q^2 values; their q^2 dependence is found to be reasonably well described by a simple pole-dominance model. In particular, f_K^+ and $A^1_{K^*}$ are well determined over the entire kinematically allowed range; these form factors dominate the $D \to K$ and $D \to K^*$ decay rates respectively. The $D \to \pi$ and $D \to \rho$ form factors were also determined.

The form factor results at $q^2 = 0$, obtained from pole-dominance fits, are in good agreement with experiment and other theoretical calculations. The $D \to K$, K^* and $D \to \pi$, ρ decay rates were also computed; the integrals over q^2 are performed analytically by assuming pole dominance. Again, these results are in good agreement with experiment. This agreement gives further confidence that lattice QCD is becoming a reliable quantitative tool for non-perturbative QCD phenomenology.

This study is one of the first calculations of weak matrix elements using the $O(a)$-improved SW action. Furthermore, a large lattice volume is used to minimise finite-size effects. Nevertheless, discretisation errors are still of order 10% for the form factors. Thus, it is important to repeat this calculation on lattices of different sizes and lattice spacings in order to study these systematic errors (except quenching) in detail. In the next few years, lattice calculations in full QCD will be performed giving control over all systematic errors.

References

[1] I. Aitchison and A. Hey, *Gauge Theories in Particke Physics*, Adam Hilger (1989).

[2] T. Cheng and L. Li, *Gauge Theory of Elementary Particle Physics*, Oxford University Press (1984).

[3] L. Ryder, *Quantum Field Theory*, Cambridge University Press (1986).

[4] N. Cabibbo, *Phys. Rev. Lett.* **10** (1963) 531.

[5] M. Kobayashi and K. Maskawa, *Prog. Theor. Phys.* **49** (1973) 652.

[6] P. Higgs, *Phys. Rev. Lett.* **12** (1964) 132.

[7] R.P Feynman and M. Gell-Mann, *Phys. Rev.* **109** (1958) 193.

[8] E. Sudarshan and R. Marshak, *Phys. Rev.* **109** (1958) 1860.

[9] J.J. Sakurai, *Nuovo Cimento* **7** (1958) 649.

[10] G. Martinelli, and C. Bernard and A. Soni in Lattice 88, *Nucl. Phys.* **B (Proc. Suppl.) 9** (1989) 134 and 155.

[11] S. Sharpe in Lattice 89, *Nucl. Phys.* **B (Proc. Suppl.) 17** (1990) 146.

[12] G. Kilcup in Lattice 90, *Nucl. Phys.* **B (Proc. Suppl.) 20** (1991) 417.

[13] G. Martinelli in Lattice 91, *Nucl. Phys.* **B (Proc. Suppl.) 26** (1992) 31.

[14] C.T. Sachrajda in Lattice 92, *Nucl. Phys.* **B (Proc. Suppl.) 30** (1993) 20.

[15] C. Bernard in Lattice 93, *Nucl. Phys.* **B (Proc. Suppl.) 34** (1994) 47.

[16] S.P. Booth *et al.* (UKQCD), *Phys. Rev. Lett.* **72** (1994) 462.

[17] K.C. Bowler *et al.* (UKQCD), *Phys. Rev. Lett.* **72** (1994) 1398.

[18] K.C. Bowler *et al.* (UKQCD), *Phys. Rev.* **D51** (1995) 4955.

[19] K.C. Bowler *et al.* (UKQCD), *Phys. Rev.* **D52** (1995) 5067.

[20] D.R.Burford *et al.* (UKQCD), *Nucl. Phys.* **B447** (1995) 425.

[21] J.M. Flynn *et al.* (UKQCD), *Nucl. Phys.* **B461** (1996) 327.

[22] M. Creutz, *Quarks, Gluons and Lattices*, Cambridge University Press (1983).

[23] I. Montvay and G. Münster, *Quantum Fields on a Lattice*, Cambridge University Press (1994).

[24] C. Rebbi, *Lattice Gauge Theories and Monte Carlo Simulations*, World Scientific (1983).

[25] H.J. Rothe, *Lattice Gauge Theories*, World Scientific (1992).

[26] D. Gross and F. Wilczek, *Phys. Rev. Lett.* **30** (1973) 1343.

[27] S. Weinberg, *Phys. Rev. Lett.* **31** (1973) 494.

[28] H. Fritzsch, M. Gell-Mann and H. Leutwyler, *Phys. Lett.* **47B** (1973) 365.

[29] A. Zee, *Phys. Rev.* **D7** (1973) 3630.

[30] S. Coleman and D.J. Gross, *Phys. Rev. Lett.* **31** (1973) 851.

[31] B. Schutz, *Geometrical Methods of Mathematical Physics*, Cambridge University Press (1980).

[32] R.P. Feynman and A.R. Hibbs, *Quantum Mechanics and Path Integrals*, McGrawHill (1965).

[33] N. Metropolis, A.W. Rosenbluth, M.N. Rosenbluth, A.H. Teller and E. Teller, *J. Chem. Phys* **21** (1953) 1087.

[34] K.G. Wilson, in *New Phenomena in Subnuclear Physics*, Erice Lectures, Ed. A.Zichichi, Plenum Press (1975).

[35] K.G. Wilson, *Phys. Rev.* **D14** (1974) 2455.

[36] M. Luscher and P. Weisz, *Commun. Math. Phys.* **97** (1985) 59.

[37] H.W. Hamber and C.M. Wu, *Phys. Lett.* **B136** (1984) 255.

[38] B. Sheikholeslami and R. Wohlert, *Nucl. Phys.* **B259** (1985) 572.

[39] G. Heatlie *et al.*, *Nucl. Phys.* **B352** (1991) 266.

[40] J. Mandula *et al.*, *Nucl. Phys.* **B228** (1983) 109.

[41] W.H. Press *et al.*, *Numerical Recipes in C, Second Edition*, Cambridge University Press (1992).

[42] S. Gusken *et al.* in Lattice 89, *Nucl. Phys.* **B (Proc. Suppl.) 17** (1990) 361; *Phys. Lett.* **B227** (1989) 266.

[43] F. Mandl and G. Shaw, *Quantum Field Theory*, Wiley (1984).

[44] C. Bernard, A. El-Khadra and A. Soni, *Nucl. Phys.* **B (Proc. Suppl.) 9** (1989) 186; 17 (1990) 499.

[45] C.R. Allton *et al.* (UKQCD), *Phys. Rev.* **D49** (1994) 474.

[46] C.R. Allton *et al.* (UKQCD), *Nucl. Phys.* **B407** (1993) 331.

[47] R.M. Baxter *et al.* (UKQCD), *Phys. Rev.* **D49** (1994) 1594.

[48] A.D. Simpson, Ph.D. Thesis, The University of Edinburgh (1991).

[49] B. Efron, *The Jackknife, the Bootstrap and other Resampling Plans*, Society for Industrial and Applied Mathematics (1982).

[50] G. Wetherill, *Elementary Statistical Methods*, Chapman and Hall (1982).

[51] W.H. Press *et al.*, *Numerical Recipes in C*, Cambridge Press (1988).

[52] Particle Properties, *Phys. Rev.* **D45** (1992).

[53] P.L. Frabetti *et al.* (E-687), *Phys. Lett.* **B315** (1993) 203.

[54] G. Crawford *et al.* (CLEO), *Phys. Rev.* **D44** (1991) 3394.

[55] Z. Bai *et al.* (MARK III), *Phys. Rev. Lett.* **66** (1991) 1011.

[56] J.C. Anjos *et al.* (E-691), *Phys. Rev. Lett.* **62** (1989) 1587.

[57] A. Bean *et al.* (CLEO), *Phys. Lett.* **B317** (1993) 647.

[58] J. Adler *et al.* (MARK III), *Phys. Rev. Lett.* **62** (1989) 1821.

[59] M.S. Alam *et al.* (CLEO), *Phys. Rev. Lett.* **71** (1993) 1311.

[60] P.L. Frabetti *et al.* (E-687), *Phys. Lett.* **B307** (1993) 262.

[61] K. Kodama *et al.* (E-653), *Phys. Lett.* **B274** (1992) 246; **B286** (1992) 187.

[62] H. Albrecht *et al.* (ARGUS), *Phys. Lett.* **B255** (1991) 634.

[63] J.C. Anjos *et al.* (E-691), *Phys. Rev. Lett.* **65** (1990) 2630; **62** (1989) 722.

[64] D.S. Henty *et al.* (UKQCD), *Phys. Rev.* **D51** (1995) 5323.

[65] E. Gabrielli *et al.*, *Nucl. Phys.* **B362** (1991) 475.

[66] A. Borrelli *et al.*, *Nucl. Phys.* **B409** (1993) 382.

[67] G.P. Lepage and P.B. MacKenzie, *Nucl. Phys.* **B (Proc. Suppl.) 20** (1991) 173.

[68] G. Bellini, talk given at *Les Rencontres de Physique de la Vallee d'Aoste*, La Thuile, Aosta Valley (1994).

[69] M.S. Witherell, talk given at the *Int. Symposium on Lepton and Photon Interactions at High Energies*, Cornell University, Ithaca, NY (1993).

[70] C.R. Allton *et al.* (APE), *Phys. Lett.* **B345** (1995) 513.

[71] T. Bhattacharya and R. Gupta, *Nucl. Phys.* **B (Proc. Suppl.) 42** (1995) 935.

[72] S. Güsken, *et al.*, preprint HLRZ-95-38.

[73] M. Crisafulli, G. Martinelli, V.J. Hill and C.T. Sachrajda, *Phys. Lett.* **B223** (1989) 90; V. Lubicz, G. Martinelli and C.T. Sachrajda, *Nucl. Phys.* **B356** (1991) 301; V. Lubicz, G. Martinelli, M.S. McCarthy and C.T. Sachrajda, *Phys. Lett.* **B274** (1992) 415.

[74] C. Bernard, A. El-Khadra and A. Soni, *Phys. Rev.* **D43** (1991) 2140; **D45** (1992) 869.

[75] A. Abada, *et al.*, *Nucl. Phys.* **B416** (1994) 675.

[76] D. Scora and N. Isgur, *Phys. Rev.* **D40** (1989) 1491;
N. Isgur, D. Scora, B. Grinstein and M. Wise, *Phys. Rev.* **D39** (1989) 799.

[77] M. Bauer, B. Stech and M. Wirbel, *Z. Phys.* **C29** (1985) 637; **C34** (1987) 103; M. Bauer and M. Wirbel, *ibid.* **42** (1989) 671.

[78] J.G. Körner and G.A. Schuler, *Z. Phys.* **C38** (1988) 511; **C46** (1990) 93; *Phys. Lett.* **B231** (1989) 306.

[79] F.J. Gilman and R.L. Singleton, *Phys. Rev.* **D41** (1990) 142.

[80] P. Ball, V.M. Braun, H.G. Dosch and M. Neubert, *Phys. Lett.* **B259** (1991) 481; P. Ball, V.M. Braun and H.G. Dosch, *Phys. Rev.* **D44** (1991) 3567.

[81] T.M. Aliev, V.L. Eletskii, and Y.I. Kogan, *Sov. J. Nucl. Phys.* **40** (1984) 527;
C.A. Dominguez and N. Paver, *Phys. Lett.* **B207** (1988) 499.